# Cell Fermentation and Microfluidics

## Zellfermentation und Mikrofluidik

Zur Erlangung des akademischen Grades eines

DOKTORS DER NATURWISSENSCHAFTEN

(Dr. rer. nat.)

von der KIT-Fakultät für Chemie und Biowissenschaften

des Karlsruher Instituts für Technologie (KIT)

genehmigte

DISSERTATION

von

M. Sc. Christina Manz

1. Referent: Prof. Dr. Peter Nick

2. Referent: Prof. Dr. Reinhard Fischer

Tag der mündlichen Prüfung: 04.02.2019

Die vorliegende Dissertation wurde am Botanischen Institut des Karlsruher Instituts für Technologie (KIT), Lehrstuhl I für molekulare Zellbiologie, im Zeitraum von Oktober 2015 bis Dezember 2018 angefertigt.

Hiermit erkläre ich, die vorliegende Dissertation, von der Verwendung der angegebenen Hilfsmittel abgesehen, selbständig verfasst zu haben.

Alle Stellen, die gemäß Wortlaut oder Inhalt aus anderen Arbeiten entnommen sind, wurden durch Angabe der Quelle kenntlich gemacht.

Diese Dissertation liegt in gleicher oder ähnlicher Form keiner anderen Prüfungsbehörde vor.

Karlsruhe, Januar 2019

# Danksagung

An erster Stelle möchte ich mich besonders bei Prof. Dr. Peter Nick bedanken, für die Möglichkeit, meine Dissertation an seinem Lehrstuhl anzufertigen und die großartige Unterstützung während der gesamten Zeit.

Mein herzlicher Dank gilt Prof. Dr. Reinhard Fischer für die Übernahme des Korreferats und den weiteren Mitgliedern des Komitees.

Dr. Jan Maisch danke ich vielmals für die zahlreichen Ratschläge, Anregungen und Bestärkungen während meiner Arbeit.

Ganz besonders bedanke ich mich bei Dr. Manish Raorane für die wunderbare Zusammenarbeit und den konstruktiven Austausch. It was a pleasure to work with you.

Sabine Purper, die mir mit ihrer Erfahrung in der Zellkultur jederzeit mit Rat und Tat zur Seite stand, gebührt großer Dank.

Dr. Michael Riemann möchte ich für die Unterstützung bei der Durchführung und Auswertung der qPCR danken.

Bei Ernst Heene bedanke ich mich für die Einführung in die HPLC-Analyse und die Lösung technischer Probleme.

Ich danke allen Auszubildenden der Botanik I, für ihre Hilfsbereitschaft und den großen Beitrag zum reibungslosen Ablauf des Laboralltags.

Vielen Dank an alle Kollegen und ehemaligen Kollegen der Botanik I, die mich während meiner Arbeit unterstützt haben, für die tolle Arbeitsatmosphäre. My sincere thanks to all members of the Botanical Institute for your support and the amazing working atmosphere.

Auch möchte ich mich bei all meinen Studenten bedanken, insbesondere bei Sarah Hildebrandt, Michaela Herschinger, Marion Mielke und Marc Thieme, für die zahlreichen Vorversuche und ergänzenden Experimente.

Für die Durchführung der LC-MS-Analyse danke ich Dr. Judith Schäfer aus der Abteilung Lebensmittelchemie und Phytochemie.

Für eine großartige Zusammenarbeit möchte ich mich bei allen Kooperationspartnern bedanken. Den Mitarbeitern der Firma Phyton Biotech GmbH danke ich für die Unterstützung durch ihre Expertise und die Bereitstellung der verwendeten Zellkulturen. Dabei danke ich Jan Lenke und Klaus Brauer als Ansprechpartnern für alle zellkultur- und HPLC-relevanten Fragen. Bei den Mitarbeitern des Instituts für Mikrostrukturtechnik, ganz besonders bei Tim Finkbeiner, bedanke ich mich für den regen Austausch und die Fertigung des mikrofluidischen Bioreaktors.

Der größte Dank gilt meiner Familie, für ihre Ermutigung und ihr Verständnis, besonders in den arbeitsintensivsten Phasen. Ich danke meinen Eltern dafür, dass sie mich stets uneingeschränkt in all meinen Vorhaben unterstützen. Ebenso sehr danke ich meiner Schwester Claudia und meinem Schwager Tony für die moralische und fachliche Unterstützung und nicht zuletzt auch dafür, dass sie unsere Familie in den letzten drei Jahren um zwei wunderbare Mitglieder bereichert haben. Ich bin froh, dass es euch gibt!

# Table of contents

# Abbreviations

| | |
|---|---|
| 2,4-D | 2,4-Dichlorophenoxyacetic acid |
| AS | Anthranilate synthase |
| bp | base pair |
| BY-2 | *Nicotiana tabacum* L. cv Bright Yellow 2 |
| Ct | cycle threshold |
| D4H | Desacetoxyvindoline 4-hydoxylase |
| DAT | Deacetylvindoline 4-O-acetyltransferase |
| DBAT | 10-deacetylbaccatin III-10-*O*-acetyltransferase |
| DBTNBT | 3'-*N*-debenzoyl-2-deoxytaxol-*N*-benzoyltransferase |
| DPI | diphenyleneiodonium |
| EXP | expressed protein (reference gene) |
| FDA | fluorescein diacetate |
| FP | fluorescent protein |
| G10H | Geraniol 10-hydroxylase |
| HPLC | high performance liquid chromatography |
| IMT | Institute of Microstructure Technology |
| JA | jasmonic acid |
| LC-MS | liquid chromatography-mass spectrometry |
| MeJA | methyl jasmonate |
| MIA | monoterpene/monoterpenoid indole alkaloid |
| MT | microtubules |
| NAA | 1-naphthaleneacetic acid |
| NTC | no template control |
| PCV | packed cell volume |
| PRX1 | Peroxidase1/α-3',4'-anhydrovonblastine synthase |
| RboH | respiratory burst oxidase homolog |
| ROS | reactive oxygen species |
| rpm | revolutions per minute |
| RT | reverse transcriptase |
| SA | salicylic acid |
| SE | standard error |
| SGD | Strictosidine β-D-glucosidase |
| STR | Strictosidine synthase |
| T16H | Tabersonine 16-hydroxylase |
| T5αH | Taxadiene 5α hydroxylase |
| TASY | Taxadiene synthase |
| TDAT | Taxadiene 5α-ol O-acetyltransferase |
| TDC | Tryptophan decarboxylase |
| TDZ | thidiazuron |
| TIA | terpene/terpenoid indole alkaloid |

# Zusammenfassung

Als sessile Organismen können Pflanzen sich ungünstigen Umwelteinflüssen nicht einfach entziehen, sondern müssen sich anpassen. Hierzu haben sie eine Vielzahl an Sekundärmetaboliten entwickelt, die beispielsweise für die Verteidigung gegen Pathogene von Bedeutung sind. Viele dieser Pflanzenmetabolite dienen Menschen als Arzneimittel. Das Alkaloid Paclitaxel (auch bekannt als Taxol) wird von verschiedenen *Taxus*-Arten gebildet und kommt als Krebsmedikament zum Einsatz. Pharmazeutisch aktive Substanzen werden in sehr geringen Mengen in Pflanzen gebildet, sodass ihre Extraktion aus natürlichen Quellen kostenintensiv und eine Gefahr für die Biodiversität ist. Aufgrund der komplexen chemischen Struktur ist eine synthetische Herstellung nicht wirtschaftlich. Pflanzliche Zellkulturen bieten einen vielversprechenden Ansatz zur Herstellung entsprechender Wirkstoffe im industriellen Maßstab. Paclitaxel wird seit einigen Jahren erfolgreich mittels pflanzlicher Zellfermentation hergestellt, obwohl der Biosyntheseweg von Paclitaxel noch nicht vollständig entschlüsselt ist. Aus diesem Grund sind *Taxus* Zellkulturen Gegenstand dieser Dissertation. Mikroskopische Untersuchungen haben zwei verschiedene Zelltypen in den verwendeten Kulturen gezeigt. Der zahlenmäßig stärker ausgeprägte Zelltyp hat einen normalen Phänotyp mit erkennbarem Zellkern und Zytoplasmasträngen, der weniger häufige Zelltyp hat eine dominante Vakuole und zeigt eine starke Reflexion im Hellfeld, weshalb diese Zellen als „shiny cells“ bezeichnet wurden. In dieser Dissertation sollte festgestellt werden, welcher Mechanismus ihrer Bildung zugrunde liegt und ob ein Zusammenhang zwischen diesen shiny cells und der Bildung von Sekundärmetaboliten besteht. Hierfür wurde die Zellkultur mit verschiedenen Substanzen behandelt und anschließend eine Quantifizierung der shiny cells und verschiedener Sekundärmetabolite durchgeführt. Dabei hat sich gezeigt, dass die Bildung von shiny cells und Sekundärmetaboliten nicht in direktem Zusammenhang steht, jedoch beide Phänomene Teil einer Stressreaktion sind und demnach ein gemeinsamer Mechanismus zugrunde liegt. Außerdem wurde anhand der Ergebnisse ein Modell zur Bildung von shiny cells entwickelt, bei dem die Bündelung von Aktinfilamenten eine entscheidende Rolle spielt.

*Catharanthus roseus* stellt die einzige Quelle der Krebswirkstoffe Vinblastin und Vincristin dar. Ihr geringer Gehalt in Pflanzen und die hohe Nachfrage machen diese Stoffe extrem teuer. Eine Herstellung mittels Zellfermentation ist trotz mehrerer Jahrzehnte intensiver Forschung bislang nicht möglich. Ein Grund dafür ist, dass die

Biosynthese in der Pflanze vier verschiedene Zelltypen involviert, die Differenzierung von Zellkulturen jedoch gehemmt ist. Mitunter wird von gänzlich undifferenzierten Zellen gesprochen oder die Summe der Zellen in Suspensionskultur vereinfacht als Biomasse bezeichnet. Für die vorliegende Arbeit standen zwei *Catharanthus* Zellkulturen (Cath 001 und Cath 004) zur Verfügung, die starke phänotypische Unterschiede zeigen, obwohl sie gleichermaßen aus Samen hergestellt wurden. Um festzustellen, ob es neben den phänotypischen Unterschieden auch andere gibt, wurden beide Kulturen hinsichtlich ihres Wachstumsverhaltens, der Genexpression, zellulärer Merkmale und Alkaloidproduktion untersucht. Die beiden Kulturen unterscheiden sich in allen zuvor genannten Punkten deutlich. Besonders auffällig waren die Unterschiede in der Alkaloidproduktion. Cath 004 produzierte schon unter Kontrollbedingungen quantifizierbare Mengen Catharanthin, einer wichtigen Vorstufe von Vinblastin und Vincristin. Diese Produktion konnte in Cath 004 durch die Behandlung mit Methyljasmonat um das Zehnfache gesteigert werden. Die Alkaloidproduktion in Cath 001 hingegen war gering und die Kultur sprach kaum auf Behandlungen an. Auch im Wachstumsverhalten wurden die Unterschiede deutlich. So wächst Cath 004 vorrangig durch Vergrößerung des Zellvolumens, während die Teilungsaktivität in Cath 001 bedeutend höher ist. In einem Versuch, Cath 001 und Cath 004 gemeinsam zu kultivieren, um die Vorzüge beider Kulturen zu nutzen, wurde Cath 004 nach wenigen Wochen vollständig durch Cath 001 verdrängt.

Einen Lösungsansatz für das Problem der räumlichen Trennung von Biosynthesewegen bieten modulare mikrofluidische Systeme. In Kooperation mit dem Institut für Mikrostrukturtechnik wurde ein mikrofluidischer Bioreaktor im Chipdesign entwickelt, der es ermöglicht, verschiedene Zelltypen über einen kontinuierlichen Mediumfluss zu koppeln. Auf diese Weise können Zellen gemeinsam kultiviert werden, ohne dass sie sich mischen oder verdrängen. Es wurde nachgewiesen, dass metabolische Prozesse auch in diesem mikrofluidischen System stattfinden und es außerdem Kommunikation zwischen Zellen in verschiedenen Chips gibt.

Zusammenfassend wurde in dieser Arbeit gezeigt, dass pflanzliche Zellen in Suspensionskulturen ein deutliches Maß an Differenzierung aufweisen und der mikrofluidische Bioreaktor konzeptionell für die technische Simulation eines pflanzlichen Gewebes geeignet ist. Dadurch wurde eine wichtige Basis für die Produktion pflanzlicher Sekundärmetabolite mittels mikrofluidischer Methoden geschaffen.

# Abstract

As sessile organisms, plants can not escape unfavorable environmental influences, but have to adapt. Therefore, they have developed a variety of secondary metabolites, which are important, for example, for the defense against pathogens. Many of these plant metabolites are used by humans as pharmaceuticals. The alkaloid paclitaxel (also known as taxol) is formed by various *Taxus* species and is used as anticancer drug. Pharmaceutically active substances are produced in very small quantities in plants, making their extraction from natural sources costly and harmful to biodiversity. Due to the complex chemical structure, synthetic production is not economical. Plant cell cultures offer a promising platform for production of complex compounds on an industrial scale. Paclitaxel has been successfully produced using plant cell fermentation for several years, although the biosynthetic pathway of paclitaxel is not fully characterized. For this reason, *Taxus* cell cultures are subject of this dissertation. By microscopic studies, two different cell types in the culture were identified. The more abundant cell type has a normal phenotype with visible nucleus and cytoplasmic strands, the less common cell type has a dominant vacuole and shows strong reflection in the bright field, which is why these cells are referred to as “shiny cells”. The aim of this dissertation was to find the mechanism of their formation and to determine if there is a relationship between these shiny cells and the formation of secondary metabolites. For this purpose, the cell culture was treated with various elicitors followed by quantification of the shiny cells and various secondary metabolites. It has been shown that the formation of shiny cells and production of secondary metabolites are not directly correlated, but both phenomena are part of a stress response and therefore based on a common mechanism. In addition, the results were used to develop a model for the formation of shiny cells, in which the bundling of actin filaments plays an important role.

*Catharanthus roseus* is the only source of the anticancer drugs vinblastine and vincristine. Their low content in plants and the high demand make these substances extremely expensive. Production by cell fermentation is not yet possible despite several decades of research. One reason is that biosynthesis in plants requires four different cell types, while differentiation of cells in culture is inhibited. Sometimes they are considered as completely undifferentiated or the cells in suspension culture are simplified referred to as biomass. Two *Catharanthus* cell cultures (Cath 001 and Cath 004) were available for the present study, which show strong phenotypic differences

although they are both derived from seeds. To determine if there are further differences, both cultures were compared in terms of growth behavior, gene expression, cellular characteristics and alkaloid production. The two cultures differ strongly in all the aforementioned points. Particularly striking were the differences in alkaloid production. Even under control conditions, Cath 004 produced quantifiable amounts of catharanthine, an important precursor of vinblastine and vincristine. This production could be increased tenfold in Cath 004 by treatment with methyl jasmonate. Alkaloid production in Cath 001 was low and the culture hardly responded to treatments. Differences also became clear in growth behavior. Cath 004 grows primarily by increasing the cell volume, while the proliferation activity in Cath 001 is much higher. In an attempt to co-cultivate Cath 001 and Cath 004 to exploit the benefits of both cultures, Cath 004 was completely displaced by Cath 001 after a few weeks.

Modular microfluidic systems are a promising approach to solve the problem of spatial separation of biosynthetic pathways in plants. In cooperation with the Institute of Microstructure Technology, a microfluidic bioreactor in chip design has been developed, which allows to couple different cell types via a continuous medium flow. In this way, cells can be cultured together without mixing or displacing each other. In this work it has been proven that metabolic processes also take place in the microfluidic system and that there is communication between cells in different chips.

In summary, this work demonstrated that plant cells in suspension cultures show a clear degree of differentiation and that the microfluidic bioreactor is in principle suitable for the technical simulation of plant tissues. This has created an important basis for the production of plant secondary metabolites using microfluidics.

# 1 Introduction

## 1.1 Plant secondary metabolites and their function

Plant metabolites can be divided into two groups: the primary metabolites needed for vital cell functions and their maintenance and secondary metabolites that are not involved in growth and development. Secondary plant metabolites are low molecular structurally complex chemical compounds and it is assumed that there are hundreds of thousands of them (Narayani & Srivastava, 2017). More than 100,000 plant secondary metabolites have already been identified (Zhong & Yue, 2005). Since plants can not articulate or escape unfavorable environmental influences, secondary metabolites have an important role in adaption and interaction between plants and their environment, for example in defense against herbivores and pathogens or protection against UV-light (Gonçalves & Romano, 2018). Secondary metabolites can also function as signal molecules to attract pollinating arthropods or seed-dispersing animals (Wink, 2010). Harborne identified the three major classes of plant secondary metabolites as terpenoids, phenolic metabolites and alkaloids and other nitrogen-containing metabolites (Harborne, 1999). Subject of this thesis are alkaloids.

## 1.2 How mankind benefits from plant secondary metabolites

Plant secondary metabolites are of great importance to the plant itself, but also to humans. Many of them possess interesting biological activities and find applications, such as pharmaceuticals, insecticides, dyes, flavors, and fragrances (Goossens et al., 2003; Barbulova et al., 2014). Of particular importance is the use of plant secondary metabolites in medicine. Since ancient times people knew how to use the pharmacological effect of plants for their benefit. One of the oldest examples is chamomile, which contains many terpenoids and flavonoids that contribute to their medicinal properties, such as anti-inflammatory, antioxidant and stringent properties (Srivastava et al., 2010). But even today, plant secondary metabolites play an increasingly important role in the treatment of disease. Some of the most significant examples are morphine and related alkaloids from *Paper somniferum* (Odell et al., 2008), the sesquiterpenoid artemisinin against malaria from *Artemisia annua* (Covello, 2008) or the anticancer drugs vinblastine and vincristine from *Catharanthus roseus* (Heijden et al., 2004) and paclitaxel from the bark of *Taxus brevifolia* and other *Taxus*

species (Zhong, 2002). Well over 50,000 plant species are used for medicinal purposes (Gómez-Galera et al., 2007) while currently, over 60 % of anticancer drugs and 75 % of drugs for infectious disease are either natural products or analogues of natural products (Newman et al., 2003). The focus of the present study is on the anticancer drugs vinblastine, vincristine and paclitaxel.

## 1.3 Origin and effect of the herbal anticancer drugs vinblastine, vincristine and paclitaxel

*C. roseus*, also known as Madagascar periwinkle is a perennial herb belonging to the family Apocynaceae and produces about 130 different terpene indole alkaloids (TIAs) also referred to as vinca alkaloids (Heijden et al., 2004). Many of them are pharmaceutically active and used in the treatment of diseases. Ajmalicine and serpentine are used as anti-hypertensive and anti-neuro-inflammatory agents, yohimbine for treatment of erectile dysfunction and vindolicine for the development of antidiabetic therapeutics (Almagro et al., 2015). *C. roseus* is the sole source of the anticancer drugs vinblastine and vincristine (Edge et al., 2018) which were discovered as a result of a drug-screening program in the late 1950s (Heijden et al., 2004). Vinblastine and vincristine were the first natural drugs used in cancer therapy and are still among the most valuable agents in cancer treatment (Costa et al., 2008). While vinblastine is mainly used against testicular carcinoma, Hodgkin and non-Hodgkin lymphomas, breast cancer and germ cell tumors, vincristine is used for treatments of leukemia, rhabdomyosarcoma, neuroblastoma, Wilm's tumor, Hodgkin's disease and other lymphomas (Moudi et al., 2013).

*Taxus* belongs to the family Taxaceae. More than 14 *Taxus* species have been identified so far. Anticancer properties of paclitaxel were discovered in *T. brevifolia* extracts. It is mainly used for treatments of ovarian and breast cancer (Malik et al., 2011; He et al., 2018). Like *Catharanthus*, *Taxus* also produces a wide range of alkaloids. There are analogues of paclitaxel which have proven bioactivities or can be converted to derivatives with activity comparable to paclitaxel. One example among others is baccatin VI (Kingston et al., 1999; Küpeli et al., 2003).

Vinblastine, vincristine and paclitaxel are antimitotic drugs, which means their anticancer activity results from their interference with microtubules (MT), causing a disruption of mitosis by affecting the mitotic spindle. The exact mechanisms of how MT

serve as a target for antimitotic drugs has been summarized in detail by Jordan & Wilson (2004). MT are highly dynamic cytoskeletal fibers, that are composed of α-tubulin and β-tubulin heterodimers. Vinblastine and vincristine bind to the Vinca domain, paclitaxel to the taxane site of the β-tubuline subunit. MT-targeted antimitotic drugs are usually classified into two main groups: MT-destabilizing agents, inhibiting MT polymerization such as vinblastine and vincristine, and MT-stabilizing agents, stimulating MT polymerization like paclitaxel. This classification can lead to confusion, as the respective drugs show their stabilizing and destabilizing effects only at high concentration. Much more crucial than the change in MT-polymer mass is the suppression of MT dynamics (Slichenmyer & Hoff, 1990; Jordan & Wilson, 2004). This effect is especially dramatic during mitosis, where MT show much higher dynamics than in the interphase (Rusan et al., 2001), wich is important as the MTs of the spindle “find” the kinetochore of the chromatids in metaphase through exploration by alternating assembly and disassembly. Cells do not satisfy the spindle assembly checkpoint if the kinetochores are not attached to the spindle, which leads to delayed mitosis and finally apoptosis (Rieder & Maiato, 2004). Since tumor cells are characterized by particularly rapid cell division, the effect of antimitotic drugs is also stronger on tumor cells. Of course, healthy body cells are affected by the drugs as well, especially rapidly proliferating tissues such as bone marrow, oral and intestinal mucosa and hair follicles or cells using MT as key component such as neurons. This interference with healthy body cells leads to side effects like hair loss, hyponatremia, constipation, peripheral neuropathy and reversible myelosuppression (van der Valk et al., 1990; Jordan & Wilson, 2004; Nagappa et al., 2009).

## 1.4 Alkaloid biosynthetic pathways – the long way to desired products

Biosynthetic pathways of plant secondary metabolites are very complex, comprise several subsections, have many branching points and include numerous intermediates and enzymatic steps. Since several intermediate products and responsible enzymes in the paclitaxel and TIA biosynthetic pathways were subject of investigation in the present work, the relevant biosynthetic pathways are described in detail below.

### 1.4.1 Paclitaxel biosynthetic pathway

The paclitaxel biosynthetic pathway (figure 1.1) consists of 19 enzymatic steps. Twelve of the enzymes involved are known. The genes encoding them were sequenced and cloned. Seven enzymes are still unknown (Cusido et al., 2014). The biosynthesis of paclitaxel starts with the formation of geranylgeranyl pyrophosphate (also diphosphate) (GGPP), which is synthesized by the condensation of three isopentenyl pyrophosphate (IPP) units with dimethylallyl pyrophosphate (DMAPP) by geranylgeranyl pyrophosphate synthase (GGPPS) (Hefner et al., 1998; Malik et al., 2011). IPP and DMAPP can be produced by plants either via the mevalonic pathway (MVA) in the cytosol or the methylerythritol phosphate pathway (MEP) in the plastids. Although it is not completely clear which of the two pathways plays a role in the formation of paclitaxel, there is evidence that both are involved (Rodríguez-Concepción, 2006; Malik et al., 2011). Subsequent to GGPP production, a cyclisation catalyzed by taxadiene synthase leads to taxadiene (Wildung & Croteau, 1996). Taxadiene is then hydroxylated at the 5-position to produce taxadien-5α-ol by the cytochrome P450 (cP450) taxadien-5α-hydroxylase (T5αH) (Jennewein et al., 2004a; Howat et al., 2014). At this point, there is a branch in the metabolic pathway. Taxadien-5α-ol is converted to either taxadien-5α-13α-diol by the cP450 taxadien-13α-hydroxylase (TαH) (Jennewein et al., 2001) or to taxadien-5α-yl acetate by the enzyme taxadien-5α-ol-O-acetyl transferase (TDAT) (Walker et al., 1999), which is then further hydroxylated at the 10-position by cP450 dependent monooxygenase taxane 10β-hydroxylase (T10βH) to form taxadien 5α-acetoxy-10β-ol (Schoendorf et al., 2001). Whether and how the intermediates of these two branches are coupled later in the biosynthetic pathway remains unclear (Nims et al., 2006; Howat et al., 2014). The next step is a series of uncharacterized reactions where neither intermediates nor responsible enzymes are described. However, it is known, that these reactions include several hydroxylations at the C1, C2, C4 and C7 positions, oxidation of C9 and epoxidation at the C4C5 double bond (Malik et al., 2011). Four ester functionalities are also attached, namely benzonate at C2, acetate at C4 and C10 and N-benzoyl-3-phenylisoserinoyl at C13. These transformations produce the hypothetical precursor 2-debenzoyltaxane (Howat et al., 2014), which is converted to 10-deacetylbaccatin III via taxane 2α-O-benzoyltransferase (DBT) (Walker & Croteau, 2000b). 10-deacetylbaccatin III is further acetylated at the C10 position by 10-deacetylbaccatin III-10-O-acetyltransferase (DBAT) to form baccatin III (Walker & Croteau, 2000a). The C13 side chain is formed from the shikimate pathway derived α-phenylalanine, which is converted into β-phenylalanine by phenylalanine aminomutase

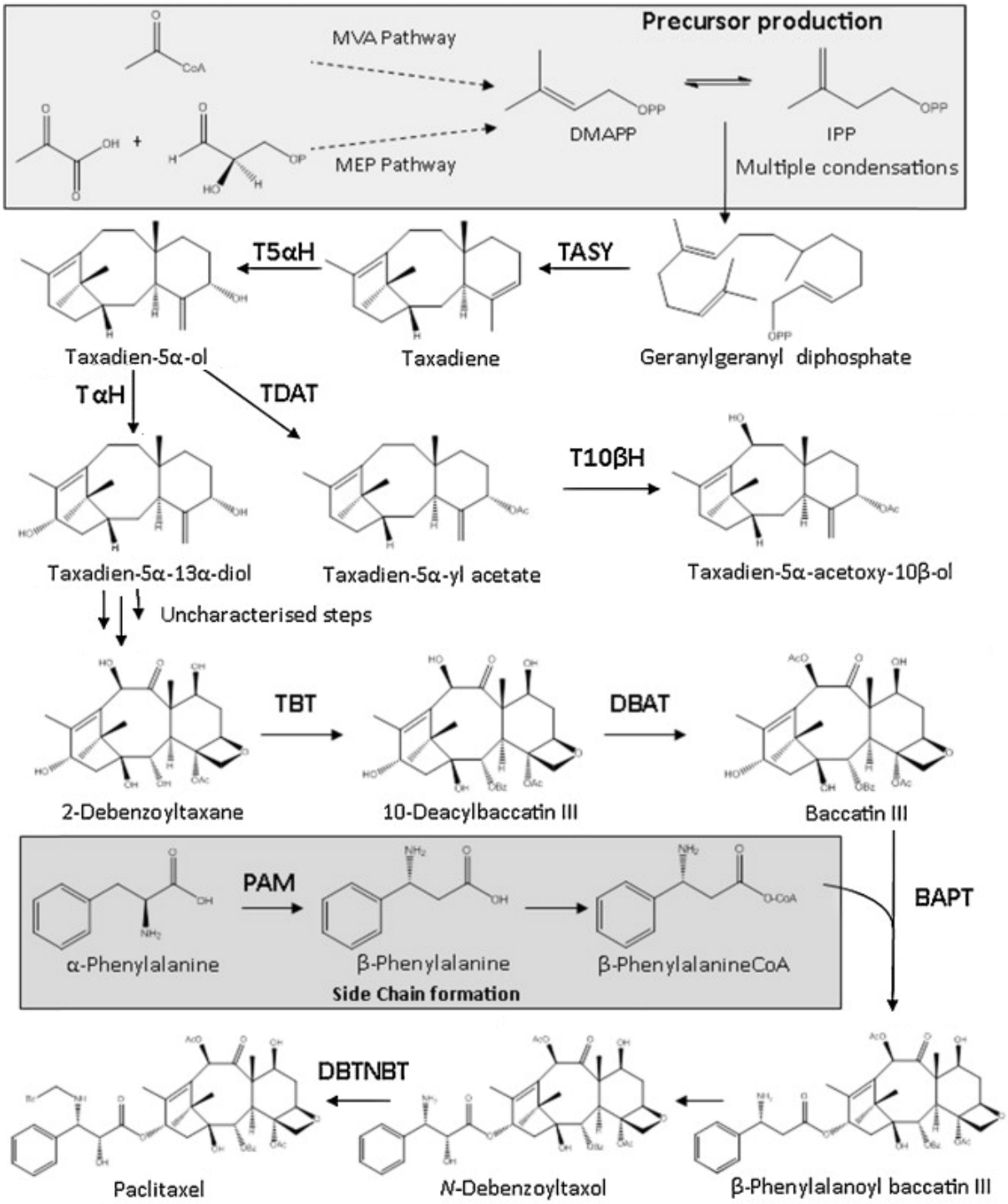


**Fig. 1.1: Biosynthetic pathway of paclitaxel**
Schematic representation of the paclitaxel biosynthetic pathway.
Abbreviations: MVA: mevalonic acid, MEP: 2-C-methyl-D-erythritol 4-phosphate, DMAPP: dimethylallyl pyrophosphate, IPP: isopentenyl pyrophosphate, TASY: taxadiene synthase, T5αH: taxadien-5α-hydroxylase, TαH: taxadien-13α-hydroxylase, TDAT: taxadien-5α-ol O-acetyltransferase, T10βH: taxoid-10β-hydroxylase, TBT: taxane 2α-O-benzoyltransferase, DBAT: 10-deacetylbaccatin III-10-*O*-acetyltransferase, PAM: phenylalanine aminomutase, BAPT: baccatin III-3-amino, 3-phenylpropanoyltransferase, DBTNBT: 3'-*N*-debenzoyl-2-deoxytaxol-*N*-benzoyltransferase
Adapted from (Roberts, 2007; Malik et al., 2011; Howat et al., 2014).

(PAM) (Jennewein et al., 2004b) and subsequently esterified by an unknown enzyme to produce β-phenylalanineCoA. The side chain is attached to the taxane core by the enzyme baccatin III-13-O-phenylpropanoyl transferase (BAPT) to produce 3‘-N-debenzoyl-2‘-deoxytaxol (Walker et al., 2002). By an unknown cP450-mediated hydroxylation of the side chain, the molecule is converted into 3‘-N-debenzoyltaxol (Lenka et al., 2015), which is converted in the final compound paclitaxel via 3‘-N-debenzoyl-2‘-deoxytaxol-N-benzoyl transferase (DBTNBT) (Nasiri et al., 2016).

### 1.4.2 Terpenoid indole alkaloid biosynthetic pathway in *Catharanthus roseus*

The biosynthetic pathway of terpenoid indole alkaloids (TIAs) in *C. roseus* is very complex (figure 1.2). Combining pathways of primary and secondary metabolism, more than 50 biosynthetic events are involved in biosynthesis of the final products vinblastine and vincristine, involving at least four different cell types, at least five different subcellular compartments and transport of pathway intermediates between these cell types and subcellular compartments (Le Zhao et al., 2013; Rai et al., 2013; Liu et al., 2016; Pan et al., 2016a).

The central intermediate in the biosynthesis of TIAs is strictosidine, which is formed by the condensation of tryptamine and secologanin. Tryptamine is derived from the indole pathway (indole moiety), while secologanin is derived from the seco-iridoid pathway (monoterpene moiety) (McKnight et al., 1990; Zhu et al., 2014).

#### MEP pathway

The MEP (2-C-methyl-D-erythritol-4-phosphate) pathway belongs to the primary metabolism and consists of seven steps starting with a condensation of pyruvate with D-glyceraldehyde-3-phosphate. The MEP pathway leads to the condensation of isopentenyl pyrophosphate (IPP) and dimethylallyl pyrophosphate (DMAPP) to geranyl pyrophosphate (GPP) (also geranyl diphosphate) catalyzed by geranyl pyrophosphate synthase (GPPS) (Oudin et al., 2007; Zhu et al., 2014).

## Seco-iridoid pathway

In the seco-iridoid pathway, also referred to as iridoid pathway (Zhu et al., 2014), terpenoid pathway (Zhu et al., 2015), monoterpenoid pathway (Simkin et al., 2013) or combinations of the aforementioned (Oudin et al., 2007), the terpene moiety of the TIAs is synthesized. In the first step GPP is hydrolysed to geraniol by the geraniol synthase (GES). Geraniol is subsequently hydroxylated to 10-hydroxygeraniol by geraniol 10-hydroxylase (G10H). Cytochrome P450 reductase, which transfers electrons from NADPH to G10H, is essential for this reaction (Meijer et al., 1993). In six subsequent steps 10-hydroxygeraniol is transformed to loganic acid, which is converted into loganin by the catalysis of loganic acid O-methyltransferase (LAMT). In the last step loganin is converted to secologanin by secologanin synthase (SLS), another cP450 enzyme. (Simkin et al., 2013; Miettinen et al., 2014)

## Shikimate and indole pathway

As autotrophic organisms, plants are able to synthesize the aromatic amino acids tyrosine, phenylalanine and tryptamine via the shikimate pathway. Phosphoenol pyruvate and erythrose 4-phosphate are converted to chorismate by a sequence of seven catalytic steps referred to as shikimate pathway (Bentley, 1990; Herrmann & Weaver, 1999). Chorismate is a major branch point to many end products including tryptophan (Roberts et al., 2002). Tryptophan is synthesized from chorismate in six enzymatically-controlled steps, the indole pathway. The first step is the formation of anthranilate by anthranilate synthase (AS). Tryptamine is derived from tryptophan by tryptophan decarboxylase (TDC) (Luca et al., 1989; Zhu et al., 2014). Both AS and TDC are considered a bottleneck in tryptamine synthesis (Noé et al., 1984; Li & Last, 1996).

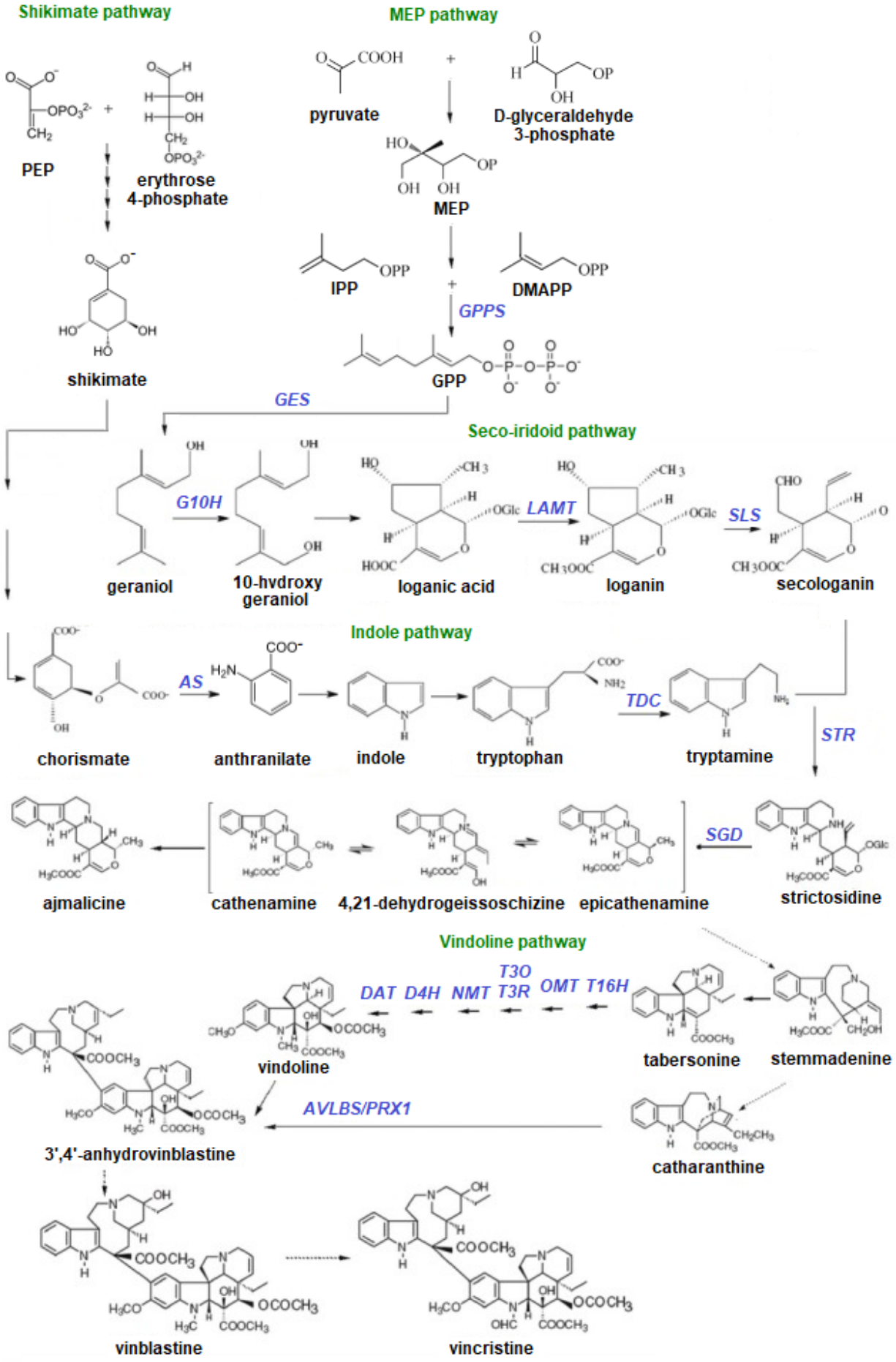
Shikimate pathway
MEP pathway
PEP
erythrose 4-phosphate
pyruvate
D-glyceraldehyde 3-phosphate
MEP
IPP
DMAPP
GPPS
GPP
shikimate
GES
Seco-iridoid pathway
G10H
LAMT
SLS
geraniol
10-hydroxy geraniol
loganic acid
loganin
secologanin
Indole pathway
AS
TDC
STR
chorismate
anthranilate
indole
tryptophan
tryptamine
SGD
ajmalicine
cathenamine
4,21-dehydrogeissoschizine
epicathenamine
strictosidine
Vindoline pathway
T3O
DAT D4H NMT T3R OMT T16H
vindoline
tabersonine
stemmadenine
AVLBS/PRX1
3',4'-anhydrovinblastine
catharanthine
vinblastine
vincristine

**Fig. 1.2: Biosynthetic pathway of terpenoid indole alkaloids in *C. roseus***
Overview of TIA biosynthesis under summary of the individual synthetic routes. Not all biosynthetic steps and the responsible enzymes are shown.
Abbreviations: Compounds: MEP: 2-C-methyl-D-erythritol-4-phosphate, PEP: phosphoenol pyruvate, IPP: isopentenyl pyrophosphate, DAMPP: dimethylallyl pyrophosphate, GPP: geranyl pyrophosphate; Enzymes: GPPS: geranyl pyrophosphate synthase, GES: geraniol synthase, G10H: geraniol 10-hydroxylase, LAMT: loganic acid methyl transferase, SLS: secologanin synthase, AS: anthranilate synthase, TDC: tryptophan decarboxylase, STR: strictosidine synthase, SGD: strictosidine β-D-glucosidase, T16H: tabersonine 16-hydrolxylase, OMT: 16-hydroxytabersonine-16-O-methyltransferase, T3O: tabersonine-3-oxygenase, T3R: tabersonine 3-reductase, NMT: N-methyltransferase, D4H: desacetoxyvindoline 4-hydroxylase, DAT: deacetylvindoline 4-O-acetyltransferase, AVLBS: α-3‘,4‘-anhydrovinblastine synthase, PRX1: peroxidase 1.
Modified according to (Zhu et al., 2014; Zhu et al., 2015).

## The enigmatic way to tabersonine and catharanthine

As described before, the two intermediates secologanin and tryptamine are fused in a condensation to strictosidine by the strictosidine synthase. While there is general agreement that the next step is catalyzed by strictosidine β-D-glucosidase (SGD), there are many different claims about the product of this step. Geerlings and his group mention cathenamine as product (Geerlings et al. 2000), whereas Zhu et al. (2014) name 4,21-dehydrogeissoschizine. Pan et al. (2015) mention tabersonine as product of SGD catalyzed reaction, while Liu et al. (2016) name strictosidine aglycoside. Thamm and his group write that the deglycosylation of strictosidine gives rise to a series of unstable intermediates for biosynthesis of different classes of MIAs (Thamm et al., 2016). There is agreement once again that this reaction is a crucial branching point for the formation of several classes of MIAs but the steps leading to these branches remain poorly characterized (Qu et al., 2018). However, these unstable intermediates lead to the formation of tabersonine and catharanthine, two important precursors in the biosynthesis of vinblastine and vincristine although nothing is known about the biochemical pathways involved in these conversions (Edge et al., 2018). There is evidence that the biosynthesis of catharanthine occurs via intermediates geissoschizine and stemmadenine (El-Sayed & Verpoorte, 2007).

## Vindoline pathway

Starting with tabersonine, the vindoline biosynthesis proceeds via seven enzymatic steps, which have all been described in the meantime, the last two only recently (figure 1.3). In a first step, tabersonine is hydroxylated by tabersonine 16-hydrolxylase (T16H) (Besseau et al., 2013), to 16-hydroxytabersonine, which is then methylated by

16-hydroxytabersonine-16-O-methyltransferase (OMT) (Levac et al., 2008) resulting in the intermediate 16-methoxytabersonine. The next step is catalysed by two enzymes: tabersonine-3-oxygenase (T3O) a cP450, which has oxidative and tabersonine 3-reductase (T3R), which has reductive properties, which leads to the formation of 16-methoxy-2,3-dihydro-3-hydroxytabersonine (Kellner et al., 2015; Qu et al., 2015). The subsequent methylation by N-methyltransferase (NMT) leads to the formation of desacetoxyvindoline (Liscombe et al., 2010), which is then hydroxylated by the desacetoxyvindoline 4-hydroxylase (D4H) to form deacetylvindoline (Vazquez-Flota et al., 1997), which is then acetylated by deacetylvindoline 4-O-acetyltransferase (DAT) to finally receive vindoline (St-Pierre et al., 1998). However, vindoline is not the only product of this biosynthetic pathway. In absence of T3R, T3O can also convert tabersonine or 16-methoxytabersonine to 2,3-epoxides. It is also involved in the synthesis of the shunt product vindorosine, which is assembled in five enzymatic reactions (figure 1.3) (Kellner et al., 2015; Qu et al., 2015; Edge et al., 2018).

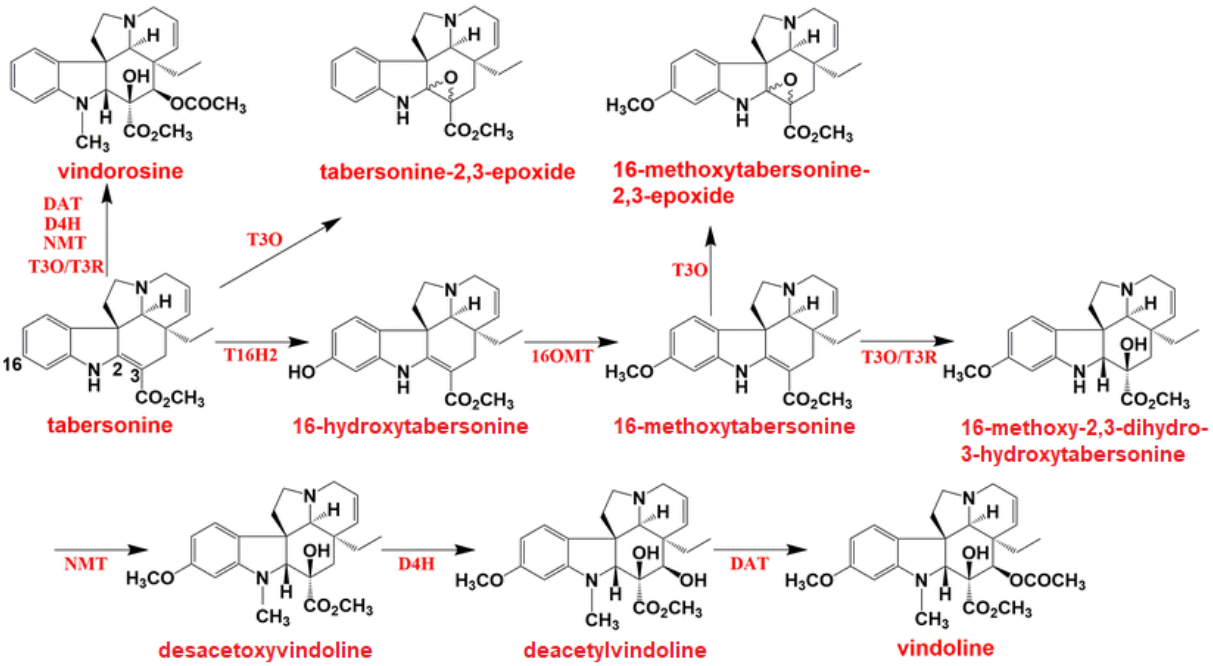


**Fig. 1.3: Vindoline pathway**
Detailed overview of the vindoline biosynthetic pathway with all intermediates, the corresponding enzymes and the shunt products.
Abbreviations: T16H: tabersonine 16-hydrolxylase, OMT: 16-hydroxytabersonine-16-O-methyltransferase, T3O: tabersonine-3-oxygenase, T3R: tabersonine 3-reductase, NMT: N-methyltransferase, D4H: desacetoxyvindoline 4-hydroxylase, DAT: deacetylvindoline 4-O-acetyltransferase. Modified according to (Edge et al., 2018).

### Biosynthesis of vinblastine and vincristine

The bisindole alkaloids vinblastine and vincristine are derived from the coupling of catharanthine and vindoline by the class III peroxidase α-3‘,4‘-anhydrovinblastine synthase (PRX1/AVLBS), forming α-3‘,4‘-anhydrovinblastine (Sottomayor et al., 1998; Costa et al., 2008). Anhydrovinblastine is then further converted to vinblastine, which is ultimately transformed into vincristine. The enzymatic steps that catalyze these last two reactions are still unknown.

## 1.4.3 Spatial organization of TIA biosynthesis

As already mentioned, TIA biosynthesis in *C. roseus* involves various cell types and intracellular compartments, resulting in a complex spatial organization of the involved synthetic pathways.

There are three modes of transport that have been reported for alkaloids in plants: inter-organ, inter-cellular and intracellular (Shitan & Yazaki, 2007; Liu et al., 2016). The place of synthesis is not always the site of action of alkaloids, which means that translocation over long distances is sometimes necessary (Yazaki, 2006). A well-known example of this would be nicotine, which is synthesized in the roots and subsequently transported to leaves and other aerial parts of the plants via the xylem (Hashimoto & Yamada, 1994). Inter-organ transport is also present in *C. roseus*, as some TIAs like vindoline and catharanthine are mainly produced in young leaves and stems, whereas synthesis of other TIAs such as ajmalicine and serpentine, which are using the same precursors, mainly occurs in roots (Blom et al., 1991).

Regarding the inter-cellular transport (figure 1.4), studies have revealed that in *C. roseus* TIA biosynthesis in aerial organs occurs in four cell types: internal phloem-associated parenchyma (IPAP), epidermal cells, laticifers and idioblasts (Burlat et al., 2004; Verma et al., 2012). The IPAP cells are found in the periphery of the pith in stems (Mahroug et al., 2007). The MEP pathway as well as the major part of the seco-iridoid pathway up to loganic acid, take place in the IPAP cells. Up to geraniol, the biosynthesis is located in the stroma of the IPAP chloroplasts, which then moves into the IPAP cytosol (Burlat et al., 2004; Mahroug et al., 2007; Oudin et al., 2007; Miettinen et al., 2014), where geraniol is hydroxylated by the ER-associated G10H (Guirimand et al., 2009). Loganic acid methyl-transferase (LAMT) and cP450 secologanin synthase (SLS), which also proved to be ER-associated (Guirimand et al., 2011a) are preferentially expressed

in the cytosol of leaf epidermis. Loganic acid is assumed to move from IPAP cells to epidermis to be converted into secologanin by LAMT and SLS (Irmler et al., 2000; Murata et al., 2008; Asada et al., 2013; Salim et al., 2013; Salim et al., 2014).

The enzymes that catalyze the reactions of the shikimate pathway were already localized in chloroplasts in the 1980s (d'Amato et al., 1984; Fiedler & Schultz, 1985; Mousdale & Coggins, 1985). Same is true for chorismate synthase and anthranilate synthase (AS) (Mousdale & Coggins, 1986). Tryptophan decarboxylase (TDC) was found in the cytosol, whereas strictosidine synthase (STR) was active in the vacuole. This suggests that tryptophan is converted in the cytosol by the TDC to tryptamine, which is then transported into the vacuole where it is condensed with secologanin to form strictosidine by STR, which passes the tonoplast (Stevens et al., 1993) to reach the strictosidine β-D-glucosidase (SGD) in the nucleus (Guirimand et al., 2010).

Catharanthine is formed in the epidermis and secreted to the wax exudates at the surface of leaves by the ATP binding cassette (ABC) transporter CrTPT2 (Yu & Luca, 2013). The first four steps of the vindoline synthesis also take place in the epidermis cells (Murata & Luca, 2005; Levac et al., 2008). T16H, the first enzyme in the vindoline pathway is an ER-anchored cP450 (Guirimand et al., 2011b) and the only enzyme in the TIA pathway, which is encoded by two different genes. They are referred to as T16H1 and T16H2. T16H1 was detected mainly in undifferentiated cells and flowers, while T16H2 was found mainly in the epidermis of young leaves, which is the site of vindoline synthesis. Silencing of T16H2 suppressed the accumulation of vindoline (Besseau et al., 2013). The fourth step of vindoline biosynthesis, the methylation by the NMT, is localized in epidermal chloroplasts (Luca & Cutler, 1987). The vindoline biosynthesis is completed by transport of desacetoxyvindoline from the epidermis into the laticifer cells and idioblast cells of stem, flowers and leaves (St-Pierre et al., 1999; Qu et al., 2015), where the last two biosynthetic steps catalyzed by DAT and D4H take place. Vindoline is transported into the vacuole by a specific proton antiporter. Same is true for catharanthine in epidermis cells (Carqueijeiro et al., 2013). Vindoline and catharanthine are fused to α-3‘,4‘-anhydrovinblastine by the vacuolar class III peroxidase α-3‘,4‘-anhydrovinblastine synthase (PRX1/AVLBS) (Costa et al., 2008). As vindoline and catharanthine are not in the vacuole of the same cell type, stimulation from external environment has to break down the spatial separation. Vinblastine and vincristine also accumulate in the vacuoles (Liu et al., 2016).

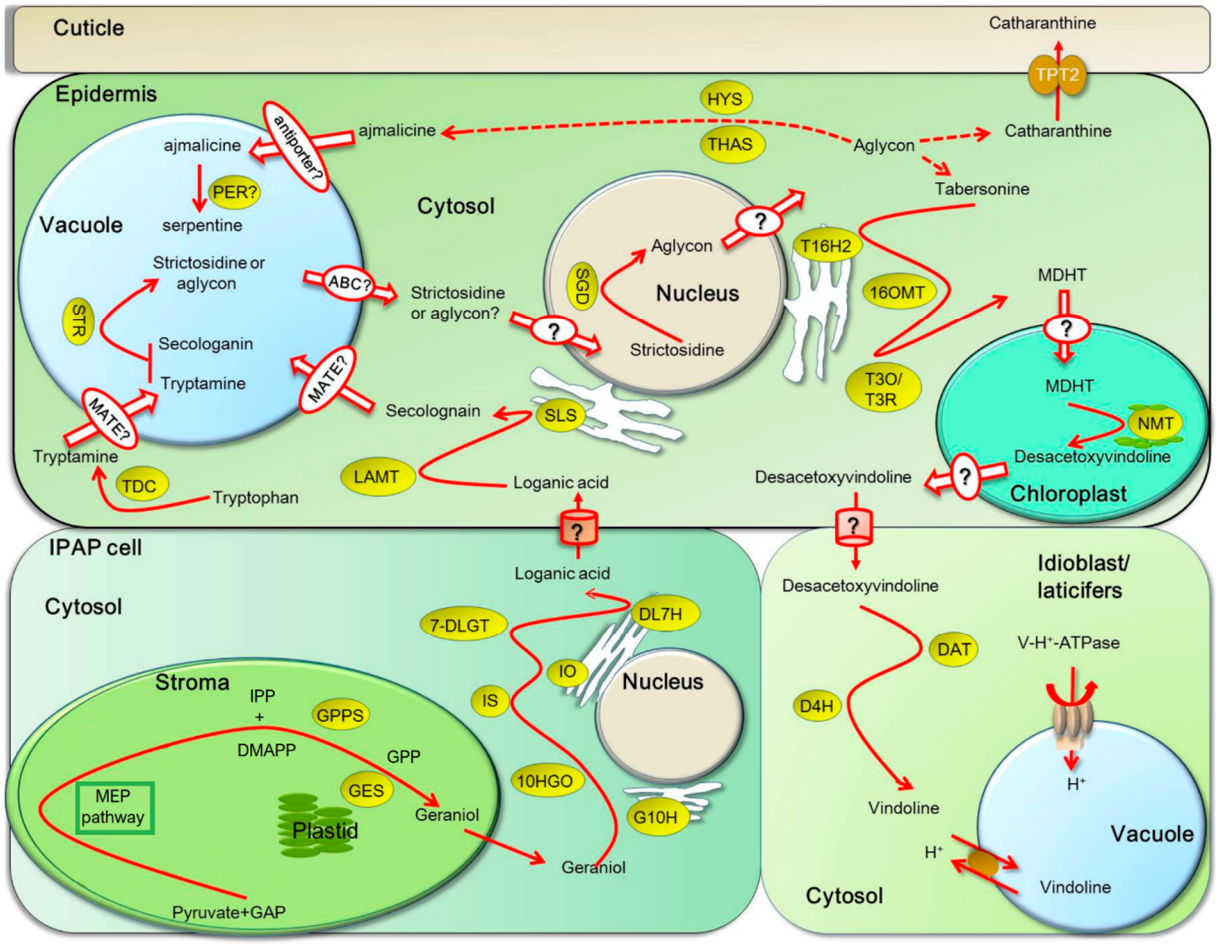


**Fig. 1.4: Spatial organization of TIA biosynthesis**
Overview of the 4 different cell types and their subcellular compartments involved in TIA biosynthesis.
Abbreviations: Compounds: GAP: D-glyceraldehyde 3-phosphate, MEP: 2-C-methyl-D-erythritol 4-phosphate, IPP: isopentenyl pyrophosphate, DMAPP: dimethylallyl pyrophosphate, GPP: geranyl pyrophosphate, MDHT: 16-methoxy-2,3-dihydro-3-hydroxytabersonine
Enzymes: GPPS: geranyl pyrophosphate synthase, GES: geraniol synthase, G10H: geraniol 10-hydroxylase, 10HGO: 10-hydroxygeraniol dehydrogenase, IS: iridoid synthase, IO: iridoid oxidase, 7-DLGT: 7-deoxyloganetic acid glucosyltransferase, DL7H: 7-deoxyloganic acid hydroxylase, LMAT: loganic acid methyltransferase, SLS: secologanin synthase, TDC: tryptophan decarboxylase, STR: strictosidine synthase, PER: putative peroxidase, SGD: strictosidine -βD-glucosidase, HYS: heteroyohimbine synthase, THAS: tetrahydroalstonine synthase, T16H2: tabersonine 16-hydroxylase, 16OMT: 16-hydroxytabersonine-16-O-methyltransferase, T3O/T3R: tabersonine 3-oxygenase/tabersonine 3-reductase, NMT: N-methyltransferase, D4H: desacetoxyvindoline 4-hydroxylase, DAT: deacetylvindoline 4-O-acetyltransferase
IPAP: internal phloem-associated parenchyma
Modified according to (Liu et al., 2016).

## 1.5 Alternative ways of production and their limitations

The main problem of extracting anticancer alkaloids from the natural sources is the low concentration of these compounds in the plant tissue. In case of *Taxus* 10,000 kg of bark are required to obtain 1 kg of paclitaxel (Vidensek et al., 1990). Therefore, 3 to 12 trees are required to treat one ovarian-cancer patient (Joyce, 1993). Another problem is the very slow growth of the trees (Vidensek et al., 1990) and the fact that the production of paclitaxel in plants is subject to seasonal fluctuations in which temperature and light play a role (Nasiri et al., 2016). In addition, extraction from the tree requires a complex system and specific purification techniques using advanced and expensive technology (Malik et al., 2011). Isolating commercial quantities of paclitaxel from original sources has proven to be unsustainable and dangerous to the environment with respect to species extinction and habitat destruction of wildlife animals. Overharvesting has already caused serious damage to wild resources of *Taxus wallichiana* (Lin et al., 2018). In the case of *Catharanthus*, values between 0.001 % (O'Keefe et al., 1997) and 0.0002 % (Miettinen et al., 2014) are given for the concentration of vinblastine and vincristine in the plant tissue. Therefore, at least 100,000 kg of plant material are needed to extract 1 kg of the desired compound. Production of vinblastine and vincristine from plants is problematic, as increasing demand is faced with growing prices (Hill & Barber, 2017). Alternatives to extraction from plant material are therefore urgently needed. Production of paclitaxel by total synthesis is possible in principle (Nicolaou et al., 1994) but commercially not viable because of the complex structure of paclitaxel and the large number of steps required (Cusido et al., 2014; Lin et al., 2018). Generally, a synthetic route for a complex molecule becomes impractial if the total process requires more than 10 separate steps, since overall yield decreases, while waste and resources increase with each step (Chemler & Koffas, 2008). Therefore, full synthesis is also not suitable for vinblastine and vincristine. Consequently, strategies for semi-synthesis are sought. Due to the complicated structure of taxol, this requires protecting group manipulations to ensure chemoselectivity, making the procedure laborious and hardly practical (Lin et al., 2018). Thornburg et al. (2017) recently managed to overcome the need of protecting group manipulation by biocatalysis of a paclitaxel analogue from the precursor baccatin III. Although this method has potential, it is still far from being economically viable. Another possibility to overcome slow growth rates, fastidious nutrient requirements and low production titers is the production of the desired compound in a well-characterized heterologous host, which is simple to culture (Zhang et al., 2011). This method has

already been used successfully to produce the paclitaxel precursor taxadiene in tomato by re-routing the GGPP which is normally utilised for making carotenoids (Kovacs et al., 2007) or in *Arabidopsis thaliana* by constitutive production of recombinant TASY (Besumbes et al., 2004). Qu et al. (2015) engineered the complete seven-gene vindoline pathway in yeast to produce vindoline from tabersonine. Brown et al. (2015) managed de novo production of strictosidine in yeast by introducing 21 genes and three gene deletions into the yeast genome. Despite these successes, the heterologous production of plant secondary metabolites is anything but simple. Gene expression and cellular environment of native and heterologous host should fit and also the heterologous host's native metabolism has to be concerned, to avoid crosstalk between pathway of interest and those of the heterologous host. The accumulating, desired product could also be toxic to the heterologous host (Zhang et al., 2011). Transgenics in plants are also a powerful tool for alternative strategies for the production of secondary plant metabolites. Only recently, an overexpression of *CrTDC* and *CrSTR* resulted in fivefold increased vinblastine production in *C. roseus* plants (Sharma et al., 2018). Nevertheless, in this approach, the gaps in knowledge about individual biosynthesis steps and the wide range of transcription factors involved cause difficulties. Moreover, the use of transgenic organisms is an economically and politically sensitive topic. A promising platform for bioproduction of desired compounds are plant tissue, organ and cell cultures. While the cultivation in an industrial system is the major obstacle to the commercial exploitation of tissue and organ cultures, such as hairy roots, plant cell cultures incorporate many advantages of the aforementioned approaches. They are not subject to seasonal changes, show rapid growth, are biosynthetically totipotent, which means that each cell in culture retains complete genetic information and hence is able to produce the range of chemicals found in the parent plant, they usually have mechanisms against self-poisoning, like storage of harmful compounds in the vacuole, upscaling to industrial levels is possible and plant cell cultures are still open for transgenics. (Ramachandra Rao & Ravishankar, 2002; Yue et al., 2016). Also, plant cell cultures provide many options for modifications by altering nutritions or by elicitation. For this reason plant cell cultures are subject of this study.

## 1.6 Plant cell cultures and elicitation

Plant cell cultures can be created from any plant through isolation of plant tissue. Explants are sterilized chemically and plated on solid growth medium containing the growth hormones and nutrients necessary for the species. With correct medium composition, explants proliferate into a callus of undifferentiated cells, which can be transferred to liquid medium to create suspension cultures (Hall, 2000; Wilson & Roberts, 2012).

Plant cell cultures are a well-established technology platform for the synthesis of natural products, which provides several advantages, especially for production of compounds with complex structures. Recent progress enabled serially assembly of bioreactors and successful scale-up from experimental platforms to commercially feasible industrial scale processes (Tekoah et al., 2015; Ochoa-Villarreal et al., 2016).

Although not even the entire biosynthetic pathway of paclitaxel has been explored, bioreactors of up to 75,000 liters are currently being employed for the commercial production of paclitaxel from cell cultures by several companies, including Phyton Biotech (Malik et al., 2011).

Since the secondary metabolites protect plants from environmental changes, their production in cell cultures in vitro is very low. Elicitation is the induction of secondary metabolite production by treatments with so called elicitors. Most secondary metabolites are associated with pathogen defense or wound response. The use of elicitors is generally intended to mimic these responses in plants by simulating pathogen attack or herbivores (Zhong, 2002; Smetanska, 2008). According to their origin, elicitors can be divided into two different types: biotic and abiotic. Biotic elicitors are substances of biological origin, like plant hormones, bacteria and fungi-derived peptides and proteins or oligosaccharins. Abiotic elicitors can be considered as substances of non-biological origin, being predominantly inorganic compounds such as salts or physical factors (Ramirez-Estrada et al., 2016). Especially methyl jasmonate (MeJA), which plays an important role in defense and plant communication (Farmer & Ryan, 1990), has been shown to be an effective elicitor and has been widely used in the production of plant secondary metabolites as summarized by Naik & Al-Khayri (2016).

Using elicitors, considerable progress has already been achieved in the production of plant secondary metabolites in plant cell cultures. Already in 1999 Laskaris et al. showed for the first time that an enzyme in the paclitaxel biosynthetic pathway (GGPPS)

was inducible by elicitation with MeJA, which also caused a taxene accumulation in the cells of the treated *Taxus baccata* suspension culture. Ramirez-Estrada et al. (2015) showed that taxene production was significantly enhanced in two different *Taxus* cell cultures by simultaneous addition of cyclodextrin and coronatine. Geerlings et al. (2000) observed an MeJA induced expression of *sgd* in *C. roseus* and van der Fits (2000) additionally found MeJA induced expression of *g10h*, *tdc* and *d4h*. Guo et al. (2013) managed to produce vinblastine in plant cell cultures in levels well above those in plants by using a mix of various elicitors and blocking the branches in the biosynthetic pathway leading to shunt products. Ramani & Jayabaskaran (2008) could increase the production of catharanthine and vindoline by UV-light.

Despite these successes, the possibilities of producing secondary metabolites in plant cell cultures have remained limited. The breakthrough in industrial-scale production of vincristine and vinblastine, despite all efforts, has not been achieved so far. One reason for this limitation is the fact that the metabolic activity in the plant is partitioned to different cell types, while plant cell fermentation in cell cultures is based on just one type of cells and therefore can not provide the interaction of different cell types required for the maturation of the metabolites (Rajabi et al., 2017). A promising approach to overcome this limitation are microfluidic systems.

## 1.7 Microfluidics

Microfluidics is the science and technology of systems that process or manipulate small amounts of fluids. It offers fundamentally new capabilities in the control of concentrations of molecules in space and time (Whitesides, 2006). Vereshchagina et al. (2013) used a novel microfluidic chip system for the screening of the antitumor chemotoxic agent mitomycin C on the HL60 myeloid leukemia cell line, taking advantage of the tight time control of the reagent exposure which is provided by the cell assay platform they used. Runge et al. (2017) used a polycarbonate-based microfluidic device for cell growth experiments and to monitor induced eGFP expression in *Saccharomyces cerevisiae* in real time.

In the context of the present work, there was a cooperation with the Institute of Microstructure Technology (IMT) from the KIT, which fabricated a microfluidic chip with a two chamber system and modular design (figure 1.5). This microfluidic chip was used in several approaches in this work and the modular design allowed to link cells with different properties in a constant medium flow.

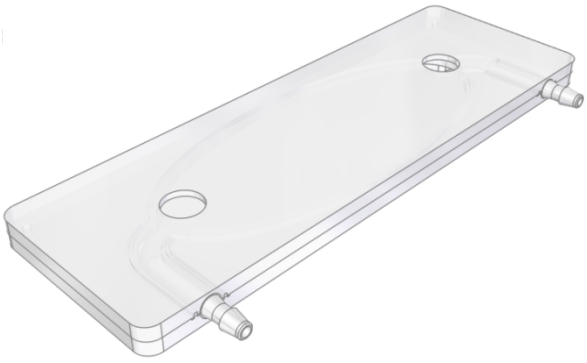

**Fig. 1.5: Model of a microfluidic chip**
Microfluidic chip with two chamber system and modular design, manufactured by IMT. Courtesy of Tim Finkbeiner (IMT)

## 1.8 Scope

In the context of this study, there was a cooperation with the company Phyton Biotech GmbH, which successfully produces paclitaxel in plant cell cultures on industrial scale. In addition to their expertise, Phyton Biotech provided the *Taxus* and *Catharanthus* cell cultures that were subject of this dissertation. Microscopic examination of the *Taxus* cell culture showed two different phenotypes among the cells (figure 2.1). A normal phenotype, displaying nucleus and cytoplasmic strands, and a bright and highly vacuolated phenotype referred to as shiny cells. In this study two major questions concerning the shiny cells should be clarified:

- Can shiny cells function as cellular predictors for paclitaxel?
- What is the mechanism of formation of shiny cells?

The two *Catharanthus* cell lines provided, showed obvious macroscopic and microscopic differences (figure 2.2). The size of the cells and cell aggregates was different, as was the structure of the cell material after removal of the medium. The two most important questions regarding the *Catharanthus* cell lines were:

- Do the cell lines Cath 001 and Cath 004 have different potential for the production of alkaloids and how is this potential reflected in phenotype, genexpression and metabolic profile?
- Can the production of alkaloids be stimulated by elicitor treatments in the two cell lines?

The microfluidic bioreactor, designed in collaboration with and manufactured by IMT, might overcome the problem that biosynthesis of important secondary metabolites in plants requires different cell types that are not present in plant cell cultures. In order to test if the system is suitable for cell fermentation application and whether it is in principle possible to technically simulate a plant tissue by means of modular chip approaches, two important questions were addressed in this study:

- Is miniaturization of cell fermentation to chip scale possible?
- Is there communication between the cells in modular chip setups?

# 2 Materials and Methods

## 2.1 Cell cultures and subcultivation

Four different cell cultures were used for experimental studies in the present work. Phyton Biotech GmbH (Ahrensburg, Germany) provided liquid cell cultures of two different cell lines of *Catharanthus roseus* (L.) G. Don, Cath 001 and Cath 004, as well as liquid growth phase cell cultures of *Taxus chinensis* (Pilg.) Rehder. The tobacco cell culture BY-2 (*Nicotiana tabacum* L. cv. Bright Yellow 2, Nagata et al., 1992) was previously used as a model organism in the BOT I.

The *Taxus* cells form aggregates in liquid cultures that range from a few to several hundred cells. Most of the cells display normal phenotype in the bright field with visible nucleus and cytoplasmic strands, whereas a few cells appear bright and highly vacuolated without displaying any expected structures. This kind of cells was referred to as shiny cells. Shiny and non shiny cells can appear within the same aggregate (figure 2.1).


**Fig. 2.1: Bright field image of *Taxus* cell aggregates containing shiny and non shiny cells**
Highly vacuolated shiny cells are present in small numbers in the same aggregates as non shiny cells. (Scale bar represents 100 µm.)

The two *Catharanthus* cell cultures also form cell aggregates, which are smaller on average compared to *Taxus*. The cells and aggregates of Cath 001 (figure 2.2 A) are smaller than those of Cath 004 (figure 2.2 B). The cell material of Cath 001 is characterized by a smooth fine structure, while Cath 004 is granular and coagulative.

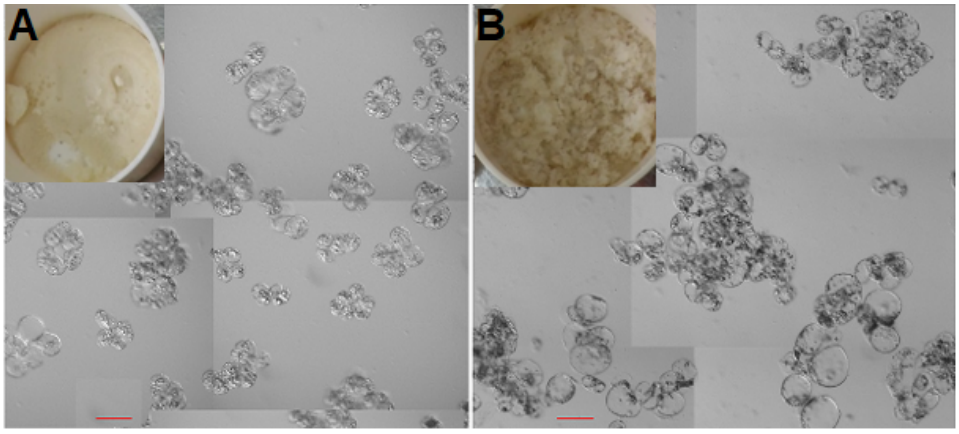


**Fig. 2.2: Cell material and microscopic images of cell aggregates of Cath 001 and Cath 004**
A: Cell aggregates and cell material (upper left corner) of Cath 001. Aggregates show smaller and fewer cells, structure of yellowish white cell material is uniform and smooth.
B: Cell aggregates and cell material (upper left corner) of Cath 004. Aggregates show larger and more cells, structure of slightly darker cell material is grainy.
(Scale bars represent 100 µm.)

The cells of BY-2 grow in simple files that comprise up to about 8 cells. Compared to *Taxus* and *Catharanthus* cells they are more elongated (figure 2.3).

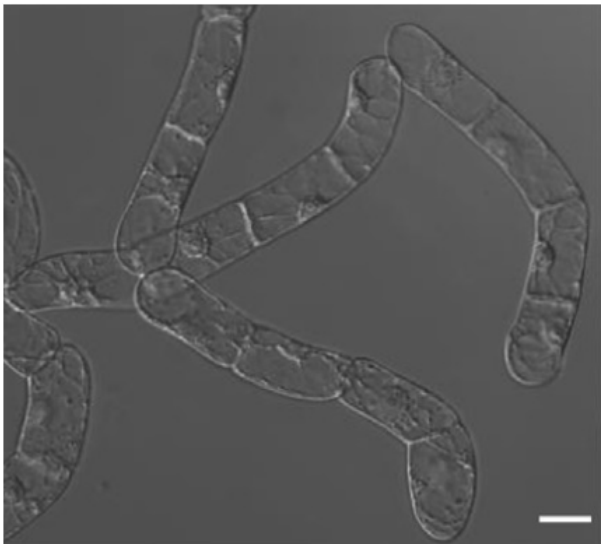

**Fig. 2.3: Cell files of BY-2 wild type**
Short files of elongated BY-2 cells in liquid cell culture.
(Scale bar represents 20 µm.)
Adapted from Durst et al., 2013.

The suspension cell cultures of *Catharanthus* and *Taxus* were subcultivated weekly, by adding 3 g (*Catharanthus*) and 1.5 g (*Taxus*) of cells to 50 ml of fresh Gamborg B5 medium (Duchefa, Haarlem, The Netherlands), respectively (Table 2.1). The cells were incubated at 26 °C (*Catharanthus*) and 23 °C (*Taxus*), respectively, under constant shaking (120 rpm) on a Unimax 2010 platform shaker (Heidolph Instruments GmbH & Co. KG, Schwabach, Germany) in 250 ml polycarbonate Erlenmeyer flasks with filter caps (Corning GmbH, Kaiserslautern, Germany). Unless stated otherwise all

experiments were performed using 125 ml polycarbonate Erlenmeyer flasks with filter caps, containing 25 ml of medium and 1.5 g (*Catharanthus*) and 0.75 g (*Taxus*) of cells, respectively.

BY-2 suspension cell cultures were subcultivated weekly, inoculating 1.0-1.5 ml of cells into 30 ml of fresh MS (Murashige and Skoog) medium (Duchefa, Haarlem, The Netherlands). The cells were incubated at 26 °C under constant shaking (150 rpm) on a KS260 basic orbital shaker (IKA Labortechnik, Staufen, Germany) in 100 ml Erlenmeyer flasks (Table 2.1).

For particular experiments Phyton Biotech GmbH provided production phase cultures of *Taxus*, producing considerable amounts of paclitaxel which were not prepared or subcultivated at the KIT. Few attempts were made on bioreactor samples. For reasons of security and confidentiality these experiments were conducted in the lab of Phyton Biotech.

**Table 2.1: Composition of medium and parameters of cultivation for *Catharanthus*, *Taxus* and BY-2 suspension cultures**

| | *Catharanthus* | *Taxus* | BY-2 |
|---|---|---|---|
| **medium** | Gamborg B5 medium 3.21 g/l<br>sucrose 30 g/l<br>2,4-D 1.1 mg/l | Gamborg B5 medium 3.21 g/l<br>maltose 10 g/l<br>picloram 2.42 mg/l<br>TDZ 0.022 mg/l | MS salts 4.3 g/l<br>sucrose 30 g/l<br>$KH_2PO_4$ 200 mg/l<br>inositol 100 mg/l<br>thiamine 1 mg/l<br>2,4-D 0.2 mg/l |
| **inoculum** | 3 g | 1.5 g | 1.5-2 ml |
| **volume** | 50 ml | 50 ml | 30 ml |
| **flask** | 250 ml polycarbonate, filter cap | 250 ml polycarbonate, filter cap | 100 ml glass |
| **temperature** | 26 °C | 23° C | 26 °C |
| **speed** | 120 rpm | 120 rpm | 150 rpm |
| **pH** | pH 5.6 | pH 5.6 | pH 5.8 |

## 2.2 Phenotyping of *Catharanthus* and *Taxus* cell lines

To analyze the phenotype of *Catharanthus roseus* and *Taxus chinensis* cells used in this study, different parameters about cell morphology and cell growth as well as subcellular compartments were investigated. Since the *Taxus* and Cath 004 cells form very large aggregates, for some experiments the cultures were previously treated with a driselase (Sigma-Aldrich, Munich, Germany) solution. A treatment with 0.25 % driselase for 20 minutes showed the best results.

### 2.2.1 Determination of growth index 7

In context of the weekly subcultivation the increase of fresh weight of the cells was determined over 5 months between March and July 2018. Growth index 7 is calculated by the amount of fresh weight at day 7 of the cell cycle divided by the amount of inoculum.

### 2.2.2 Cell size, volume and aspect ratio

For cell size measurements microscopic images were captured using an AxioImager Z.1 microscope (Zeiss, Jena, Germany). The MosaiX-module sampling system (Zeiss, Jena, Germany) was used to record a large number of cells at once, covering an area of approximately 2.5 $mm^2$ consisting of 25 individual images. Cell length and width were measured from the central section of the cell using the AxioVision software (Rel. 4.8.2) (Zeiss, Jena, Germany) according to Maisch and Nick (2007). For studies conducted over several days, cells were taken from the same flask to prevent distortions of the results.

Based on the values measured for the cell size, the volume and aspect ratio of the cells were also calculated. The aspect ratio allows conclusions about the cell shape. A relationship between cell shape and alkaloid production has already been demonstrated (Kim et al., 1994) and a connection between volume and alkaloid production is at least not excluded, since the vacuole, where metabolic products are often stored, accounts for the largest part of the cell volume (Marty, 1999).

To calculate the aspect ratio, the value for the breadth of the cell was divided by the value for the length. This way, all values are between 0 and 1, with a value near 1 indicating an increasingly round shape, while decreasing values indicate an elongation of the cell.

The calculation of the cell volume was based on the assumption that the cell shape corresponds approximately to that of a cylinder (Sakano et al., 1995). The formula used is therefore the one used to calculate the volume of a cylinder.

$$V = \pi \times \left(\frac{d}{2}\right)^2 \times h$$

The value measured for cell breadth was used as diameter d, the value of the cell length as height h.

### 2.2.3 Cell number and cell cycle

The cell density was estimated by a hemocytometer (Fuchs-Rosenthal) under bright field illumination to determine the number of cells in suspension and the average length of the cell cycle. The latter was implemented using an exponential model for proliferation ($N_t = N_0 \times e^{kt}$ with $N_t$ = cell density at time point t, $N_0$ = cell density at inoculation, e = Euler constant, and k = time constant).

### 2.2.4 Packed cell volume (PCV)

Growth of the *Catharanthus* and *Taxus* cell cultures was approximated by measuring the packed cell volume as described by Jovanović et al. (2010) for BY-2 cell cultures. For calculation of the PCV one 125 ml Erlenmeyer flask was set up for every measurement, containing 25 ml of medium and 1.5 g (*Catharanthus*) or 0.75 g (*Taxus*) of cells, respectively. At the appropriate time the cell suspension was mixed properly by vigorous shaking and 10 ml were poured directly in two 15 ml falcons (Carl Roth, Karlsruhe, Germany), respectively. The falcons were kept in an upright position in the fridge for three days to allow the cells to settle down. Afterwards the PCV was ascertained using the scale of the falcon and calculated in percent. (A PCV of e.g. 20 % means that the settled cells reached the 2 ml mark of the falcon.)

### 2.2.5 Determination of fresh weight/dry weight

The setup for the fresh and dry weight determination corresponds to the PCV experiment (2.2.4). To provide the fresh weight, the medium was removed from the cell suspension by vacuum filtration (Vacuum pump ME 4 NT, Vacuubrand GmbH & Co KG, Wertheim, Germany). The remaining cell material was kept in a hot air oven at 60 °C for three days to provide the dry weight of the cells.

### 2.2.6 Viability

To quantify the amount of viable cells in the suspension culture 0.1 % of a 5 mg/ml fluorescein diacetate (FDA; Merck Chemicals GmbH, Darmstadt, Germany) stock solution was used to stain the living cells according to Widholm (1972).
If the non-fluorescent FDA enters a living cell, lipases, esterases and proteases cleave the fluorescein, which then fluoresces green. For dead cells in which no enzyme activity is present, no signal can be detected. The stained cells were examined by an AxioImager Z.1 microscope (Zeiss, Jena, Germany), using the filter set 38 HE (excitation: 470 nm, beamsplitter: 495 nm and emission: 525 nm, Zeiss).

### 2.2.7 Sugar consumption

The sugar consumption of *Catharanthus* and *Taxus* cells was calculated by means of the sugar concentration which was measured over time by a portable brix refractometer. The refractive index of the sample medium is measured via the light deflection, which changes depending on the sugar concentration. 20 µl of vacuum filtered supernatant were applied and the brix values documented.

### 2.2.8 Transient transformation for visualization of subcellular compartments

Transient transformation by particle bombardment was implemented to visualize subcellular compartments of *Catharanthus* and *Taxus* cells for further investigation and comparison of cell traits. Three day old cells were used for transformation, following the method described by Guirimand et al. (2009). Transformed cells were examined after 24 h of incubation time under an AxioImager Z.1 microscope (Zeiss, Jena, Germany) equipped with an ApoTome microscope slider for optical sectioning and a cooled digital CCD camera (AxioCam MRm; Zeiss). YFP and GFP were observed through the filter sets 46 HE (excitation 500 nm, beamsplitter: 515 nm, emission: 535 nm) and 38 HE (excitation 470 nm, beamsplitter: 495 nm, emission: 525 nm), respectively (Zeiss).
The constructs, their properties and references are listed in Table 2.2.

**Table 2.2: Constructs used in this study, antibiotics for selection in *E. coli*, localization in the cell, fused fluorescent protein (FP) and origin reference**

| | selection E. coli | localization | FP | reference |
|---|---|---|---|---|
| **FABD2-GFP** | spectinomycin | actin | GFP | (Maisch et al., 2009) |
| **ST-GFP Golgi-GFP** | kanamycin | golgi | GFP | (Brandizzi, 2002) |
| **Peroxi-YFP** | ampicillin | peroxisomes | YFP | (Mathur et al., 2002) |
| **NtTPC1A** | spectinomycin | tonoplast | GFP | (Liu, 2014) |

## 2.2.9 Mitochondria shape analysis

The shape of mitochondria was studied by staining with MitoTracker Red FM (Thermo Fisher Scientific Inc., Waltham, MA, USA), a far red-fluorescent dye that stains mitochondria depending on the membrane potential, unlike MitoTracker Green FM, which is independent of membrane potential (Presley et al., 2003). The dye was added to the cell suspension culture at a final concentration of 100 nM freshly prepared from a 100 µM stock solution in DMSO (dimethyl sulfoxid). The cells were observed immediately without incubation or washing (Agnello et al., 2008). In order to get high-resolution images, an AxioObserver Z1 inverted microscope (Zeiss, Jena, Germany) was used, equipped with a laser dual spinning disc device from Yokogawa (Yokogawa CSU-X1 Spinning Disc Unit, Yokogawa Electric Dorporation, Tokyo, Japan) and a cooled digital CCD camera (AxioCam MRm; Zeiss). Pictures were taken using the 488 nm emission line of the Ar-Kr laser and a Plan-Apochromat 63x/1.44 DIC oil objective operated via the Zen 2012 (Blue edition, Zeiss) software.

## 2.2.10 Mitochondria quantification

The images taken for the shape analysis of mitochondria were also used for their quantification. To quantify the mitochondria within a cell, their coverage was calculated in percent, using ImageJ (https://imagej.nih.gov/ij/). The area of the cell was determined as 100 %. A value of 50 % implies that half of this area was covered with mitochondria. Although the three-dimensionality of the cell is neglected, this method takes into consideration that mitochondria are sometimes interconnected and form large networks, so quantification in absolute numbers is not conclusive.

## 2.3 Immunofluorescence for cellular localization of paclitaxel

For immunofluorescent staining of paclitaxel, *Taxus* cells of the production phase were fixed with 1 % (w/v) paraformaldehyde at 4 °C for 1 h (Naill, Roberts, 2005b). The double-immunofluorescence staining and confocal laser-scanning microscopy was conducted as described by Nick et al. (2000), using a mouse monoclonal anti-taxol (Santa Cruz Biotechnology, Inc., Dallas, USA) as primary antibody and a goat polyclonal anti-mouse IgG-TRITC (Sigma-Aldrich, Munich, Germany) as secondary antibody. High-resolution microscopic images were taken as described in 2.2.9.

## 2.4 Nile red as marker for paclitaxel

Growth phase, production phase and bioreactor samples of *Taxus* were stained with Nile red (Carl Roth, Karlsruhe, Germany) to investigate whether the dye is useful as marker for the production of paclitaxel in living cells.

The stock solution was prepared in acetone, the final concentration of the dye was 1 µg/ml. After 1 h of incubation time the stained cells were observed under an AxioImager Z.1 microscope (Zeiss, Jena, Germany) using the filter set 43 HE (excitation 550 nm, beamsplitter: 570 nm, emission: 605 nm).

## 2.5 Elicitor treatment and precursor feeding

In scope of this study various elicitors were used to treat the cell cultures in order to investigate morphological and metabolic changes. In case of *Taxus*, elicitors were used to modify the number of shiny cells in the culture and to find out if changes in gene expression and alkaloid production are linked to the number of these cells.

With respect to *Catharanthus*, elicitor studies were conducted to stimulate alkaloid biosynthesis as well as expression of the biosynthetic genes and to monitor whether the cell lines respond to the treatment in a different manner. Since the *Catharanthus* cell lines have been shown to be unable to produce vindoline, which is essential for the biosynthesis of the final products vincristine and vinblastine, it was added to the cells in precursor-feeding experiments. In order to determine whether a higher content of precursors also leads to a higher yield of subsequent intermediates, tabersonine and catharanthine were also added to the cell cultures. Table 2.3 shows a list of all elicitors and precursors and their concentration used in this study.

**Table 2.3: List of elicitors and their concentration for cell culture treatment**

| | producer | concentration | cell culture |
|---|---|---|---|
| **JA** | Duchefa (Haarlem, The Netherlands) | 100, 200 µM | *Catharanthus* |
| **MeJA** | Duchefa (Haarlem, The Netherlands) | 100 µM | *Catharanthus* *Taxus* |
| **SA** | Sigma-Aldrich (Munich, Germany) | 100 µM | *Taxus* |
| **$AlCl_3$** | Merck (Darmstadt, Germany) | 10, 50, 100 µM | *Taxus* |
| **$AgNO_3$** | Carl Roth (Karlsruhe, Germany) | 50 µM, 100 µM | *Taxus* |
| **NAA** | Duchefa (Haarlem, The Netherlands) | 5 µM | *Catharanthus* |
| **kinetin** | Duchefa (Haarlem, The Netherlands) | 2, 2,5 µM | *Catharanthus* |
| **DPI** | Sigma-Aldrich (Munich, Germany) | 20 µM | *Taxus* |
| **sucrose** | Carl Roth (Karlsruhe, Germany) | 15 – 100 g/l | *Catharanthus* |
| **tabersonine** | Sigma-Aldrich (Munich, Germany) | 1.2, 2.4, 3.6 µM | *Catharanthus* |
| **catharanthine** | Sigma-Aldrich (Munich, Germany) | 1.2 µM | *Catharanthus* |
| **vindoline** | Sigma-Aldrich (Munich, Germany) | 0.8, 1.6, 2.4 µM | *Catharanthus* |

## 2.6 Quantification of vinca alkaloids by high performance liquid chromatography

For alkaloid extraction, samples were frozen and lyophilized for 72 h. The dried material was dissolved in pure methanol (*Catharanthus*) or methanol with 0.1 % acetic acid (*Taxus*), respectively. Samples containing cell material were lysed by ultrasonication for 2 minutes (amplitude 100 %, 0.5 s pulse) using a high-efficiency ultrasound device (UP 100H, Hielscher Ultrasonics GmbH, Teltow, Germany). Samples were centrifuged for 10 minutes with 10,000 g at room temperature. The supernatant containing the alkaloids was filtered with a Chromafil PET-20/15 MS filter with 0.2 µm pore size (Macherey-Nagel GmbH & Co. KG, Düren, Germany), sealed in autosampler vials (WIC4200, WICOM Germany GmbH, Heppenheim, Germany) and stored at -20 °C.

The chromatographic system used for the analysis of vinca alkaloids was an Agilent-1200-Series HPLC system (Agilent Technologies, Santa Clara, USA) equipped with a diode array detector (G1315D), Agilent ChemStation software and an Agilent Eclipse XDB-C18 column (4.6 x 250 mm, 5 µm particle size). The method was adapted from (Pan et al., 2016b).

The composition of the mobile phase is given in Table 2.4. The flow rate was 1 ml/min, the injection volume was 30 µl.

Identification of alkaloids was implemented by comparison of UV spectra and retention time to those of authentic standards (Sigma-Aldrich, Munich, Germany) dissolved in methanol. Quantification of alkaloids was performed using the calibration curves of the standards. Standards and their retention times are listed in Table 2.5. The total run of each sample took 20 minutes.

**Table 2.4: Composition of ammonium acetate buffer system for HPLC analysis**

| solvent | percentage |
|---|---|
| acetonitrile | 45 % |
| MeOH | 15 % |
| 25 mM ammonium acetate<br>0.1 % triethylamine | 40 % |

**Table 2.5: Retention times of standards in ammonium acetate buffer system, analyzed via HPLC**

| standard | retention time (+/-0.05) [min] |
|---|---|
| tryptophan | 2.17 |
| tryptamine | 2.58 |
| vindoline | 8.81 |
| vincristine | 10.91 |
| catharanthine | 12.38 |
| vinblastine | 16.92 |

## 2.7 Detection of vinca alkaloids by LC-MS

To detect even smallest traces of pharmaceutically important vinca alkaloids that could not be found by HPLC, a more sensitive non-quantitative LXQ Linear Ion Trap $MS^n$ system (Thermo Fisher Scientific, Waltham, MA, USA) equipped with a Finnigan Surveyor HPLC-PDA was used (Hildebrand et al., 2015). Separation was carried out on a Phenomenex Luna C18 (2), 250 x 4.6 mm, 5 µM column. The metabolites were characterized with MS operating in ESI positive mode. Mass spectra were recorded for *m/z* 337, 457, 811 and 825. $MS^2$ experiments of the $[M + H]^+$ ions were recorded. Spray voltage was 4 kV, capillary voltage 33 V, capillary temperature 350 °C and the tube lens voltage was 70 V. The LC-MS analysis was conducted at the Institute for Applied Biosciences at KIT. The buffer system is described in Table 2.6, the retention times and fragmentation patterns for the analyzed alkaloids are given in Table 2.7. A detailed chromatogram of the standards is shown in figure 2.4.

**Table 2.6: Buffer exchange system for LC-MS analysis**

| time [min] | 0 | 5 | 23 |
|---|---|---|---|
| 10 mM ammonium acetate buffer, pH 6.0 [%] | 30 | 10 | 30 |
| methanol [%] | 70 | 90 | 70 |

**Table 2.7: Retention times and fragmentation patterns of standards analyzed by LC-MS**

| | retention time [min] | MS fragmentation pattern | |
|---|---|---|---|
| **tabersonine** | 16.7 (+/- 0.7) | 337.3 > 305.22 | 337.3 > 228.02 |
| **catharanthine** | 11.4 (+/- 0.2) | 337.32 > 173.23 | 337.32 > 144.12 |
| **vindoline** | 10.2 (+/- 0.1) | 457.43 > 188.27 | 457.43 > 397.46 |
| **vinblastine** | 10.8 | 811.58 > 224.41 | 811.58 > 751.68 |
| **vincristine** | 10.1 | 825.55 > 807.70 | 825.55 > 765.66 |

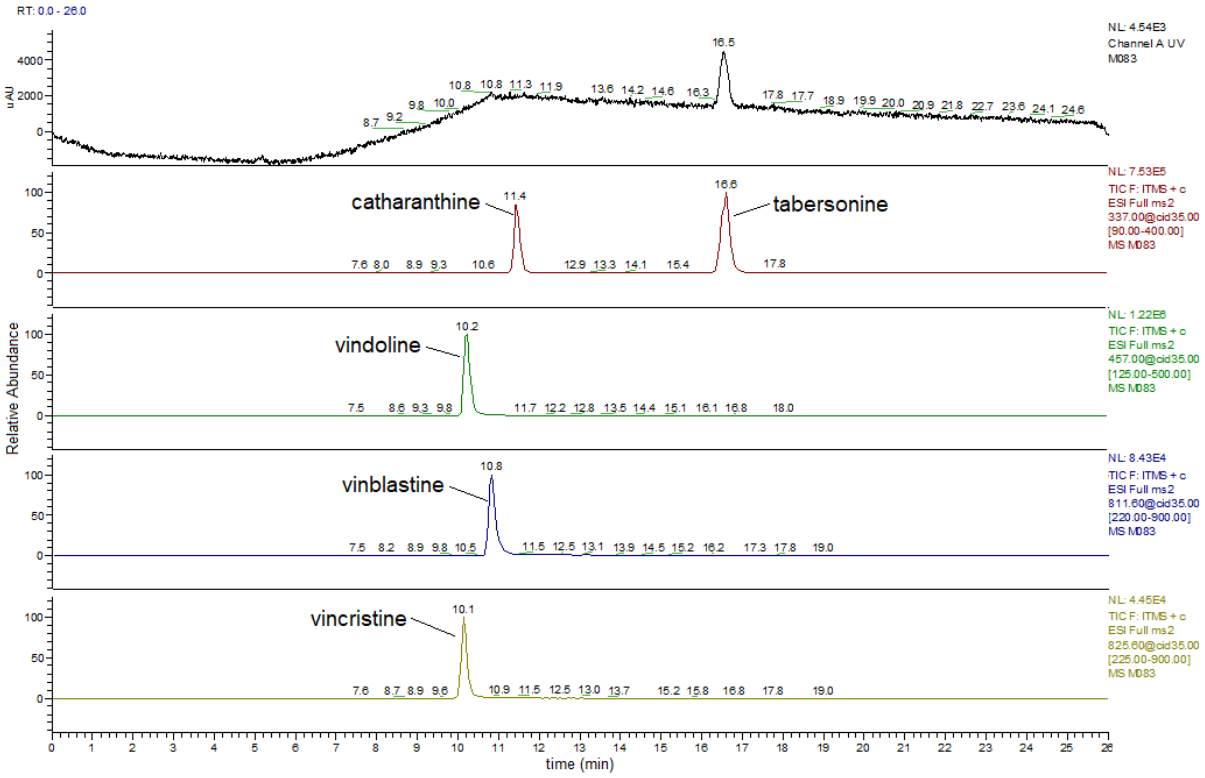


**Fig. 2.4: LC-MS profile of standards**
Different masses are shown in different colors. Red: chromatogram of *m/z* 337 (catharanthine and tabersonine), green: chromatogram of *m/z* 457 (vindoline), blue: chromatogram of *m/z* 811 (vinblastine), yellow: chromatogram of *m/z* 825 (vincristine). Height of the peak indicates the relative abundance of a molecule, normalized according to the highest peak in each spectrum.

## 2.8 RNA-extraction and cDNA synthesis

For sampling of the cell suspension cultures, medium was removed by a vacuum pump and approximately 100 mg of cells were transferfed to 2.0 ml reaction tubes, frozen in liquid nitrogen and kept at -80 °C until further processing. Prior to extraction, frozen cells were homogenized into a powder physically, using quartz sand and pestle. RNA was extracted by means of the innuPREP Plant RNA Kit (Analytik Jena, Jena, Germany), a column-based extraction method, following the manufacturer's instructions. Possible contaminations by genomic DNA were removed by incubating the RNA on the column with RNAse-free DNAse (Qiagen, Hilden, Germany) for 15 min at 37 °C.

High quality and integrity of RNA was verified via spectrophotometry by NanoDrop (peqlab Biotechnologie GmbH, ND-1000 Spectrophotometer, Erlangen, Germany) and gel electrophoresis.

For cDNA synthesis 2 µg of RNA were added to 1.4 µl of mastermix I (Table 2.8). Total volume of 16 µl was adjusted with nuclease free $H_2O$. This approach was kept in a

thermocycler for 5 min at 70 °C. Subsequently, 4 µl of mastermix II (Table 2.8) were added and samples returned to the cycler for 60 min at 42 °C followed by 10 min at 90 °C.

**Table 2.8: Protocol and cycler program for cDNA synthesis**

| | | |
|---|---|---|
| **mastermix I** | | |
| dNTPs (10 mM) | 1 µl | New England Biolabs GmbH, Ipswich, USA |
| oligodT (100 µM) | 0.4 µl | Thermo Fischer Scientific, Waltham, USA |
| | | |
| **cycler step I** | | |
| 70 °C | 5 min | |
| | | |
| **mastermix II** | | |
| MulV RT buffer | 2 µl | New England Biolabs GmbH, Ipswich, USA |
| RNase inhibitor | 0.5 µl | New England Biolabs GmbH, Ipswich, USA |
| MulV RT | 0.25 µl | New England Biolabs GmbH, Ipswich, USA |
| nuclease free water | 1.25 µl | Qiagen, Hilden, Germany |
| | | |
| **cycler step II** | | |
| 42 °C | 60 min | |
| 90 °C | 10 min | |
| 12 °C | ∞ | |

## 2.9 Semi quantitative RT-PCR

Reverse transcriptase (RT)-PCR was performed using the components and concentrations shown exemplarily for a single reaction of 20 µl in Table 2.9. Taq DNA Polymerase and reaction buffer were purchased from New England Biolabs GmbH (Ipswich, USA). Cycling conditions are given in Table 2.10. Primers which were utilized for gene expression analysis in *Catharanthus* are listed in Table 2.11, those which were used for *Taxus* are listed in Table 2.12. Primers were synthesized by Sigma-Aldrich (Munich, Germany) and designed with the Primer3 software (http://primer3.ut.ee/) if no references are given.

Remark: Nomenclature of genes is inconsistent between different references. Genes, which were examined in the present study, are all written in lower case letters and in italics.

**Table 2.9: (RT)-PCR single reaction**

| volume [µl] | component |
|---|---|
| 2 | Taq Reaction Buffer 10x |
| 1 | dNTPs (10 µM) |
| 1 | forward primer (10 µM) |
| 1 | reverse primer (10 µM) |
| 1.5 | template DNA |
| up to 20 µl | nuclease free $H_2O$ |
| 0.5 | Taq DNA polymerase |
| **20** | **final volume** |

**Table 2.10: (RT)-PCR cycling conditions**

| temperature | duration | repeats |
|---|---|---|
| 95 °C | 3 min | 1x |
| 95 °C | 30 s | 30x |
| 50 °C – 58°C | 30 s | |
| 68 °C | 30 s | |
| 68 °C | 5 min | 1x |
| 12 °C | ∞ | |

**Table 2.11: Primers used for investigation of the TIA pathway of *Catharanthus roseus***

| gene | sequence | size of transcript [bp] | annealing Tm [°C] | reference |
|---|---|---|---|---|
| *exp* | 5‘ ACAATACCATCGCCATCAC | 172 | 50 | (Pollier et al., 2014) |
| | 5‘ AAGAGGACTGCTGGAAGG | | | |
| *rsp9* | 5‘ GAGGGCCAAAACAAACTTGA | 145 | 58 | (Peebles et al., 2009) |
| | 5‘ CCCTTATGTGCCTTTGCCTA | | | |
| *g10h* | 5‘ CATTTATTAGGCGACCAACC | 148 | 50 | |
| | 5‘GAACTTCTTTCGCCATTGTT | | | |
| *as* | 5‘ GCGAACATTTGCAGATCCAT | 156 | 50 | |
| | 5‘ GGCCGATTTGTTATTGTTCC | | | |
| *tdc* | 5‘ ATCCGATCAAACCCATACCA | 143 | 50 | |
| | 5‘ CGTCATCCTCGACCATTTTT | | | |
| *str* | 5‘ ACCATTGTGTGGGAGGACAT | 152 | 50 | |
| | 5‘ ATTTGAATGGCACTCCTTGC | | | |
| *sgd* | 5‘ GGAGGCTTCTTGAGTGATCG | 149 | 50 | |
| | 5‘ GCAAATTCACCAGTGGCATA | | | |
| *t16h1* | 5‘ GCCCAAAACAGCCAATATTCAAACC | 154 | 55 | |
| | 5‘ ATGTGATGAGTATGGCCACCGC | | | |
| *t16h2* | 5‘ GATCAACTCACAGTGGCAGTC | 147 | 52 | |
| | 5‘ GACTTGAGGACTTGTGATTGGC | | | |
| *d4h* | 5‘ ATAGTTAATCATGGGATTCCACAAGATGTT | 140 | 52 | |
| | 5‘ GTTCATGAAACTTACGAACTCCATCTAC | | | |
| *dat* | 5‘ GGTTTCAATTTATTTCTCACGTAC | 150 | 50 | |
| | 5‘ AACTATCAGAAAGGTAAGCATCGA | | | |
| *prx1* | 5‘ AGGGGTGCGATTCATCAGTG | 142 | 54 | |
| | 5‘ ATCCTGAAAGCCTGCTGACG | | | |

**Table 2.12: Primers used for investigation of paclitaxel biosynthesis pathway of *Taxus chinensis***

| gene | sequence | size of transcript [bp] | annealing Tm [°C] | reference |
|---|---|---|---|---|
| *maturase* | 5‘ TTGATTCGTCGGATACGTCA | 418 | 58 | (Expósito et al., 2009) |
| | 5‘ GTGGAACCAGAGCTTTCTGC | | | |
| *18S rRNA* | 5‘ CCGCGGTAATTCCGCTCCAAT | 111 | 58 | (Onrubia et al., 2010) |
| | 5‘ GAGGGCCAGTGCACACCGAGTA | | | |
| *tasy* | 5‘ AATGCAGCGCTGAAGATGAATGCA | 608 | 58 | (Nims et al., 2006) |
| | 5‘ TTGGCTGTGCCCTGTTTTCCAAAC | | | |
| *t5αh* | 5‘ TTAGGCATCCCTTTCATTGG | 202 | 56 | |
| | 5‘ ACATCTGCACCAGCTTCTCC | | | |
| *dbat* | 5‘ GGGATCTTGAAGTGGAGTGC | 227 | 58 | |
| | 5‘ ACCATGGCAGAAACTCATCC | | | |
| *dbtnbt* | 5‘ GCAGGGGAATTTTTAACACG | 196 | 52 | |
| | 5‘ ATGGCTTCCACAAACAGAGC | | | |

## 2.10 qPCR

The analysis of gene expression by qPCR was performed using the components and concentrations shown exemplarily for a single reaction of 20 µl in Table 2.13. GoTaq polymerase and buffer were obtained from Promega GmbH (Mannheim, Germany), SYBR Green I from Invitrogen (Darmstadt, Germany).

**Table 2.13: qPCR single reaction**

| volume [µl] | component |
|---|---|
| 1 | cDNA (1:10 diluted) |
| 4 | GoTaq buffer |
| 11.75 | $H_2O$ (nuclease-free) |
| 0.4 | dNTPs (10 mM) |
| 0.8 | primer mix (10 µM) |
| 1 | $MgCl_2$ (50 mM) |
| 0.1 | GoTaq polymerase |
| 0.95 | 20x SybrGreen I |
| **20** | **final volume** |
| | |
| **triplet mix** | |
| 61.8 µl | mastermix |
| 3.25 µl | cDNA |

A mastermix, containing all components excluding template cDNA was prepared for each gene. The last component added was SYBR Green due to its photosensitivity. Each sample was analyzed in three technical replicates by mixing one aliquot of mastermix with sample cDNA (Table 2.13) and distributing it to three wells of a 96-well plate.

The qPCR was performed on a CFX96 Touch Real-Time PCR Detection System (Bio-Rad Laboratories Inc., Munich, Germany). Cycling conditions are listed in Table 2.14.

**Table 2.14: qPCR cycling conditions**

| temperature | duration | repeats |
|---|---|---|
| 95 °C | 3 min | 1x |
| 95 °C | 20 s | 40x |
| 52 – 58 °C | 30 s | |
| 70 °C | 40 s | |
| melting curve from 50 °C to 95 °C in 0.5 °C increments | | |

All primers were tested by running a standard curve with tenfold dilutions of cDNA (Hellemans et al., 2007). Efficiency of primers was determined by calculating a linear regression of the cycle threshold (Ct)-values of these dilution series. The calculation of the relative expression was performed with adjusted primer efficiency. A no template control (NTC) was set up for each primer pair on each plate, substituting cDNA with nuclease-free $H_2O$ to monitor potential formation of PCR by-products. Signals in the NTC were classified as insignificant if the peaks of dissociation curve and sample product accured at different temperatures, or if the Ct-value of the NTC signal was at least 5 cycles later than the latest sample peak (D'haene et al., 2010).
Samples with extremely variable Ct-values within technical repeats as well as samples whose dissociation curve peaks deviated from the calculated product melting temperature, were neglected during analysis.

Analysis of qPCR raw data was conducted using the modified $2^{-\Delta\Delta CT}$ method described in Hellemans et al. (2007). As recommended for example by Vandesompele et al. (2002) and Jain et al. (2006), two reference genes were used for normalization of gene expression for *Catharanthus* (Table 2.11) and *Taxus* (Table 2.12), respectively.

## 2.11 Chip experiments

In cooperation with the working group for Molecular Cell Biology of the Botanical Institute I (BOT I), the Institute of Microstructure Technology (IMT) from the KIT developed a microfluidic chamber system, where plant cells can be integrated into a process flow, which has also been patented (Maisch et al., 2016a).
A single microfluidic chip consists of an upper cell chamber and a lower medium perfusion chamber. Cells can be introduced and removed from the upper chamber via two openings. The perfusion chamber has one inlet and one outlet, which can be connected to pipes to realize a constant flow of medium (figure 2.5). This also allows to connect two or more chips together. By providing the different chips with different cell types, a plant tissue can be technically reproduced in this way.

The chip parts were fabricated with polycarbonate (Makrolon® GP clear 099, Bayer Material Science AG, Leverkusen, Germany) by hot embossing with a brass molding tool (i-sys Mikro- und Feinwerktechnik GmbH, Karlsruhe, Germany). Chip parts were assembled by ultrasonic welding. The membrane with a pore size of 5 µm (Sterlitech Corporation, Kent, USA) was welded on the cell chamber and the membrane-sealed cell chamber was welded on the perfusion chamber and in between the two chambers, the connectors (dba Nordson MEDICAL, Loveland, USA) were integrated at the same time.

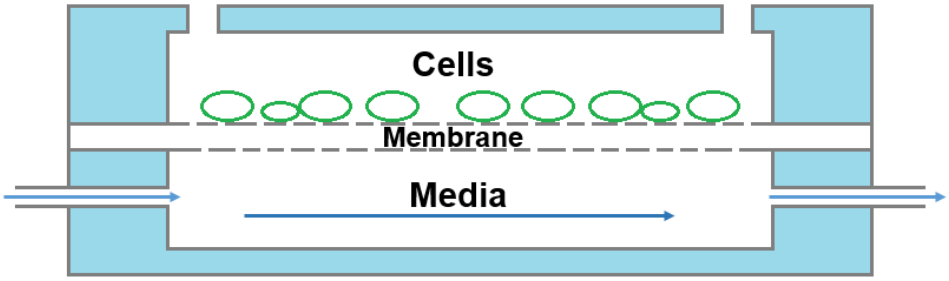


**Fig. 2.5: Schematic layout of a microfluidic bioreactor developed by IMT and BOT I**
The upper cell chamber and the lower medium chamber are separated by a semipermeable membrane, which allows the exchange of nutrients and cellular signals.

The chip is manufactured by the IMT in various designs, which differ in their volume and the diameter of the cell chamber openings. The version, which was mainly used in this work, holds 800 µl and has 3 mm openings in the cell chamber (figure 2.6).

**Fig. 2.6: Model of a microfluidic chip**
Microfluidic chip manufactured by IMT with chamber volume of 800 µl and 3 mm openings of the cell chamber. Courtesy of Tim Finkbeiner (IMT)

In each experiment, the chips were connected to transparent Tygon tubing (Reichelt Chemietechnik GmbH & Co., Heidelberg, Germany) with an inner diameter of 1.6 mm, which fits exactly to the connectors of the chip. The openings of the cell chamber of the chip were closed using 3M Polyester Tape Green (Röckelein GmbH, Nürnberg, Germany). The chips were connected to a 4-channel Ismatec REGLO Digital peristaltic pump (Cole-Parmer GmbH, Wertheim, Germany). The flow rate of the medium was 20 µl/min (figure 2.7).

**Fig. 2.7: Experimental setup for chip experiments**
The cell compartment of the chip is loaded with *Catharanthus* cells. There is a continuous medium flow by which multiple chips can be connected.

In various experimental approaches using the cell lines Cath 001 and Cath 004 it was examined whether detection of vinca alkaloids by means of LC-MS is possible on this scale (Table 2.15). In this way, it should be confirmed that the microfluidic approach is suitable for cell fermentation. Fermentation processes, which normally run on an industrial scale of several thousand liters, could be miniaturized with the aid of the microfluidic chip in order to simplify experiments for these processes. Cell cultures on the chip were elicitated by 100 µM MeJA. The volume of the circulating medium was 25 ml.

**Table 2.15: Setup of chip experiments for detection of vinca alkaloids in *Catharanthus***

| number of experiment | number of chips | volume of chips | cell line used | treatment |
|---|---|---|---|---|
| 1 | 2 | 200 µl | Cath 001 + Cath 004 | MeJA 100 µM |
| 2 | 2 | 200 µl | Cath 004 | MeJA 100 µM |
| 3 | 2 | 200 µl | Cath 001 + Cath 004 | MeJA 100 µM |
| 4 | 2 | 200 µl | Cath 004 + Cath 001 | MeJA 100 µM |
| 5 | 1 | 100 µl | Cath 004 | MeJA 100 µM |
| 6 | 1 | 200 µl | Cath 004 | MeJA 100 µM |
| 7 | 1 | 800 µl | Cath 004 | MeJA 100 µM |
| 8 | 1 | 100 µl | Cath 004 | MeJA 100 µM, vindoline 0.8 µM |
| 9 | 1 | 200 µl | Cath 004 | MeJA 100 µM, vindoline 0.8 µM |
| 10 | 1 | 800 µl | Cath 004 | MeJA 100 µM, vindoline 0.8 µM |
| 11 | 1 | 100 µl | Cath 004 | MeJA 100 µM, vindoline 1.6 µM |
| 12 | 1 | 200 µl | Cath 004 | MeJA 100 µM, vindoline 1.6 µM |
| 13 | 1 | 800 µl | Cath 004 | MeJA 100 µM, vindoline 1.6 µM |
| 14 | 3 | 800 µl | Cath 004 | MeJA 100 µM, vindoline 1.6 µM |
| 15 | 2 | 800 µl | Caht 001 + Cath 004 | MeJA 100 µM |
| 16 | 2 | 800 µl | Cath 004 + Cath 001 | MeJA 100 µM |
| 17 | 1 | 800 µl | Cath 004 | MeJA 100 µM |
| 18 | 1 | 800 µl | Cath 004 | MeJA 100 µM |

BY2 cell cultures were used as a proof of concept of the interaction of the cells in the two-chip system. When plant cells in liquid cell cultures are strongly diluted, they stop dividing. If diluted cells are complemented with medium of dividing cells they start proliferating again, which indicates communication between the cells.

In this experiment two setups were started, using 7 day old cells. In the control experiment, two chips were connected, each containing cell culture in high dilution (1:300). In the second setup one chip was used corresponding to the chips from the control setup, the other chip was loaded with cells of lower dilution (1:30) which corresponds to the normal cell concentration after the weekly subcultivation (figure 2.8).

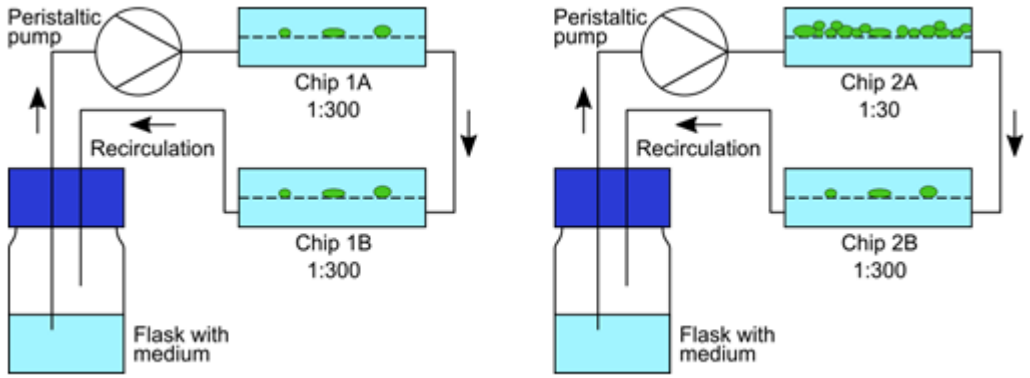


**Fig. 2.8: Setup of the BY-2 chip experiment for proof of cell communication on the chip.** Left side: control setup using two chips with strong dilution. Right side: experimental setup using one chip with strong dilution and one with regular concentration. Courtesy of Tim Finkbeiner (IMT)

Cells were harvested after three days in the chip, which corresponds to the proliferation phase of BY-2 and quantified using a hemocytometer (Fuchs-Rosenthal).
In the work of Maisch et al. (2016b) it was shown that BY-2 cells behave in the same way with regard to viability and division in the chip as they do in flask cultures.

## 2.12 Statistical analysis of data

Significance tests between individual samples were performed by two-tailed student‘s *t*-test assuming a confidence interval of 95 % using excel.

Significance tests between several samples were performed using ANOVA followed by Tukey HSD post-hoc test with R version 3.5.0 assuming independence and normal distribution of values and confidence interval of 95 %.

# 3. Results

In this chapter, the results of the present study are presented in three main sections. The first part is about the work on *Taxus*, starting with aspects of growth and phenotype. This section is focusing on the search for a marker of paclitaxel production and the investigation of a specific cell type found in *Taxus* suspension cultures which was referred to as shiny cells. Another key point of this part is the relationship between elicitor treatment and the shiny cell phenotype, paclitaxel production, and the expression of paclitaxel biosynthesis genes. The questions to be answered were whether cellular predictors for paclitaxel exist and if the discovered shiny cells could function as such. Furthermore, it should be clarified which mechanism underlies the formation of shiny cells and if they are linked to production of secondary metabolites and expression of paclitaxel biosynthesis genes.

The second section deals with the work on *Catharanthus* cell cultures. The main point of this part is the comparison of cell traits and metabolic potential between the two cell lines Cath 001 and Cath 004. For this purpose, treatments with different elicitors and precursors were performed and changes in alkaloid production, gene expression and cellular parameters were investigated. The major questions of this section were if the differences in phenotype and growth behavior of Cath 001 and Cath 004 are linked to a difference in their potential to produce alkaloids and how this production could be stimulated.

The third section is about the experiments performed with the microfluidic bioreactor. The first part of this section examines whether chip-scale detection of vinca alkaloids is possible to clarify whether the microfluidic bioreactor is suitable for research on fermentation processes. In the second part, a proof of concept experiment uses BY-2 cells to investigate whether there is communication between cells in coupled chips. The questions to be answered in this section were whether miniaturization and cell communication in chip experiments are possible and thus, whether a technical simulation of a plant tissue using the microfluidic bioreactor is possible in principle.

## 3.1 Work on cell cultures of *Taxus chinensis*

The following part of the result chapter is about the work that has been done on *Taxus* cell cultures. Besides the investigation of phenotypic aspects of this cell culture, the search for a marker for paclitaxel production is subject of this section. In addition, the investigation of the machanism of the shiny cell formation is described and a correlation between the number of shiny cells and paclitaxel production and gene expression is examined.

### 3.1.1 Phenotyping of *Taxus chinensis* cell cultures

The *Taxus* cells used in this study form aggregates in liquid culture, which may comprise only a few (figure 3.1 A) up to several hundred cells (figure 3.1 B).

Microscopy of *Taxus* cells in bright field showed two different cell types – one which displayed normal phenotype with visible nucleus and cytoplasmic strands (figure 3.2 A) and one which appeared bright and highly vacuolated without showing any expected structures (figure 3.2 B). This kind of cells was less common and referred to as shiny cells. Shiny cells and non shiny cells could be found within the same aggregates (figure 3.1 C).

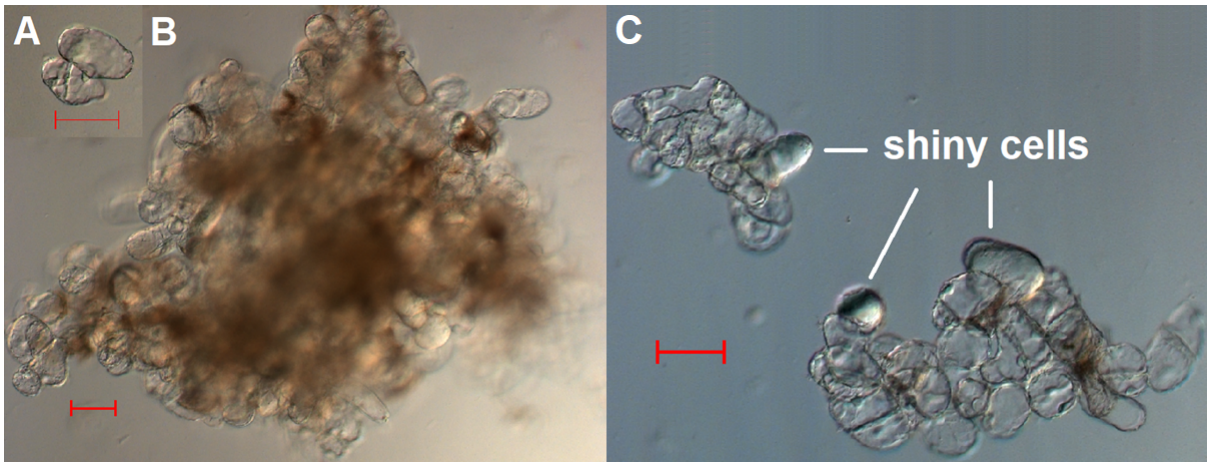


**Fig. 3.1: Bright field images of *Taxus* cell aggregates of different sizes containing shiny and non shiny cells**
A: Small cell aggregate consisting of few cells.
B: Aggregate containing several hundred cells.
C: Medium sized aggregates containing shiny and non shiny cells
(Scale bars represent 100 µm.)

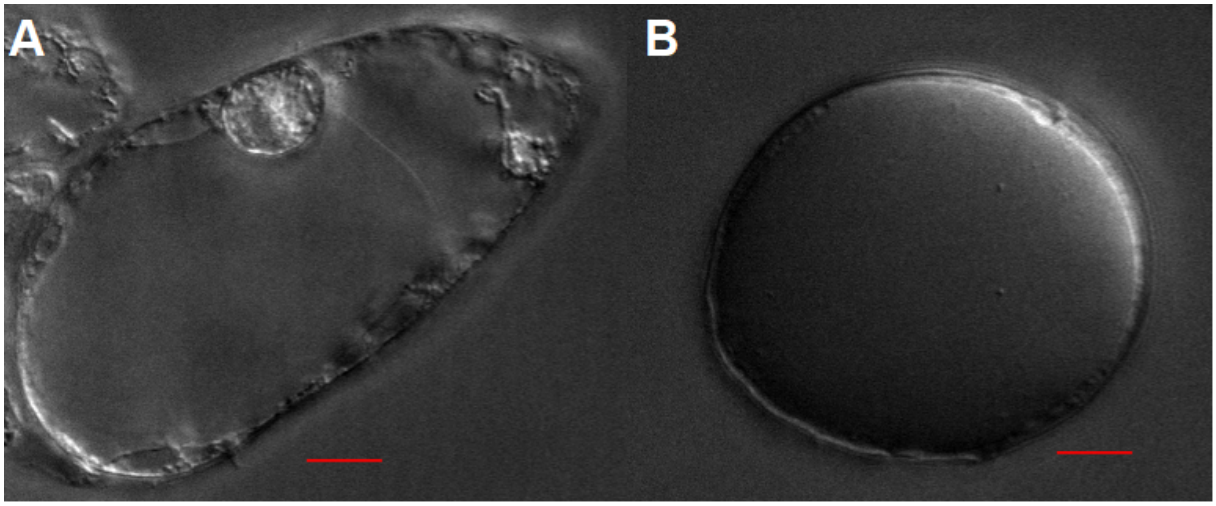


**Fig. 3.2: High-resolution bright field images of non shiny and shiny cells**
A: Non shiny cell showing nucleus and cytoplasmic strands.
B: Highly vacuolated optically largely unstructured shiny cell.
(Scale bars represent 10 µm.)

## *Taxus* cell growth and cell cycle

Growth index 7, cell size, cell number, PCV, fresh weight and dry weight were determined like described in 2.2.1 to 2.2.5 and summarized graphically in figure 3.3.

Figure 3.3 A shows the results for *Taxus* growth index 7 for two independent cultures that were subcultivated weekly on different days. The factor of increase in fresh weight varies between 1.5 and 3.0. On average, there is about a doubling of the cell weight during one week. The culture transferred on Fridays shows a slightly higher increase over the investigation period (average growth factor 2.4) than the culture transferred on Tuesdays (average growth factor 2.2).

The development of cell size over a period of 15 days is shown in figure 3.3 B. During this time, the cells were not transferred to fresh medium. At least 1000 cells were measured for each day. Cell length varies between 72 and 90 µm, cell breadth between 51 and 61 µm. During the first two days the cell size increases. The largest values were measured at day 2. On day 3 there is a decrease in cell size, which then remains more or less stable until day 7. On day 8, there is an increase in the cell size followed by a strong decrease on days 9 and 10, where the lowest values for length and breadth were measured. On day 11 there is a high increase again. Towards the end of the measurement period, the cell size decreases. Ratio of cell breadth and cell length indicates that *Taxus* cells are initially more elongated and later rather round.

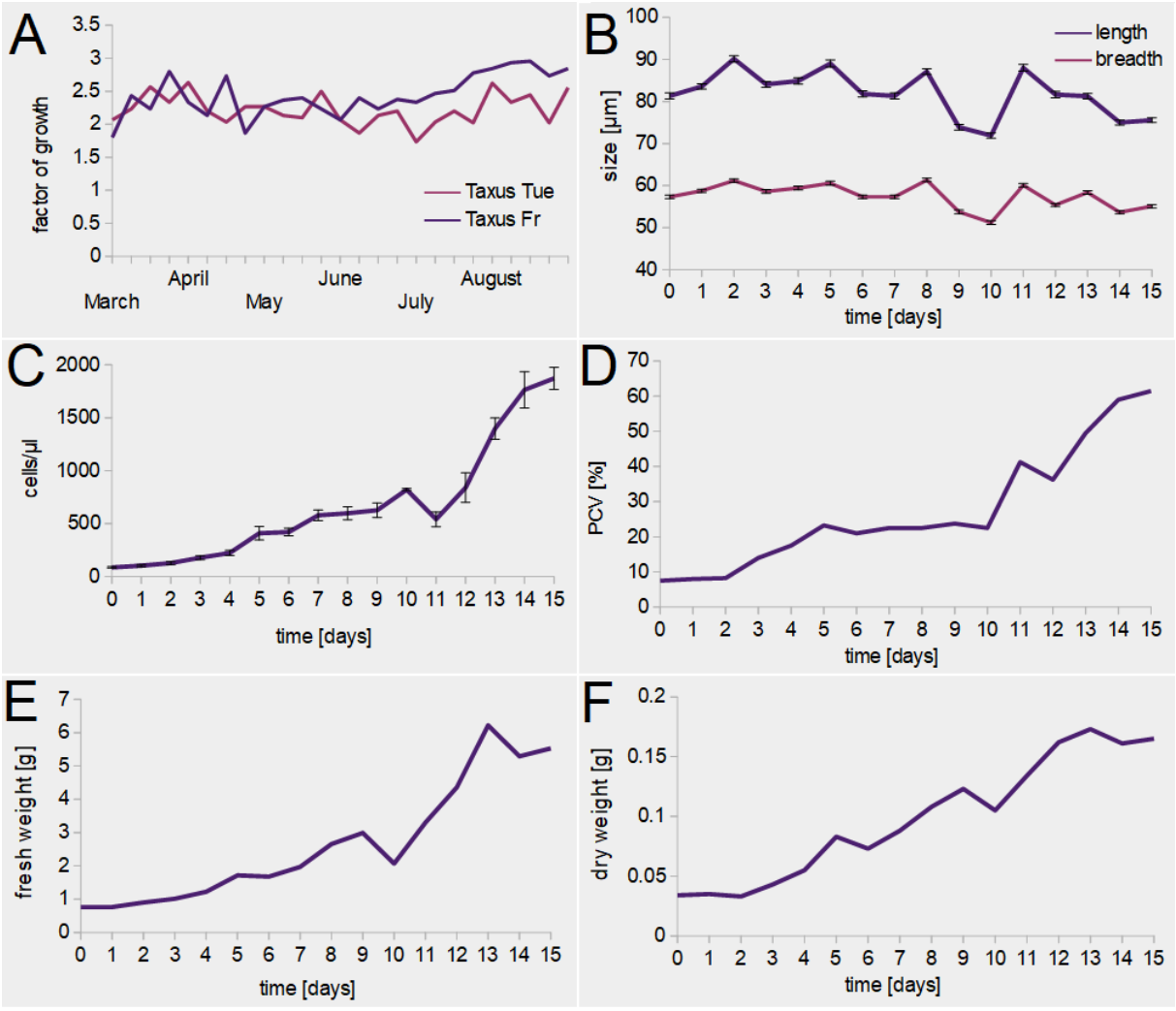


**Fig. 3.3: Phenotypic parameters of *Taxus* cells regarding cell growth and division**
A: Growth Index 7 of two independent *Taxus* cell cultures assayed over 6 months from March to August 2018 based on the fresh weight at the day of subcultivation. B: Measurement of *Taxus* cell size over 15 days. Each data point represents an average of at least 1000 cells. Error bars indicate ±SE. C: Cell counting over time. Each data point represents an average of 5 technical replicates. Error bars indicate ±SE. D: PCV over time. Data represents the average of two technical replicates. E: Fresh weight over time. F: Dry weight over time.

The development of cell number in 1 µl of cell suspension over 15 days is shown in figure 3.3 C. Until day 4 there is a slight, steady climb, followed by a slightly faster increase until day 10, after which there is a kind of exponential growth phase. The average length of cell cycle was calculated as described in 2.2.3. For this purpose, only the values from day 0 to day 7 were used, since this period corresponds to the weekly cell transfer. This resulted in a doubling time of 2.4 days.

Figure 3.3 D shows the PCV over a period of 15 days. During the first two days, there is no change. Between day 3 and 5 the PCV rises evenly and reaches a plateau phase

of approximately 25 % that lasts until day 10, whereupon it again rises sharply up to 61 % at day 15. The course correlates with the development of cell number.

The results of fresh and dry weight (shown in figure 3.3 E and F) are very similar to the PCV data. For the fresh weight data, there is a mild increase in the first days, followed by a slightly stronger one until day 9. From day 10 there is a rapid increase, which reaches a plateau around day 13. For dry weight, the increase over the measurement period is more uniform. From this data the water content of *Taxus* cells can be calculated, which is between 95 % and 97 % and is especially high towards the end of the sampling period, while it is lower in the middle.

## Uniform sugar consumption in *Taxus*

The content of sugar in the medium of liquid *Taxus* cell culture was measured by brix refractometer over 15 days and is shown in figure 3.4. The sugar consumption is relatively even over the entire culture cycle. Between day 10 and 12 a slightly faster decrease is observed.

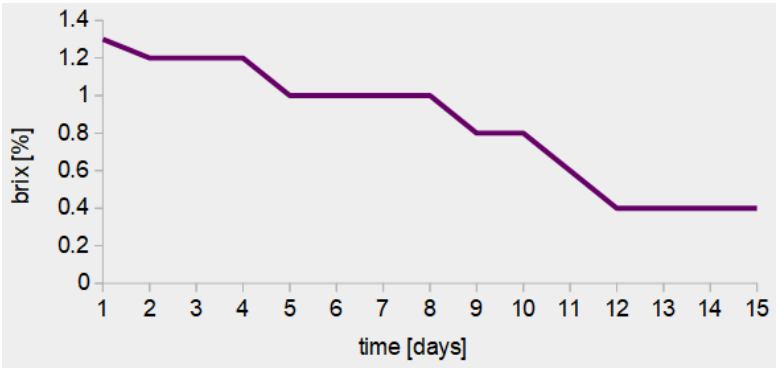


**Fig. 3.4: Sugar content in *Taxus* cell culture medium**
Sugar content of *Taxus* medium over time measured in brix.

## Visualization of tonoplast and actin by transient transformation

Tonoplast and actin of *Taxus* cells were visualized by transient transformation with GFP-coupled constructs. Further information on the constructs used, are given in Table 2.2 in the materials and methods section. The tonoplast is strongly folded, especially in the periphery of the cell (figure 3.5 A), while actin is relatively evenly distributed, showing stronger as well as finer, higly branched filaments (figure 3.5 B).

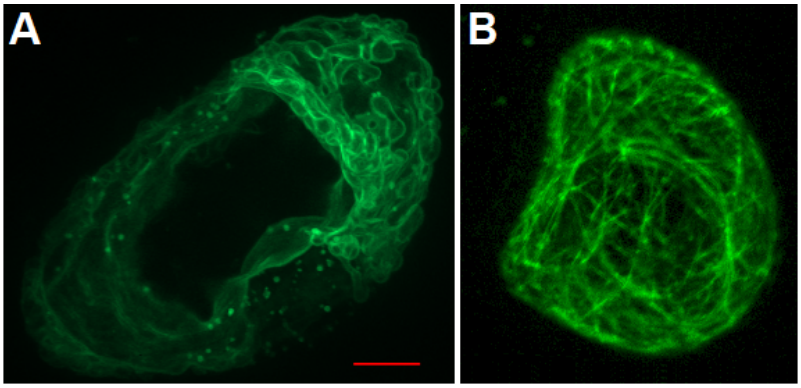


**Fig. 3.5: Transient transformation of *Taxus* by gene gun**
A: Labeling of tonoplast by GFP-coupled NtTPC1A.
B: Labeling of actin by FABD2-GFP.
(Scale bar represents 10 µm.)

## Mitochondria shape analysis

To investigate the energy level of *Taxus* cells in growth and production phase, cells were stained with Mito Tracker Red FM and z-stack images taken like described in 2.2.9. Noteworthy was the wide range of structure and shape of mitochondria. To further investigate the evolution of the shape, images were taken at various time points during cell cycle and the shape of mitochondria assessed by establishing three categories to which the cells were assigned. Examples of these categories are shown in figure 3.6. A pattern called dots was assigned to all cells that had exclusively or predominantly punctuated mitochondria (figure 3.6 A). Cells whose mitochondria were predominantly elongated were assigned to the category called lines (figure 3.6 B). When all or most of the mitochondria were connected, this was called a mesh pattern (figure 3.6 C).

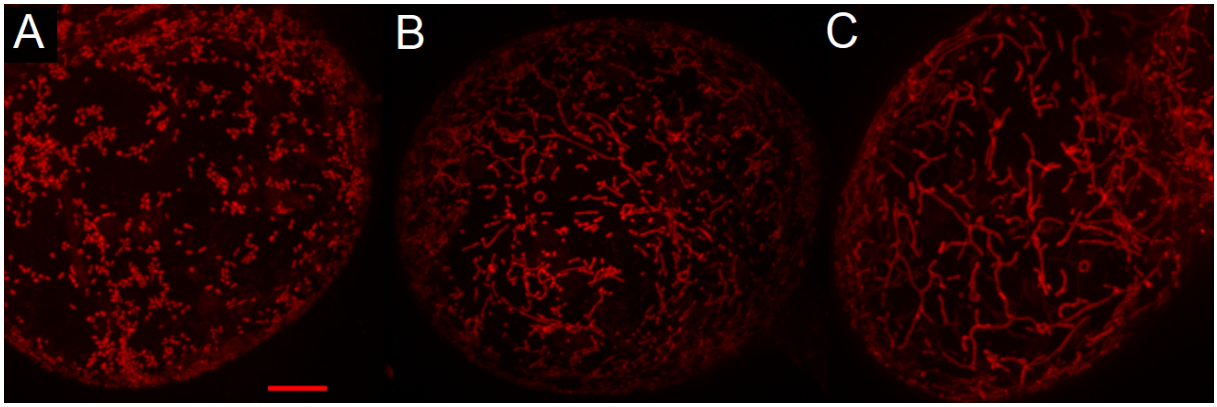


**Fig. 3.6: Categories for mitochondrial shape in *Taxus***
Z-stack images of optical sections of *Taxus* cells stained with Mito Tracker Red FM and the name of categories: (A) dots: punctuated mitochondria (B) lines: elongated mitochondria (C) mesh: elongated and connected mitochondria.
(Scale bar represents 10 µm.)

Figure 3.7 shows the distribution and evolution of mitochondrial shape over time. Figure 3.7 A shows the situation in the growth phase culture, figure 3.7 B and C display the pattern in the production phase, differentiated between non shiny (B) and shiny (C) cells. For the growth phase at least 68 up to 83 cells were analyzed per time point. In production phase the signal of the Mito Tracker was often very low. For this reason, fewer cells were used for this analysis (16 to 23 for non shiny cells and between 8 and 12 for the less common shiny cells). In the case of growth culture, the days indicated refer to the time after the last subcultivation. In the production culture, the days represent the time after the transfer into production medium.

In the growth culture, the mesh pattern is dominant at the beginning of the culture cycle and accounts for about half on day 1, while the dot pattern is below 10 %. Over time, the mesh pattern disappears almost entirely, while the dot pattern increases sharply, which is particularly evident between day 6 and 9 until it reaches 50 % on day 15. The line pattern is quite stable over the measurement period.

In the non shiny cells of the production culture, the dot pattern is about 30 % nine days after the transfer to production medium while the mesh pattern is hardly pronounced. The strongest representation is the line pattern. Occasionally, cells with mitochondrial nonspecific Mito Tracker signal appeared in the production culture. These cells were referred to as no pattern and accounted for 20 % on days 16 and 19 in the non shiny cell production medium.

In the shiny cells, the dot pattern barely appears, while the mesh pattern is much more pronounced than in the non shiny cells. Again, at the beginning and the end of the sampling period there were cells with unspecific signals.

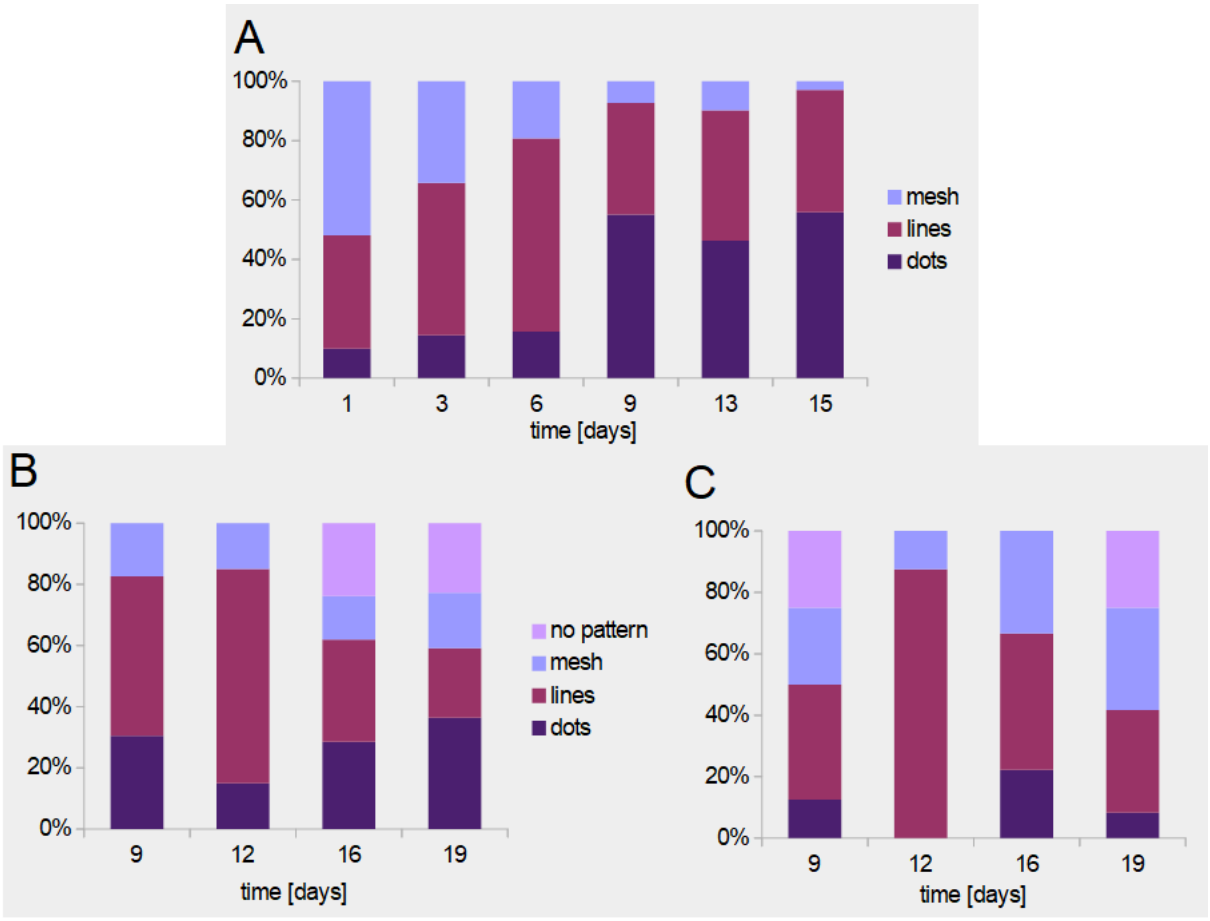


**Fig. 3.7: Shape of mitochondria in *Taxus* cells over time**
A: Shape of mitochondria in *Taxus* growth phase culture. 68 to 83 analyzed cells per data point. B: Shape of mitochondria in non shiny *Taxus* cells in production phase. 16 to 23 analyzed cells per data point. C: Shape of mitochondria in shiny *Taxus* cells in production phase 8 to 12 analyzed cells per data point.

## Mitochondria quantification

In addition to shape, the number of mitochondria was investigated. The same microscopic images were used for this purpose. To quantify the mitochondria, their percentage coverage of the cell was calculated (see 2.2.10). Figure 3.8 shows the results of this study. During the growth phase, there is a significant decrease in mitochondria over time. On day 1 the coverage is about 30 %, on day 15 it has dropped to 22 % (figure 3.8 A)

The non shiny cells of the production phase show a reverse trend. Nine days after transfer to production medium the mitochondrial coverage is 24 % and increases to 36 % within ten days. Between day 9 and day 12 there is also a significant increase for the shiny cells, but mitochondrial coverage decreases again. After 19 days in production medium, the number of mitochondria in the non shiny cells is significantly higher than in the shiny cells (figure 3.8 B).

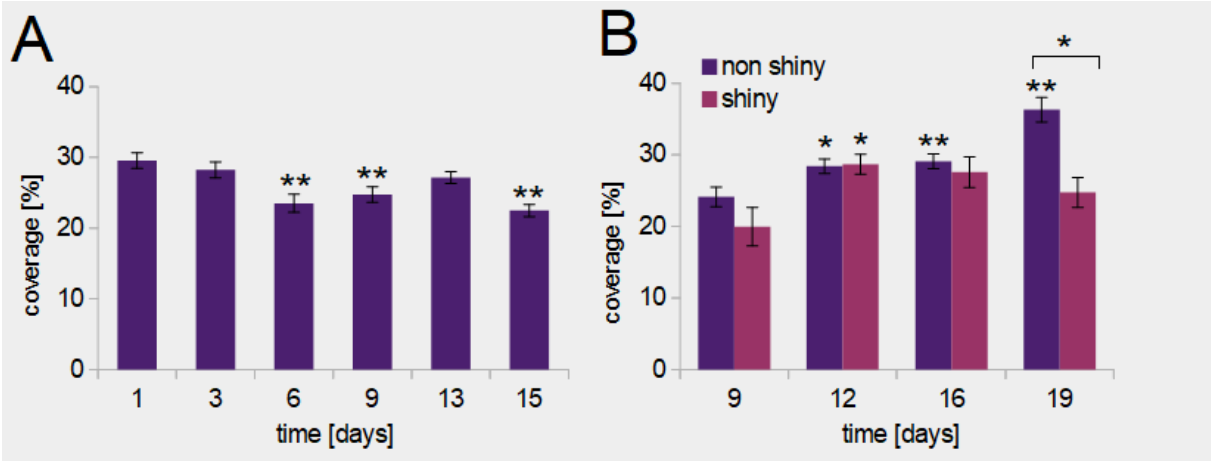


**Fig 3.8: Quantification of mitochondria in *Taxus* growth and production cell culture**
A: Percentage of mitochondrial coverage in *Taxus* growth phase culture. Error bars indicate ± SE. Statistically significant differences to the starting point (day 1) are indicated by two asterisks (student's *t*-test, $p < 0.01$). B: Percentage of mitochondrial coverage in *Taxus* production phase culture distinguished between shiny and non shiny cells. Error bars indicate ± SE. Statistically significant differences to the starting point (day 9) are indicated by one or two asterisks above the bar. Statistically significant differences between shiny and non shiny cells are indicated by an asterisk above the bracket (student's *t*-test, *: $p < 0.05$, **: $p < 0.01$).

### 3.1.2 Immunofluorescence localizes paclitaxel between cell wall and membrane

To localize paclitaxel within the cell a double-immunofluorescence staining of production phase cells was conducted as described in 2.3. Since *Taxus* cells form large agglomerates and are highly vacuolated, a large number of cells was destroyed during fixation or the fixed cells exhibited plasmolysis. Nonetheless, high-resolution images of some cells could be taken after antibody treatment. Figure 3.9 shows two examples of cells after immunofluorescence staining. The staining showed two rings around the cell wall and the cell membrane, suggesting that paclitaxel is accumulated in notable amounts at these sites.

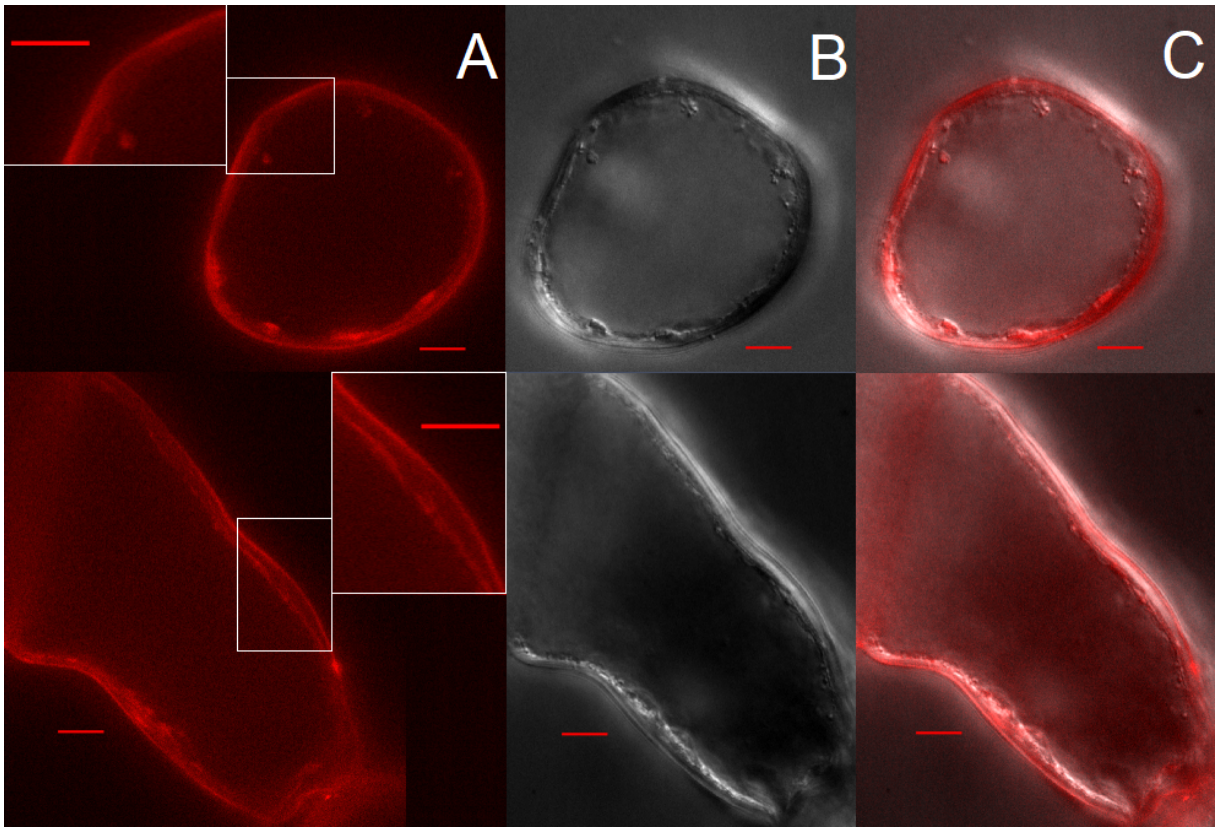


**Fig. 3.9: Subcellular localization of paclitaxel in *Taxus***
Two cells of *Taxus* production phase after double-immunofluorescence staining. A: RFP channel with detail magnification, B: DIC, C: merged RFP and DIC.
(Scale bars represent 10 µm.)

### 3.1.3 Nile red as marker for paclitaxel

Since immunofluorescence staining has shown that paclitaxel is localized in the area of cell wall and cell membrane, the lipophilic dye Nile red was tested as a marker for paclitaxel production. Cells from growth, production and bioreactor samples were stained with Nile red as described in 2.4.

Figure 3.10 shows an example of the result of Nile red staining for the growth phase (figure 3.10 A), the production phase (figure 3.10 B) and the bioreactor sample (figure 3.10 C). There is a minor difference between growth and production culture. The staining of the cells in production medium is slightly stronger. In the bioreactor sample about half of the cells are unstained, the remaining cells have a very strong color, which can be seen even in the bright field image, where the colored cells are very dark.

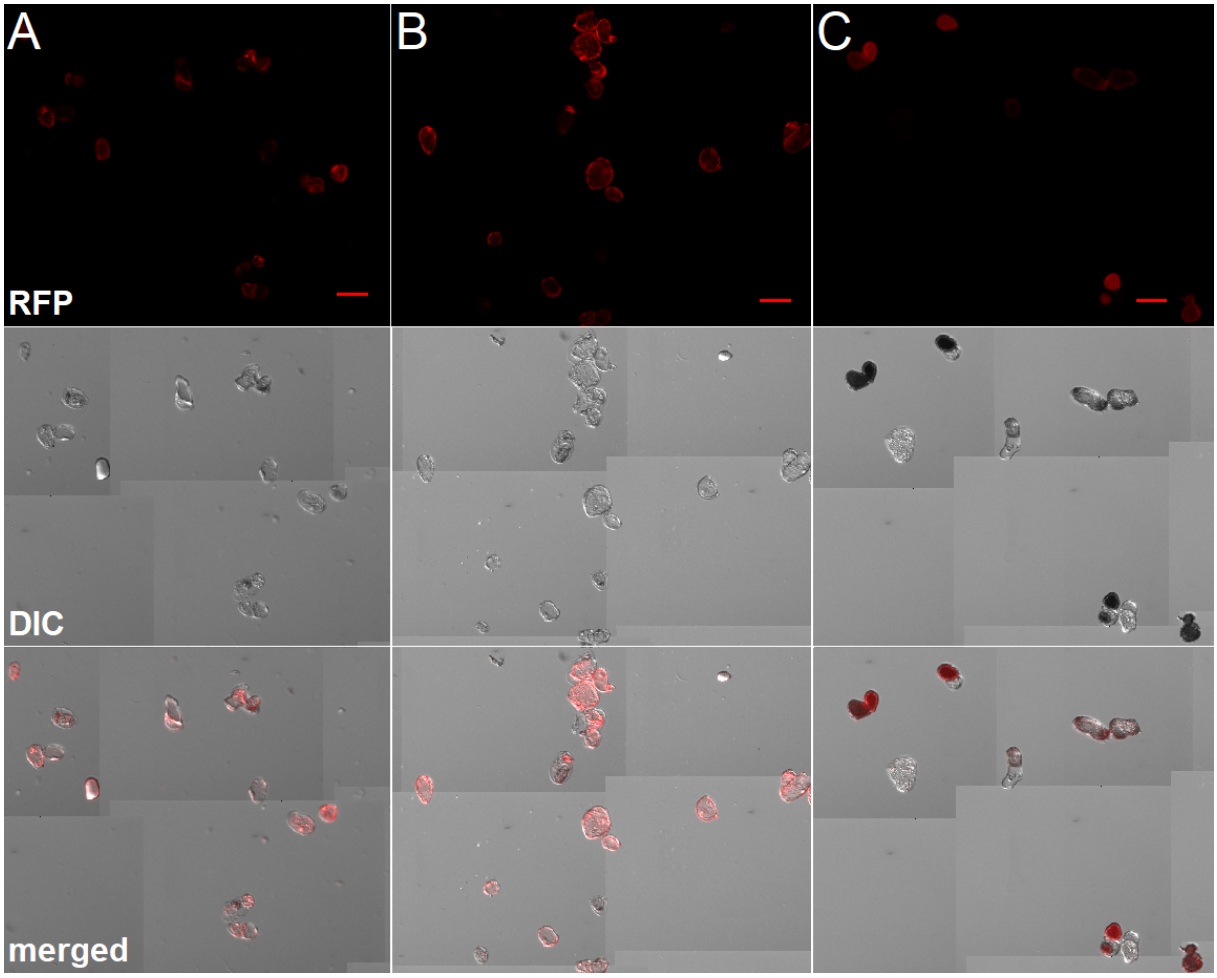


**Fig. 3.10: Overview images of Nile red stained *Taxus* cells**
A: Growth phase cell culture. B: Production phase culture. C: Bioreactor sample. Upper panel: RFP channel, middle panel: DIC, lower panel: merged RFP and DIC.
(Scale bars represent 100 µm.)

Figure 3.11 shows stained cells of the respective samples in larger magnification. It is notable that the Nile red pattern is very similar to the immunofluorescence staining, since the dye is mainly located in two rings in the area of cell wall and membrane. The intensity of the fluorescent signal is slightly higher in production than in growth phase. In the bioreactor sample, the staining is very strong throughout the cell.

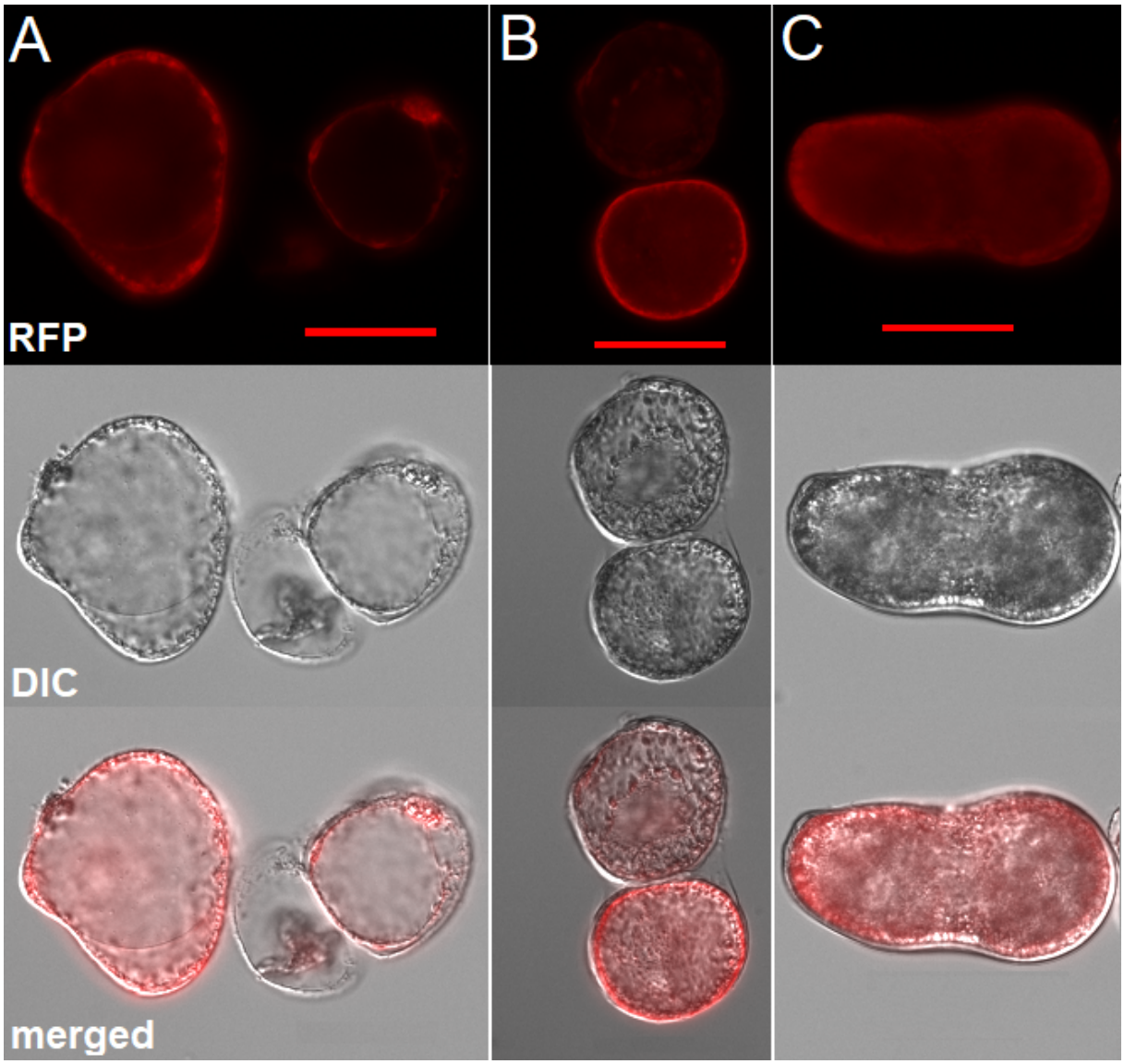


**Fig. 3.11: Nile red stained *Taxus* cells**
A: Growth phase. B: Production phase. C: Bioreactor. Upper panel: RFP channel, middel panel: DIC, lower panel: merged RFP and DIC.
(Scale bars represent 50 µm.)

### 3.1.4 *Taxus* shiny cell study

The following section is about investigation of the shiny cell type observed in microscopic studies. It describes the change in the percentage of shiny cells after different treatments and the relationship between shiny cells and production of secondary metabolites and gene expression

#### Number of shiny cells increases in production culture over time

Figure 3.12 shows the abundance of shiny cells in *Taxus* production culture where this phenotype was first observed. The number of days stands for the time point after the transfer to production medium. After 8 days in production medium, the proportion of shiny cells is 6 % and increases to 28 % by day 13.

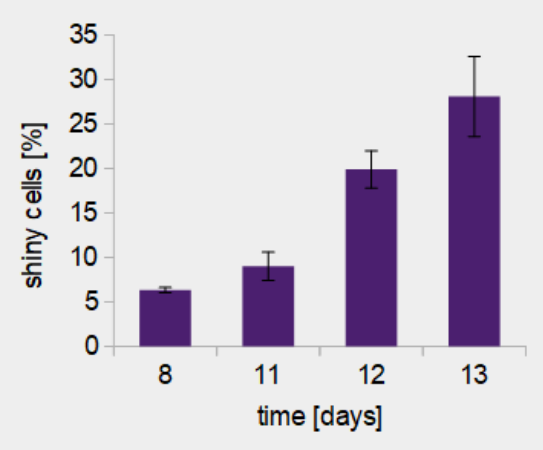


**Fig. 3.12: Proportion of shiny cells in production medium**
Emergence of shiny cells at certain time points after transfer to production medium. Data represents the average of three technical replicates.
Error bars indicate ±SE.

#### *Taxus* shiny cells decrease after driselase treatment

Since the shiny cell phenotype was first detected in driselase-treated samples, *Taxus* growth phase cells were treated with the enzyme and the number of shiny cells subsequently quantified every 15 minutes. This should determine if the digestion causes the appearance of the shiny cells and if the shininess is just an optical phenomenon. The experiment was performed on cells of different ages (day 1 and day 6) to determine if the response to driselase treatment depends on the cell cycle. Figure 3.13 illustrates the result of this experiment. Prior to the treatment, the number of shiny cells is around 7 % and decreases continuously over the measurement period, down to approximately 2 % after 45 minutes. The day 1 sample shows a slightly higher level of shiny cells compared to the day 6 sample, but the trend is the same.

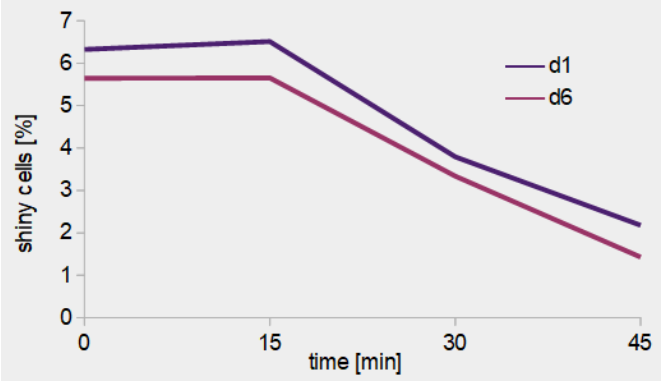


**Fig. 3.13: Shiny cells after driselase**
Development of number of shiny cells after digestion with 0.25 % driselase in cell cultures of different ages.

## *Taxus* shiny cell study after elicitation

It was already known that shiny cells occur in large numbers in the production medium and less in the growth phase. To elucidate the background of the formation of these cells, treatments were performed with different elicitors and the number of shiny cells was quantified on days 1, 3 and 6 after treatment. This way it should be tested, whether the formation of shiny cells is stress related. Since the previous experiment showed that shiny cells are sensitive to the driselase treatment, a digestion for the quantification was omitted.

In a first pilot study different concentrations of $AlCl_3$ (10, 50 and 100 µM) were added to the cells. $AlCl_3$ causes an oxidative burst and actinbundling in plants by activation of ROS (reactive oxygen species) production by the NADPH oxidase RboH (respiratory burst oxidase homolog). The results are shown in figure 3.14 A. For each data point, 20 microscopic images were evaluated. As the cell density increases during the cell cycle, the number of cells evaluated varies between 600 and 2300. The values for day 1 are therefore subject to large variation. The values for day 3 show no trend On day 6 it is clearly visible that the number of shiny cells increases with the concentration of $AlCl_3$. Since MeJA is known as an effective elicitor for alkaloid production, treatment with 100 µM MeJA was also performed in the pilot study and evaluated on day 3 (figure 3.14 B). MeJA is a stress related phytohormone involved in plant defense. There is a remarkable increase in the number of shiny cells compared to the control.

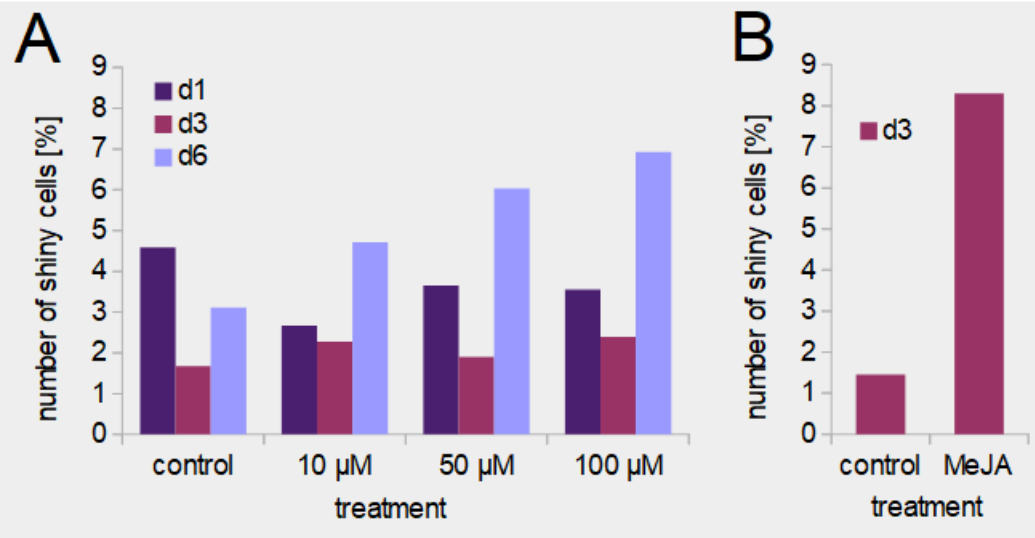


**Fig. 3.14: Shiny cell quantification after $AlCl_3$ and MeJA treatment**
A: Percentage of shiny cells after treatment with 10, 50 and 100 µM $AlCl_3$. B: Percentage of shiny cells after treatment with 100 µM MeJA. Data represents one biological replicate, with 600 to 2300 evaluated cells per data point.

Since $AlCl_3$ and MeJA showed great potential to increase the number of shiny cells in the pilot study, these elicitors were used for further investigation. In concentrations of 100 µM they were added to the cells combined and separated. In addition, picloram (10 µM) and $AgNO_3$ (10, 50 and 100 µM) were used as elicitors since auxins are known to promote cell growth and inhibit cell differentiation, while $AgNO_3$ acts as an antagonist to the plant hormone ethylene. In case of silver nitrate, a high level of cell mortality was found in some samples, even at low concentrations, and was therefore not considered for further study. Since some elicitors used are not soluble in water, a respective solvent control was conducted, which served as an internal standard. The values for the treatments are normalized to the values for the solvent control. Figure 3.15 shows the results of the experiment and gives the factor of increase in shiny cells compared to the corresponding internal standard. Each treatment was carried out in three biological replicates and at least 4000 cells were evaluated for each data point.

The treatment with picloram leads to a severe inhibition of the formation of shiny cells especially 6 days after the treatment. Addition of MeJA leads to an early increase in shiny cells by a factor of around 1.5 and remains relatively stable over the observation period. In case of $AlCl_3$ the effect becomes clear after six days. A combination of MeJA and $AlCl_3$ leads to an early and strong increase. In the further course, the proportion of shiny cells decreases again.

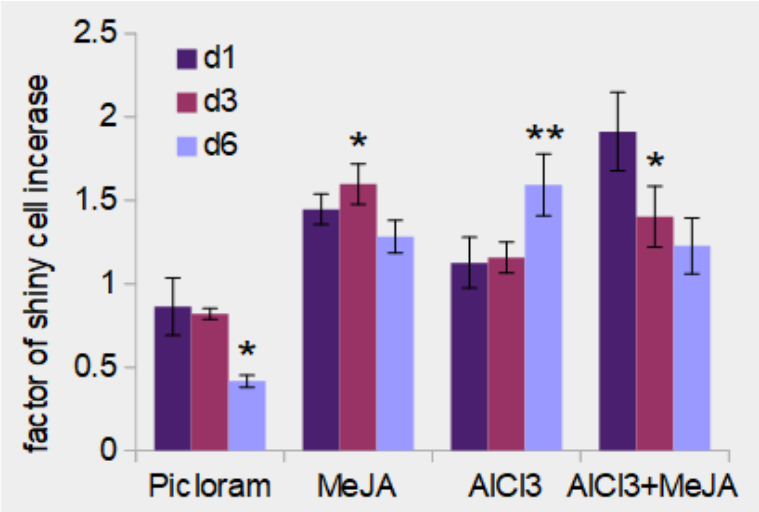


**Fig. 3.15: Shiny cell increase after picloram, MeJA and $AlCl_3$ elicitation**
Factor of increase of shiny cells after treatment with picloram (10 µM), MeJA (100 µM) and $AlCl_3$ (100 µM) over time. Error bars indicate ± SE. Statistically significant differences to the respective internal standard are indicated by one or two asterisks above the bars (student's *t*-test, *: $p < 0.05$, **: $p < 0.01$).

To shed light on the causes of the formation of the shiny cells, a second set of experiments was carried out. MeJA and $AlCl_3$ from the first set were combined with salicylic acid (SA) and diphenyleneiodonium (DPI). SA is antagonistic to MeJA while DPI blocks the NADPH oxidase RboH so there is no formation of ROS and no subsequent oxidative burst or actinbundling. For this reason, DPI is antagonistic to $AlCl_3$. The idea of the experiment was to find out if DPI and SA could reverse the MeJA and $AlCl_3$ induced formation of shiny cells. Figure 3.16 illustrates the results of this second set of experiments which was also conducted in three biological replicates with at least 4000 evaluated cells per data point.

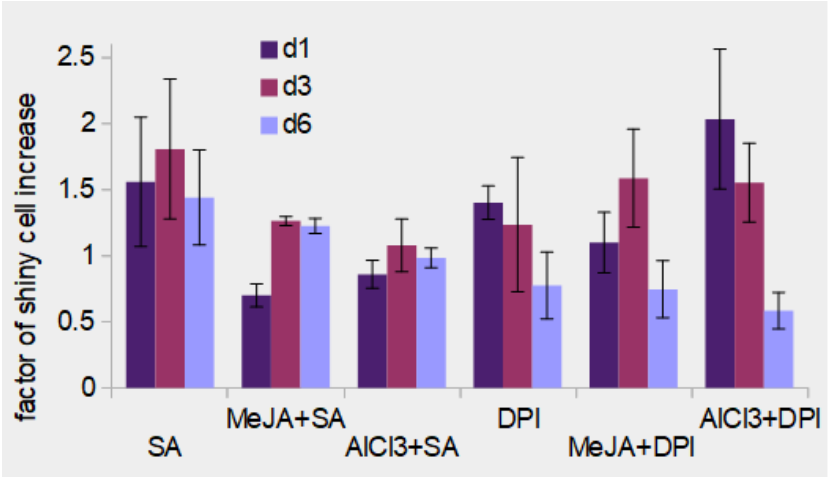


**Fig. 3.16: Change in shiny cell frequency after combination of elicitors**
Factor of increase of shiny cells after treatment with SA (100 µM), DPI (20 µM) and their combination with MeJA and $AlCl_3$ over time. Error bars indicate ± SE.

Figure 3.17 shows the comparison between the two data sets (figure 3.15 and 3.16). An ANOVA analysis followed by a Tukey HSD post-hoc test was used to test whether the course of the shiny cell number from day 1 to day 6 differs between the treatments. For this purpose, differences were calculated from the values of day 6 and day 1. There was a significant difference between the course of $AlCl_3$ and the course in the combination of $AlCl_3$ and DPI, whereas DPI alone showed no significant difference. Between the MeJA treatment and the combined MeJA and SA treatment no significant difference could be found in the course of shiny cell number. This result shows that treatment with DPI can actually block the effect of $AlCl_3$.

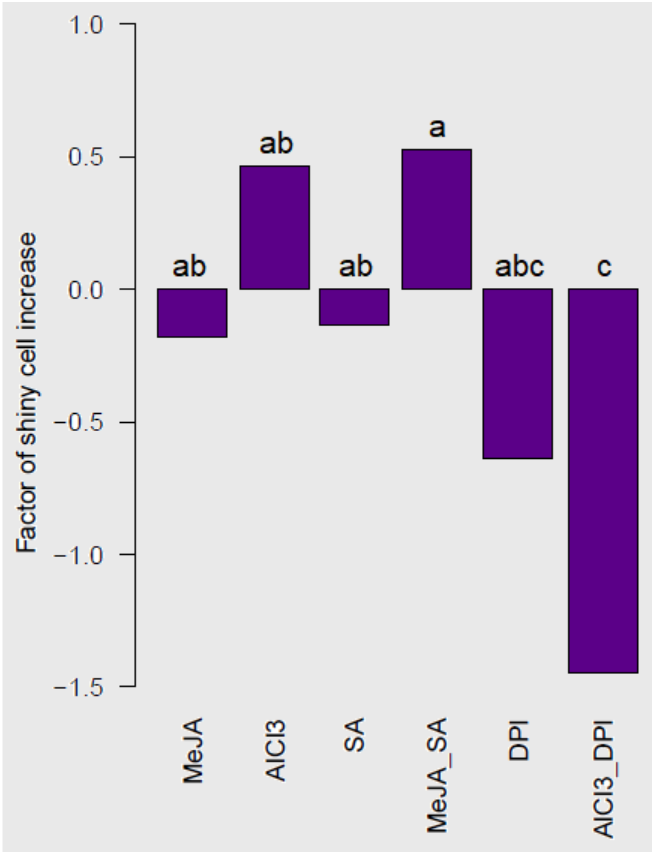


**Fig. 3.17: Change in the course of shiny cell number after combined elicitor treatments**
Comparative summary of data from figure 3.15 and 3.16.
ANOVA analysis followed by Tukey HSD post-hoc test to check for significance over time of the shiny cell number between different treatments.
Different letters indicate statistically significant differences.

### 3.1.5 Quantification of secondary metabolites via HPLC

To determine whether the number of shiny cells is linked to the production of secondary metabolites, their extraction followed by HPLC was performed on the cells after completion of the shiny cell quantification on day 6. Figure 3.18 summarizes the results of the HPLC analysis. Paclitaxel was not detected in any sample. In some samples the paclitaxel precursor baccatin III and the paclitaxel analouge baccatin VI could be measured. Baccatin III was detected in several samples, including the control. While the baccatin III levels in the treatments do not exceed the control values, there is a clear correlation between MeJA treatment and production of baccatin VI. MeJA induces baccatin VI production most effectively, when administered alone.

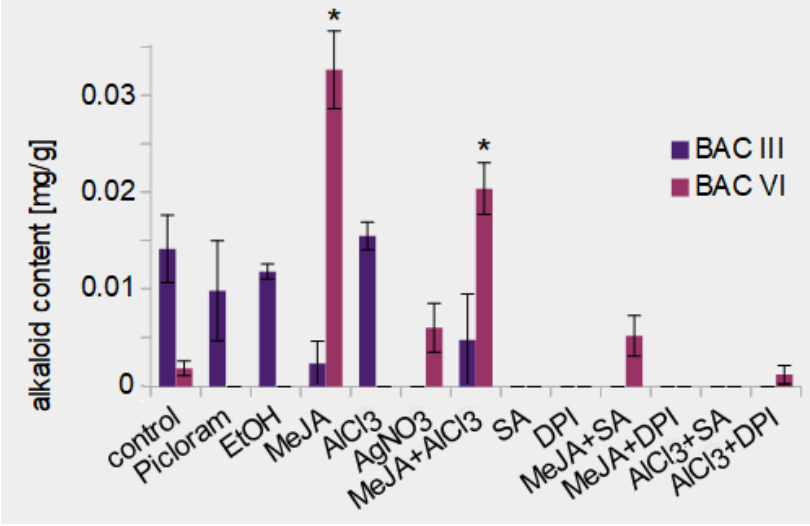


**Fig. 3.18: Content of secondary metabolites in the shiny cell study**
Amount of baccatin III and baccatin VI at day 6 after the treatment. Content of compounds is given in mg/g dry weight. Error bars indicate ± SE.
Statistically significant differences to the control are indicated by an asterisk above the bar (student's *t*-test, *: $p < 0.05$).

### 3.1.6 qPCR analysis of paclitaxel biosynthesis genes

In order to investigate whether the change in the amount of shiny cells results in a change in gene expression, an expression analysis of 4 different paclitaxel biosynthetic genes (*tasy*, *t5αh*, *dbat* and *dbtnbt*), located in different parts of the pathway, was performed by qPCR. RNA extraction and cDNA synthesis were carried out as described in 2.8. The primers used for this analysis are listed in Table 2.12. Since auxin and $AlCl_3$ had the greatest effect on the proportion of shiny cells among all treatments performed, these treatments were selected for gene expression analysis. The cells were transferred to auxin and $AlCl_3$ containing medium on day 0, respectively. Untreated auxin-free cultures served as control. Samples were taken at day 3 and day 6 for gene expression analysis. Samples taken at day 0 prior to the treatment were used as calibrator. Normalization was achieved by the housekeeping genes *maturase* and *18S rRNA*.

Three biological replicates with three technical replicates each were used for evaluation. Data was analyzed as described under 2.10. The results of qPCR analysis are shown in figure 3.19.

Treatments with auxin did not significantly affect the expression of the selected genes. Differences between time points and treatment and control do not show any pattern. Auxin is obviously not regulating the expression of the genes under investigation, which is also indicated by the high error bars (figure 3.19 A). $AlCl_3$ seems to slightly induce the expression of *tasy* and *dbat* at d6, while *dbtnbt* is downregulated at this time point (figure 3.19 B).

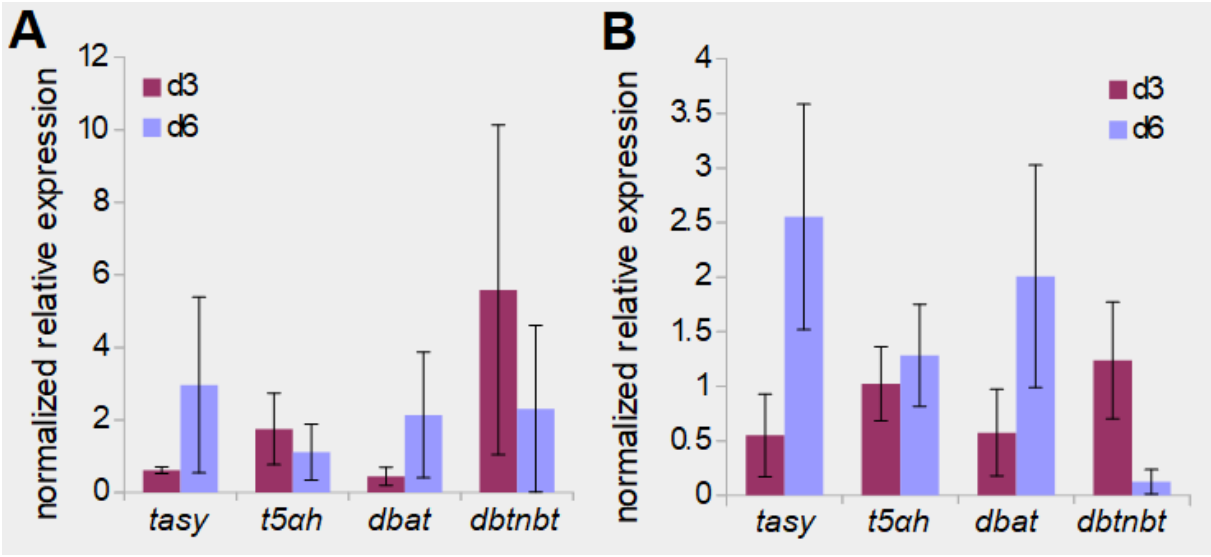


**Fig. 3.19: Results of gene expression analysis in *Taxus* by qPCR**
A: Normalized relative expression of paclitaxel biosynthesis genes after treatment with auxin. B: Normalized relative expression of paclitaxel biosynthesis genes after treatment with $AlCl_3$. The genes studied are *tasy* (*taxadiene synthase*), *t5αh* (*taxadiene 5α hydroxylase*), *dbat* (*10-deacetylbaccatin III-10-O-acetyltransferase*), and *dbtnbt* (*3'-N-debenzoyl-2-deoxytaxol-N-benzoyltransferase*). *Maturase* and *18S rRNA* are the housekeeping genes used. Untreated samples at d0 were used as calibrator. Error bars indicate ± SE.

### 3.1.7 Summary *Taxus*

The aim of this part of the work was to clarify, whether there are cellular markers for paclitaxel production to predict whether a cell line will yield high amounts. It should also be shown whether there is a relationship between shiny cells and paclitaxel production and what mechanism underlies the formation of shiny cells. The experiments performed on *Taxus* cell cultures resulted in the following main findings:

- Immunofluorescence staining showed localization of paclitaxel at the cell wall and membrane.
- Staining with Nile red showed a similar pattern. Intensity of the staining showed a dependency on paclitaxel production and that some cells in the bioreactor were undyed and therefore probably not very active.
- Treatments with MeJA clearly stimulated the production of shiny cells and baccatin VI.
- While auxin had a strong inhibitory effect on the number of shiny cells, there was no significant effect on the expression of the biosynthetic genes or production of secondary metabolites.
- Aluminum chloride did not affect the production of secondary metabolites but slightly induced expression of *tasy* and *dbat* after 6 days of treatment. It also had an enhancing effect on the number of shiny cells, which was inhibited by the administration of DPI.

## 3.2 Work on cell cultures of *Catharanthus roseus*

The subsequent section of the results chapter deals with the work performed on *Catharanthus* cell cultures. Phenotypic aspects of the two cell cultures Cath 001 and Cath 004 are compared as well as their growth behavior, metabolic potential, differences in gene expression and the effect of various elicitor treatments on alkaloid production.

### 3.2.1 Phenotyping of *Catharanthus roseus* cell cultures Cath 001 and Cath 004

In this work, two cell lines of *Catharanthus roseus* were used, designated Cath 001 and Cath 004, which differed widely in phenotype, growth behavior, and metabolic potential. Both cell lines form aggregates in liquid culture. The aggregates of Cath 004 are much larger than those of Cath 001, which is clearly visible, when looking at the cell material in the filter during the weekly cell transfer (figure 3.20), where Cath 001 is characterized by a smooth fine structure, while Cath 004 is granular and coagulative.

**Fig. 3.20: Structure of cell material of two *Catharanthus* cell lines**
Uniform and fine structure of the yellowish white cell material of Cath 001 (left) and the coarser, grainy structure of the slightly darker cell material of Cath 004.

The difference in size of the aggregates is more evident when examined microscopically, where it also becomes clear that higher number of cells as well as larger cell size play a role in the size of aggregates (figure 3.21).

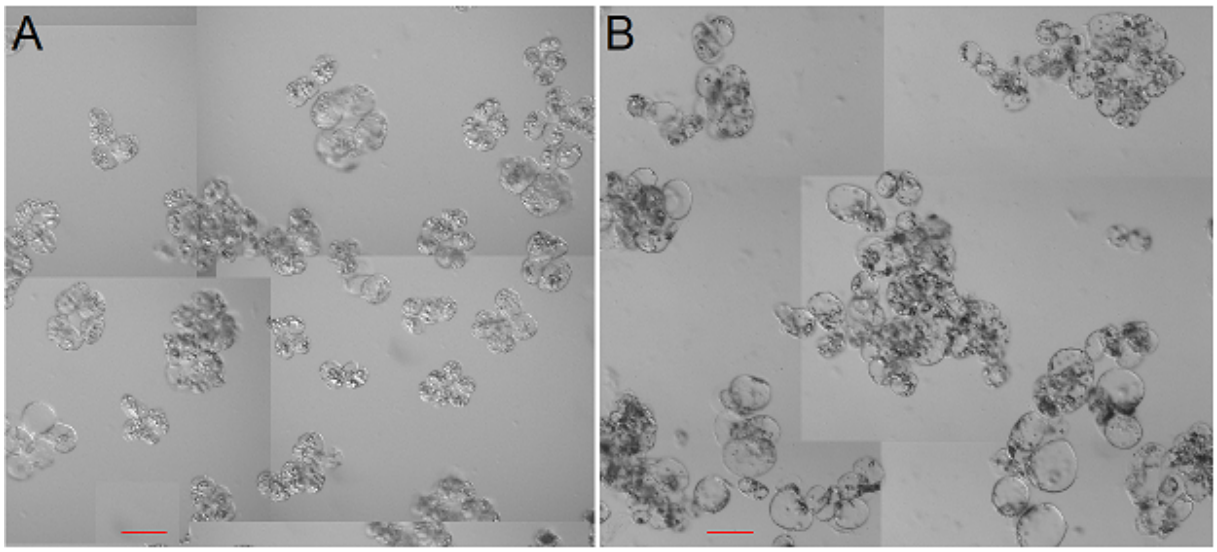


**Fig. 3.21: Microscopic images of cell aggregates of Cath 001 and Cath 004**
A: Cell aggregates of Cath 001 with smaller and fewer cells. B: Cell aggregates of Cath 004 with more and larger cells.
(Scale bars represent 100 µm.)

## *Catharanthus* cell growth and cell cycle

Various aspects of cell growth and division have been studied in comparison between Cath 001 and Cath 004 and summarized graphically in figure 3.22. Figure 3.22 A shows the growth index 7 over 5 months for two cultures with different subcultivation days for both cell lines. The growth index was determined on the basis of the fresh weight after 7 days as part of the regular cell transfer. It can clearly be seen that the weekly increase in fresh weight for Cath 004 is much higher, although it fluctuates widely, while the increase in Cath 001 is lower but much more stable.

The measurements of cell size for Cath 001 and Cath 004 are shown in figure 3.22 B. Each data point shows the mean of at least 500 cells. The cells of the Cath 004 cell line are significantly larger. Cell length and width are on average 54.6 and 43.8 µm for Cath 001 and 67.7 and 52.8 µm for Cath 004, respectively. Assuming that the cell shape is approximately a cylinder, this means that the volume of Cath 004 cells is on average 1.6 times larger than that of Cath 001. With regard to the development of the cell size over time, the result is similar to that of growth index 7. Cath 004 shows larger values but also larger fluctuations. Although the changes in Cath 004 are more obvious, the course is approximately the same for both cell lines. Cell size increases first, then around day 4, there is a rapid decline until day 6, whereupon it is quite stable for three days before returning to a rise lasting four to five days, followed by another decrease. The course is delayed by a day or two in Cath 001 from day 8 onwards.

For both cell lines the cell number was determined over a cultivation period of 15 days. In order to get an impression of the division activity in a smaller volume, as it is used for the experiments with the microfluidic chip, 15 wells of a 24 well plate were filled with 800 µl of cell suspension each on day 0 and counted on the appropriate days. The results are shown in figure 3.22 C (Cath 001) and 3.22 D (Cath 004). The average length of cell cycle was calculated as described in 2.2.3. For this purpose, only the values from day 0 to day 7 were used, since this period corresponds to the weekly cell transfer. Obvious outliers were not taken into account. This resulted in an average doubling time of 4.8 days for Cath 001 and 4.2 days for Cath 004. While these values were fairly close, the doubling time of the cells cultured in the well plate was 8.2 days for Cath 001 and 2.6 days for Cath 004. Thus, the cell division activity of Cath 004 is higher in the smaller volume in the well plate, while the same conditions have a clearly negative effect on the cell cycle of Cath 001. There are also clear differences between Cath 001 and Cath 004 in the time course of the cell number. On day 0, the cell number for both lines is quite similar. While Cath 004 shows a fourfold increase in cell number over the measurement period, the number of cells increases sevenfold in the case of Cath 001. The peak for Cath 004 appears already on day 9, while the highest values for Cath 001 were counted on day 13.

Fresh and dry weight were determined for both cell lines over a period of 15 days and the results summarized in figure 3.22 E and 3.22 F. The fresh weight shows an exponential course for Cath 004 until day 8, followed by a plateau phase, with only minor changes. The increase in fresh weight in Cath 001 is much slower and smoother with small jumps between day 5 and day 6 as well as day 12 and day 13. The fresh weight values correlate with the values for cell number. For the dry weight there is a reverse situation compared to the fresh weight. Here, the values of Cath 001 are much higher than those of Cath 004 over the entire measurement period. In contrast to the fresh weight, the dry weight profile is very similar for both cell lines. In both the values increase evenly until day 8/day 9 whereupon there is a decrease. The much slower increase of Cath 004 dry weight, compared to the fresh weight suggests that the rapid increase in fresh weight is mainly due to cell growth by water uptake rather than cell division. This is confirmed by the values of cell measurement and cell counting. The decrease in dry weight towards the end of measurement period also indicates a high water content in both cell lines.

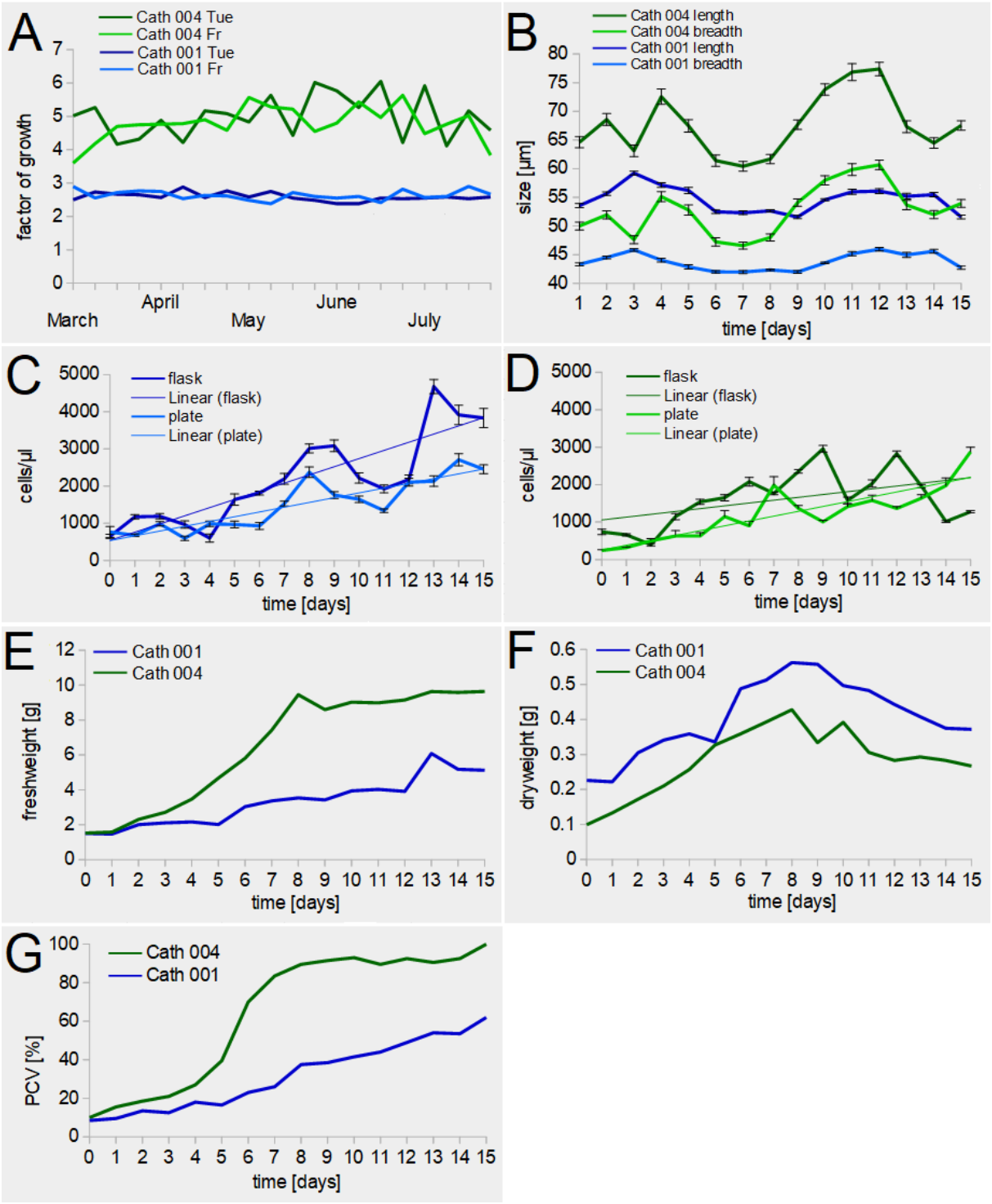


**Fig. 3.22: Phenotypic parameters of *Catharanthus* cell lines regarding cell growth and division**

A: Growth Index 7 of two independent *Catharanthus* cell cultures for Cath 001 and Cath 004, respectively assayed over 5 months from March to July 2018 based on the fresh weight at the day of subcultivation. B: Measurement of Cath 001 and Cath 004 cell size over time. Each data point represents an average of at least 500 cells. Error bars indicate ±SE. C: Cell counting of Cath 001 over time in flask cell culture and in 800 µl of cell suspension cultivated in a well plate. Regression line was inserted. Each data point represents an average of 5 technical replicates. Error bars indicate ±SE. D: Cell counting of Cath 004 over time in flask and plate with regression line. Each data point represents an average of 5 technical replicates. Error bars indicate ±SE. E: Fresh weight of Cath 001 and Cath 004 over time. F: Dry weight of Cath 001 and Cath 004 over time. G: PCV over time. Data represents an average of two technical replicates.

Figure 3.22 G shows the PCV for both cell lines over a 15-day period. While the course for Cath 001 is nearly linear, there is an exponential phase for Cath 004 between day 4 and 7 after a slow increase until day 4, followed by a plateau phase. The highest value for Cath 001 is 62 % on day 15, while Cath 004 reaches over 80 % on day 7 and 100 % on day 15.

## Faster sugar consumption in Cath 001

The sugar content in the medium of Cath 001 and Cath 004 liquid cell cultures was measured over a 15 day period using brix refractometer. The results are shown in figure 3.23. In the medium of Cath 001, the sugar concentration drops sharply after a short time, especially from day 3. Already on day 6, the sugar content has dropped to a barely detectable level. In contrast, the sugar content in Cath 004 medium decreases much slower. There is only a decline starting from day 4, which then continues less rapidly compared to Cath 001 until day 8, after which it stabilizes at a value around 0.5 %.

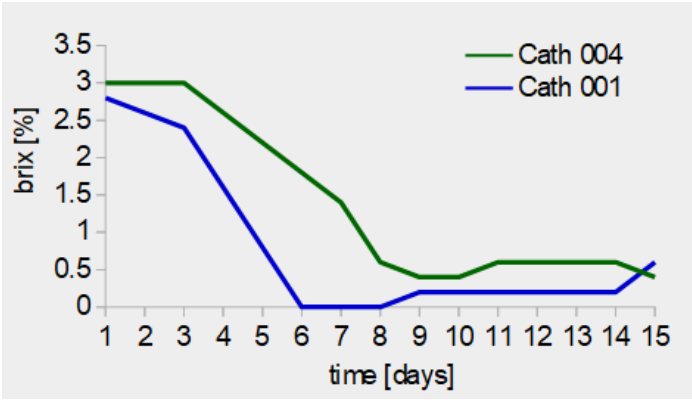


**Fig. 3.23: Sugar content in *Catharanthus* cell culture medium**
Sugar content of Cath 001 and Cath 004 cell culture medium over time measured in brix.

## Visualization of subcellular compartments by transient transformation

For comparison of subcellular compartments between Cath 001 and Cath 004 transient transformation was conducted with different constructs labeling actin, golgi apparatus, peroxisomes and tonoplast, respectively. Further information on the constructs used, are given in Table 2.2 in the materials and methods section. Representative microscopic images are shown in figure 3.24. At the qualitative level, there are no salient differences. It seems that actin and tonoplast are a little more structured in Cath 001, whereas peroxisomes appear to be more abundant in Cath 004.

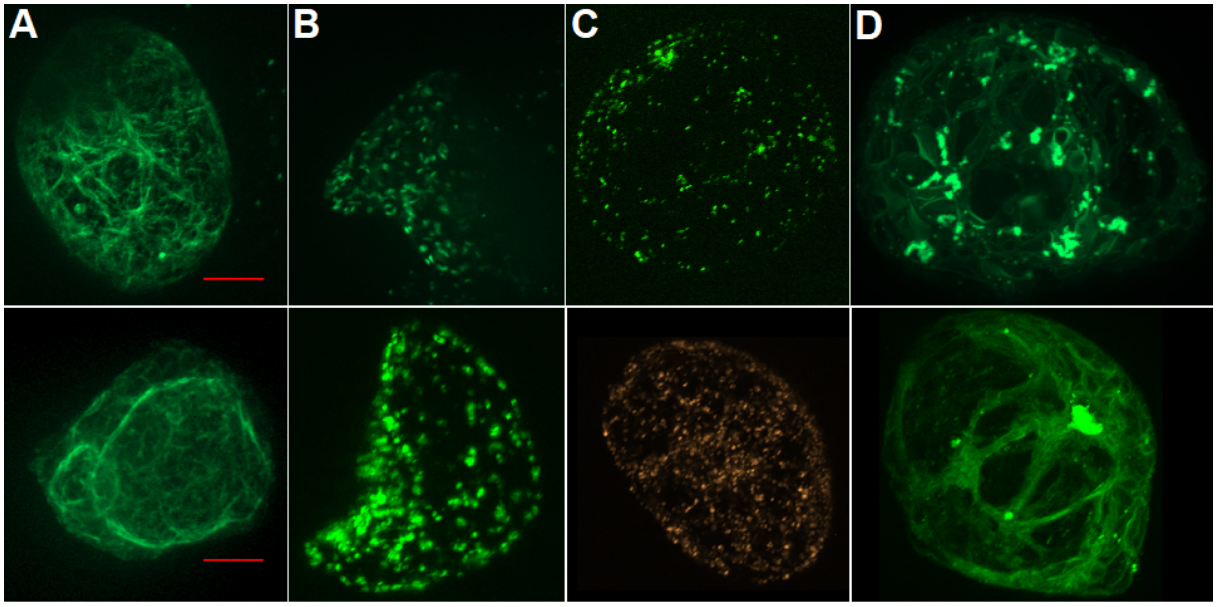


**Fig. 3.24: Transient transformation of Cath 001 and Cath 004 by gene gun**
Visualization of some subcellular compartments in Cath 001 (upper panel) and Cath 004 (lower panel). A: Labeling of actin by FABD2-GFP. B: Labeling of golgi by ST-GFP. C: Labeling of peroxisomes by Peroxi-YFP. D: Labeling of tonoplast by GFP-coupled NtTPC1A.
(Scale bars represent 10 µm.)

## Comparative mitochondria shape analysis

To investigate differences in energy level between Cath 001 and Cath 004, cells were stained with Mito Tracker Red FM and z-stack images taken for analysis of mitochondrial shape and coverage. The mitochondria in *Catharanthus* showed similar pattern like in *Taxus* and were therefore classified in the same categories, which are shown in figure 3.25.

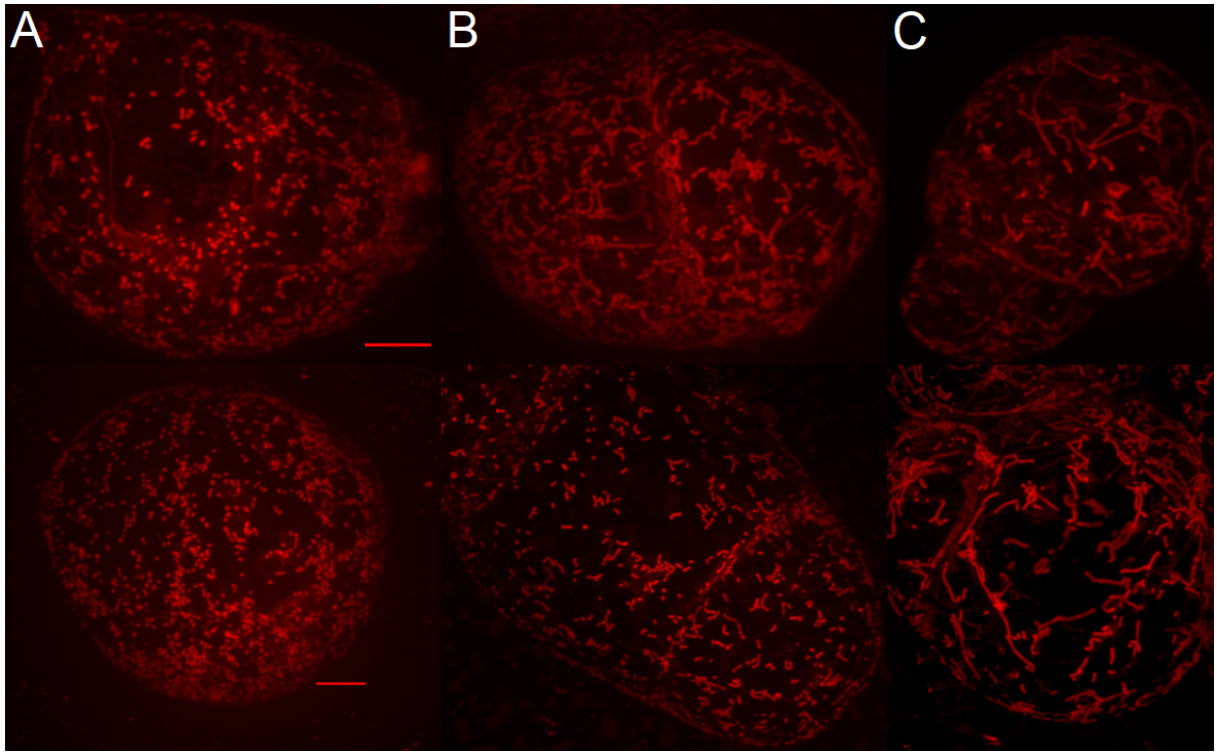


**Fig. 3.25: Categories for mitochondrial shape in *Catharanthus***
Z-stack images of optical sections of *Catharanthus* cells stained with Mito Tracker Red FM and the name of categories. Upper panel: Cath 001; lower panel: Cath 004. A: Dots: punctuated mitochondria, B: Lines: elongated mitochondria, C: Mesh: elongated and connected mitochondria.
(Scale bars represent 10 µm.)

Figure 3.26 shows the development of the mitochondrial shape over 15 days comparing between Cath 001 (figure 3.26 A) and Cath 004 (figure 3.26 B). In Cath 001, the dot pattern is dominant and its proportion is at least 40 % on each day examined. On day 7 it reaches 80 %. Calculating the average of all Cath 001 cells examined, it makes up 66 %. The mesh pattern, on the other hand, hardly appears. It has a maximum of 20 % on days 8 and 9. On days 3, 4, 14 and 15, it does not appear at all. Over the course of time, the dot pattern continuously increases until day 7, displacing the line and mesh pattern. Then it comes to a drop in the dot pattern until day 10, whereupon it rises again. In Cath 004, this course is similar. However, the dot pattern is less dominant from the beginning. It is around 49 % over the entire study period. In Cath 004 the line and mesh pattern are more common than in Cath 001. Also in Cath 004 there is an increase in the dot pattern, which reaches a plateau of 60 % between day 4 and 8 and then drops to 20 % on day 10, whereupon it rises again. In summary, the course in both *Catharanthus* cell lines is similar, but in the case of Cath 004 there is a shift towards the line and mesh pattern.

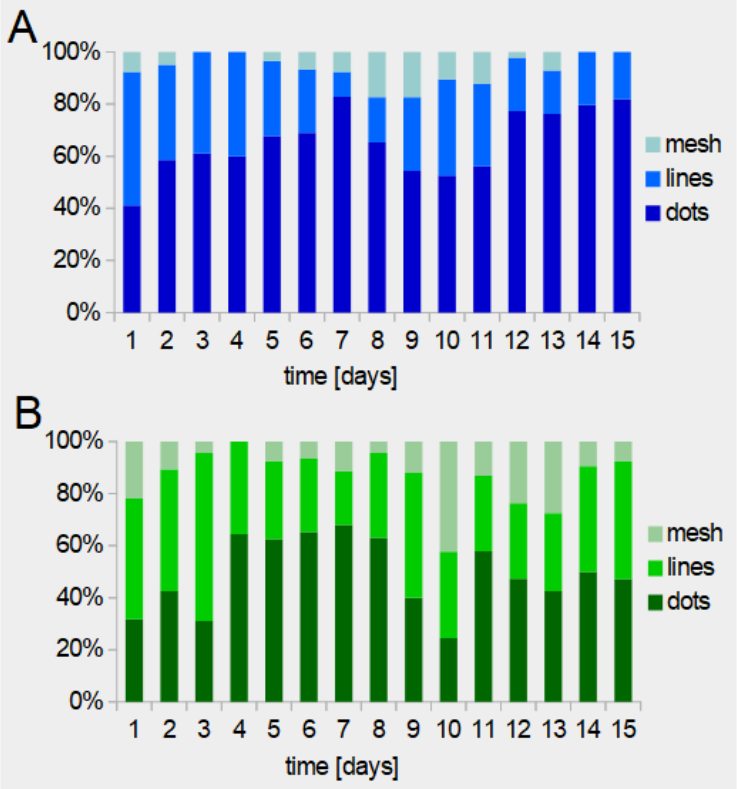


**Fig. 3.26: shape of mitochondria in *Catharanthus* cells over time**
A: Shape of mitochondria in Cath 001 with 38 to 59 analyzed cells per data point. B: Shape of mitochondria in Cath 004 with 38 to 53 analyzed cells per data point.

## Mitochondria quantification

In addition to the shape, the amount of mitochondria was also compared between Cath 001 and Cath 004. Figure 3.27 shows the results of this study. To quantify the mitochondria, the proportion of the cell they cover is expressed as a percentage. The microscopic images used for this study were the same as those used to analyze the mitochondrial shape. Overall, both cell lines show an irregular course in mitochondrial coverage. There are many outliers in both directions. A comparison of individual measurement points therefore is not conclusive. Considering the overall course of both curves in comparison, there is still a clear difference between Cath 001 and Cath 004. Especially when looking at the regression line, it becomes clear that the amount of mitochondria in Cath 001 is much higher compared to Cath 004 at the beginning, but decreases very fast and rapidly to a level well below that of Cath 004 at the end of the measurement period, while the amount of mitochondria in Cath 004 remains relatively constant over the entire measurement period, with a slight decrease.

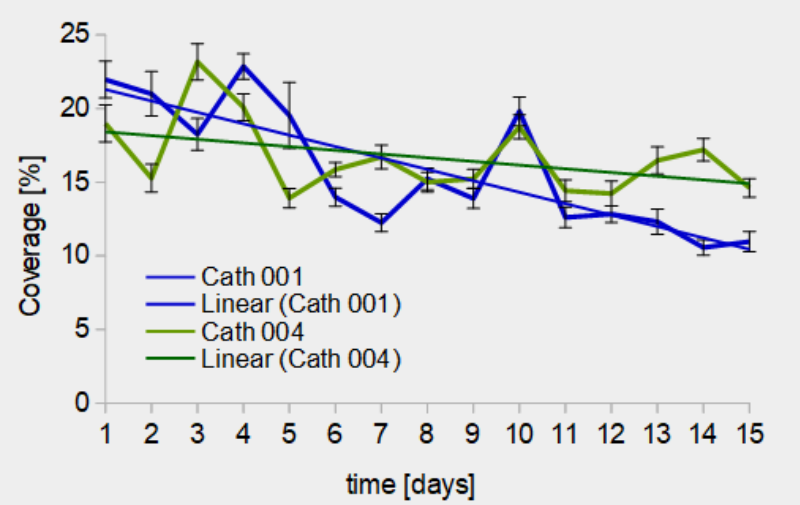


**Fig. 3.27: Quantification of mitochondria in Cath 001 and Cath 004 over time**
Percentage of mitochondrial coverage in Cath 001 (38 to 59 cells analyzed per data point) and Cath 004 (38 to 53 cells analyzed per data point). Error bars indicate ± SE. Regression lines were inserted.

### 3.2.2 Comparative gene expression analysis of important vinca alkaloid biosynthesis pathway genes in Cath 001 and Cath 004 by semi-quantitative RT-PCR and qPCR

After investigating the growth behavior and phenotypic properties, the expression of important vinca alkaloid biosynthesis genes should also be analyzed. Again, comparison was made between Cath 001 and Cath 004 – first by semi-quantitative RT-PCR and then for a smaller selection of genes also by qPCR.

### Gene expression analysis of vinca alkaloid biosynthesis pathway genes by semi-quantitative RT-PCR

For the gene expression analysis by semi-quantitative RT-PCR samples were taken from day 1 to day 7 of the culture cycle, RNA extracted and transcribed into cDNA. The genes analyzed were *g10h* (*geraniol 10-hydroxylase*) of the seco-iridoid pathway, *as* (*anthranilate synthase*) and *tdc* (*tryptophan decarboxylase*) of the indole pathway, *str* (*strictosidine synthase*) and *sgd* (*strictosidineβ-D-glucosidase*) of the connective pathway, *t16h1* (*tabersonine 16-hydroxylase 1*), *t16h2* (*tabersonine 16-hydroxylase 2*), *d4h* (*desacetoxyvindoline 4-hydoxylase*) and *dat* (*deacetylvindoline 4-O-acetyltransferase*) of the vindoline pathway and *prx1* (*peroxidase 1*) combining vindoline and catharanthine. *Exp* (*expressed protein*) was used as reference gene. Figure 3.28 shows the results of the semi-quantitative RT-PCR. The reference gene *exp* was expressed continuously strong in all seven days of the cell cycle in both cell lines with stronger expression in Cath 001. The expression of *g10h* was strong from day 2 to day 6 and slightly lower at day 1 and 7 in Cath 001, while it was very strong in Cath 004. The

expression of *as* was uniformly strong in Cath 001 while it was a little weaker in Cath 004 where it also showed an increase until day 3, followed by a decrease until day 7. For *tdc* the expression was equally strong on all days and stronger in Cath 004 compared to Cath 001. *str* and *sgd* showed a higher expression in Cath 001 and were expressed equally on all days except for *str* in Cath 001 where it showed an increase over time. *T16h1* was expressed evenly moderate in Cath 004, while there was a higher level of expression for Cath 001 at days 4, 6 and 7. The expression of *t16h2* was weak in cell line Cath 001 with a stronger expression at day 3, while a very weak expression could be detected in Cath 004 at days 2, 3 and 7. For *d4h* and *dat* no expression could be detected in Cath 001. In Cath 004, a very weak expression signal was found for *d4h* on days 3, 5, 6 and 7 and a comparably weak signal for *dat* on days 3, 4 and 7. *Prx1* was expressed continuously strong in Cath 001 and with a much weaker signal and an increase over time in Cath 004.

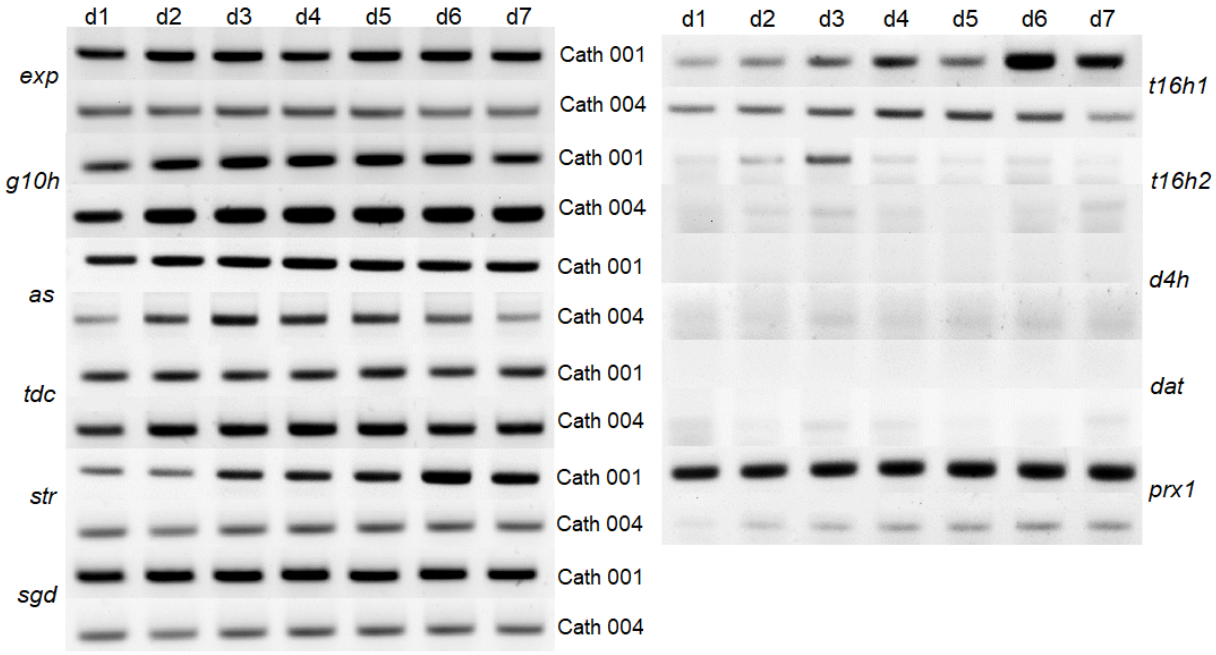


**Fig. 3.28: Expression profile of Cath 001 and Cath 004 TIA biosynthesis pathway genes**
Expression was analyzed for Cath 001 and Cath 004 at days 1 to 7 of the cultivation cycle. Genes under investigation are *g10h* (*geraniol 10-hydroxylase*), *as* (*anthranilate synthase*), *tdc* (*tryptophan decarboxylase*), *str* (*strictosidine synthase*), *sgd* (*strictosidine β-D-glucosidase*), *t16h1* (*tabersonine 16-hydrolxylase 1*), *t16h2* (*tabersonine 16-hydrolxylase 2*), *d4h* (*desacetoxyvindoline 4-hydroxylase*), *dat* (*deacetylvindoline 4-O-acetyltransferase*), and *prx1* (*peroxidase 1*). *Exp* (*expressed protein*) served as houskeeping gene.

In summary, it can be said that the genes studied are relatively strongly and uniformly expressed up to the vindoline pathway, whereas there are large deficits in the expression of the genes within the vindoline pathway. Visible differences in gene expression between Cath 001 and Cath 004 were found in the genes *as*, *tdc*, *str*, *sgd*, *t16h1* and *prx1*. Weak expression was found in Cath 004 for *dat* and *d4h* on some days, while it was not detected in Cath 001.

## Gene expression analysis of certain TIA biosynthesis pathway genes by qPCR

To confirm the differences found for Cath 001 and Cath 004 in expression of numerous TIA biosynthesis genes by semi-quantitative RT-PCR, qPCR was performed for selected genes (*str*, *t16h1*, *d4h*, *prx1*). The housekeeping genes used in this study are *exp* and *rsp9*. As the study was performed on untreated samples, there was neither a calibrator nor a control. Therefore, the efficiency-adjusted normalized expression of Cath 004 was related to Cath 001. For better assessment of the differences, the data is presented as a binary logarithm. Three biological replicates, each with three technical replicates, were used for the study. Results of the gene expression analysis are shown in figure 3.29.

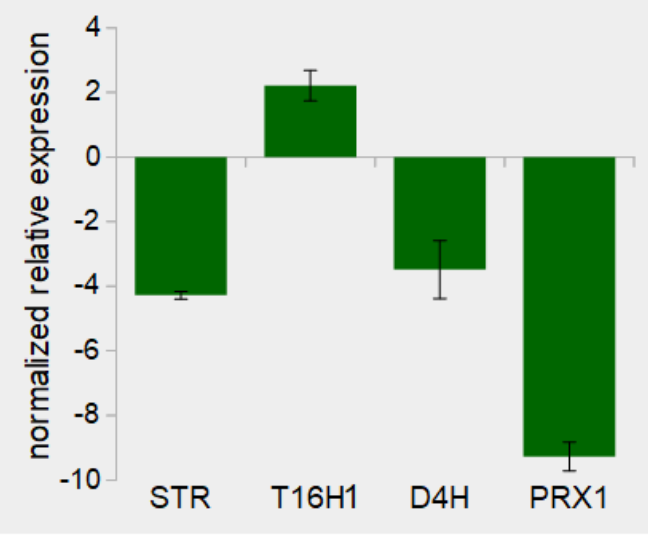


**Fig. 3.29: Results of qPCR analysis of Cath 001 and Cath 004**
Normalized relative expression of TIA biosynthesis genes in Cath 004 compared to Cath 001 at day 6 of the subcultivation cycle. The genes studied are *str* (*strictosidine synthase*), *t16h1* (*tabersonine 16-hydrolxylase 1*), *d4h* (*desacetoxyvindoline 4-hydroxylase*), and *prx1* (*peroxidase 1*). *Exp* and *rsp9* served as housekeeping genes. Error bars indicate ± SE.

Results of the qPCR confirmed that *prx1* expression is much stronger in Cath 001 than in Cath 004. The stronger expression of *str* is also clearly visible. However, the expression of *d4h* in Cath 001 was also elevated compared to Cath 004, although no

*d4h* expression was observed in semi-quantitative PCR for Cath 001. *T16h1* on the other hand shows a slightly stronger expression in Cath 004 than in Cath 001 although semi-quantitative PCR suggested otherwise. In summary, there is a notable difference between Cath 001 and Cath 004 in expression of the investigated genes even under control conditions.

### 3.2.3 Metabolic potential, elicitation and precursor feeding of Cath 001 and Cath 004

After characterizing the phenotypic properties and expression of the vinca alkaloid pathway genes, the metabolic potential and effect of elicitors and precursors on various properties of Cath 001 and Cath 004 cell line should be investigated. The elicitors used were various phytohormones, such as JA and MeJA, which are important in the stress response, as well as NAA and kinetin, artificial auxins or cytokinins, which play a role in growth regulation. In addition, various concentrations of sucrose were used, which serves as a carbon source in the medium of the cells. In addition, the precursors tabersonine and vindoline, which were not formed by the cells or in small quantities, were administered, to see whether downstream biosynthetic products are formed.

#### Decreasing viability of *Catharanthus* cells after elicitor and precursor treatments

In a first step, it was tested whether the treatments and solvents have an effect on the viability of the cells and whether this effect is different in Cath 001 and Cath 004. JA and MeJA were dissolved in ethanol, the precursors in methanol. Since Cath 004 trials sometimes included treatments with two precursors, two different methanol concentrations were tested. Since MeJA is volatile, the air-permeable filters in the culture bottles were closed with tissue paper and aluminum foil after the treatment. Therefore, it was also examined whether this measure affects the viability. The growth medium of the cells contains 2,4-D, a synthetic auxin. As the production of secondary metabolites occurs rather in the stationary phase, all experiments were performed in auxin-free medium. Therefore, it was checked whether the lack of auxin has an influence on the viability. The auxin-free sample is referred to as control, the auxin containing sample as 2,4-D. Due to the osmotic activity of sugars, the effect on viability of the various sucrose concentrations used was also tested. Since the results for Cath

004 listed below have shown an increasingly positive effect for various sucrose concentrations up to 60 g/l, higher sucrose concentrations were tested for this cell line and therefore their influence on viability was also determined. The results for Cath 001 are summarized in figure 3.30 A and C, those for Cath 004 in figure 3.30 B and D.

The viability for both cell lines was very high in auxin-containing medium and barely changed over time (figure 3.30 A and B). In auxin-free medium, however, the viability of Cath 004 visibly decreases to 93 % on day 6. The additional closing of the filters has a slight negative effect on Cath 001 and again lowers the viability on Cath 004. As a result of EtOH treatment, the viability of Cath 001 decreases from 97 % on day 1 to 89 % on day 6. Thus, Cath 001 is more sensitive to EtOH than Cath 004, where it drops only from 94 % to 90 % over the same period. The effect of MeOH on Cath 004 is lower than the effect of EtOH even at higher concentrations. As a result of the MeJA treatment, which summed up the effects of EtOH, closed filter, and hormone treatment, Cath 001 showed a reduction in viability from 96 % to 80 %, whereas Cath 004 remains quite stable with a decrease from 95 % to 90 %.

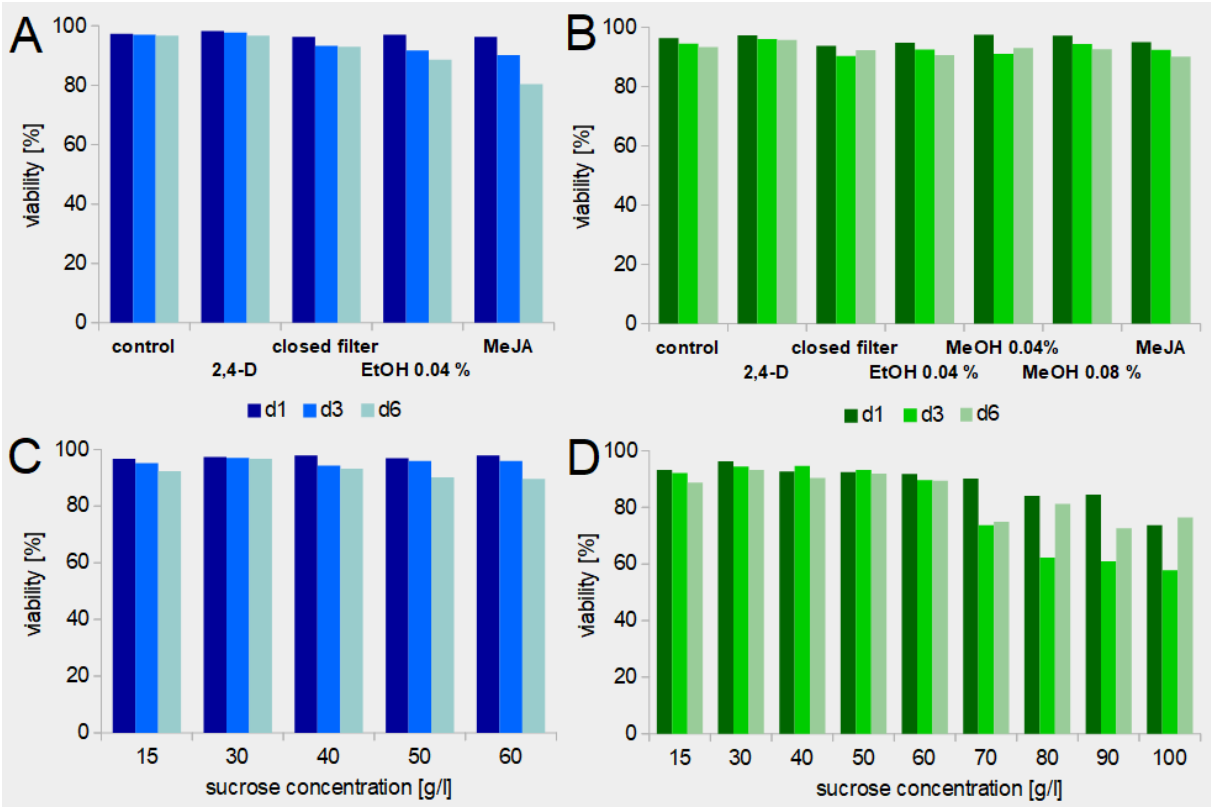


**Fig. 3.30: Effect of treatments and solvents on the viability of Cath 001 and Cath 004**
A: Viability of Cath 001 after treatment over time. B: Viability of Cath 004 after treatment over time. C: Viability of Cath 001 at different sugar concentrations. D: Viability of Cath 004 at different sugar concentrations.
Each data point represents the result of at least 300 evaluated cells.

In summary, the viability of Cath 004 is at a slightly lower level for untreated samples, but remains more stable than Cath 001 when treatments are given.

At different sucrose concentrations, the highest viability in both cell lines was found at 30 g/l, which corresponds to the sugar concentration present in the growth medium (figure 3.30 C and D). At 15 and 40 g/l there is a slight decrease in viability, which is more pronounced at 50 g/l and clearly visible at 60 g/l. It shows the same pattern as in the viability tests of the treatments and solvent controls – Cath 004 starts at a lower level, but remains more stable over time. At 60 g/l, the viability of Cath 001 decreases from 98 % to 90 % between day 1 and day 6, that of Cath 004 from 92 % to 89 %. If the sugar concentration in Cath 004 is increased further, there is a massive decline in viability. At 100 g/l sucrose, it is about 75 % on days 1 and 6 and down to 58 % on day 3.

## Alkaloid profile of Cath 001 and Cath 004 in growth and stationary phase

To determine and compare the alkaloid profile of Cath 001 and Cath 004, normal growth cultures were sampled in which the cells grew in presence of auxin. Cells and medium were separated by vacuum filtration and lyophilized. Subsequently, the alkaloids were extracted and analyzed by HPLC as described in 2.6. Standards for tryptophan, tryptamine, vindoline, catharanthine, vinblastine and vincristine were available for HPLC analysis. Among these alkaloids, catharanthine was the only one that could be detected in small amounts in Cath 004 by HPLC, in Cath 001 no alkaloids could be detected under these conditions.

Figure 3.31 shows the result of HPLC analysis for Cath 004. The amount of catharanthine in the cells increases visibly over time. In the supernatant, where the amount of catharanthine is much lower, the level remains about the same.

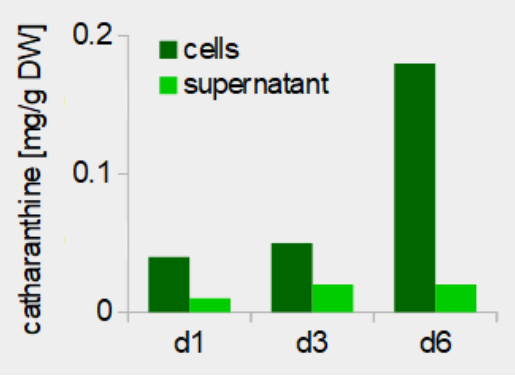


**Fig. 3.31: HPLC Profile of Cath 004 in growth medium**
Catharanthine content of Cath 004 in mg/g dry weight (after lyophilization) in cells and supernatant over time.

The alkaloid profile of Cath 001 and Cath 004 was also tested by LC-MS. The standards used for LC-MS are tabersonine, catharanthine, vindoline, vinblastine and vincristine. With this more sensitive but non-quantitative method catharanthine could also be detected in Cath 001 and, moreover, tabersonine was detected in both cell lines. Figure 3.32 shows a section of the MS spectra. Catharanthine and tabersonine both have a mass of 337. Catharanthine is detected at about 11.4 minutes, tabersonine after about 16.7 minutes. In the spectra of the other alkaloids there was only noise, which is why they are not shown here.

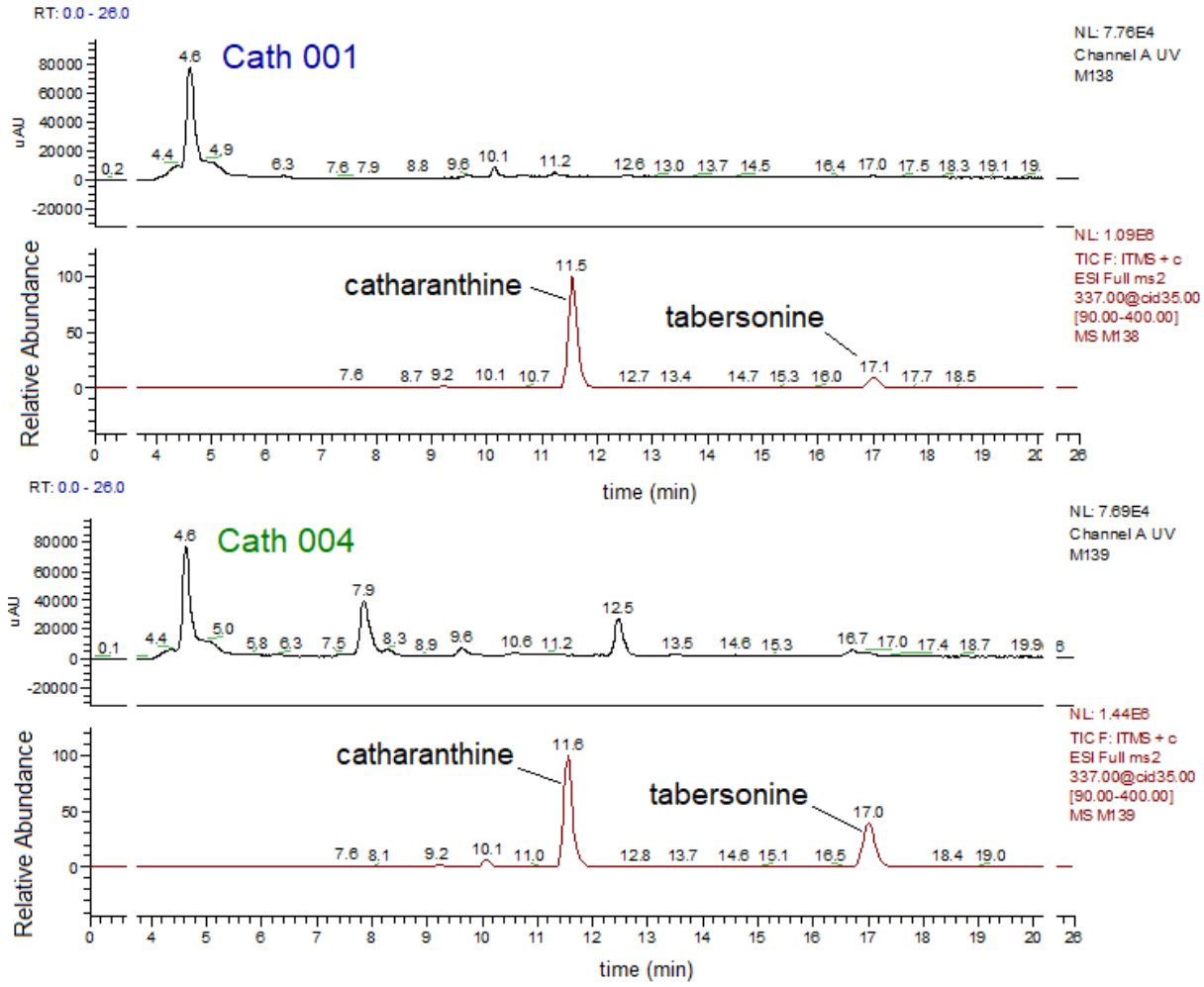


**Fig. 3.32: LC-MS profile of Cath 001 and Cath 004**
Section of the chromatogram of *m/z* 337 for Cath 001 (top) and Cath 004 (bottom). Labeled peaks are tabersonine and catharanthine, the corresponding retention times are given above.

In the next step, the alkaloid profile was determined by HPLC in the stationary phase of the cell cycle, which means in the absence of auxin. Since it has been shown that the alkaloid content increases over time, early, middle and late stationary phase were sampled (early: d1-d4, middle: d5-d7, late: from d8).

The results are given in figure 3.33. Again, Catharanthine was the only alkaloid among the standards that could be detected. This time small amounts could also be detected in Cath 001. For Cath 004, there was a clear increase over the amount in the auxin-containing growth medium. While the level was just under 0.2 mg/g in the presence of auxin on day 6, it is already 3 mg/g in the middle stationary phase. Again, an increase in the amount of catharanthine is detectable over time.

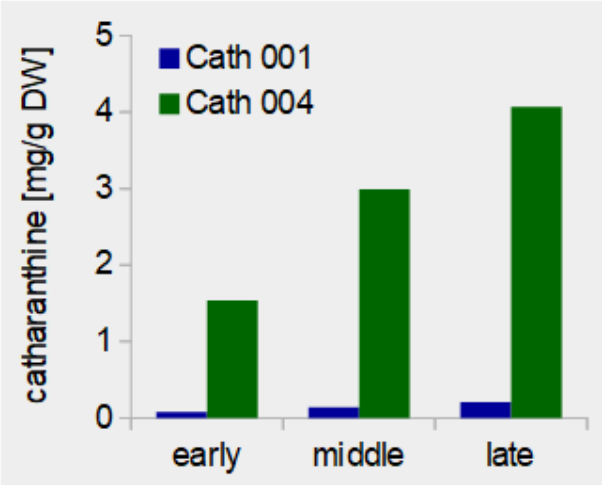


**Fig. 3.33: HPLC Profile of Cath 001 and Cath 004 in stationary phase**
Catharanthine content of Cath 001 and Cath 004 in mg/g dry weight (after lyophilization) in early (d1-d4), middle (d5-d7) and late (from d8) stationary phase.

## Elicitation with jasmonic acid increases catharanthine in Cath 004

For the JA treatment, the cells were transferred to auxin-free medium on weekly cell transfer and JA was added at a final concentration of 100 µM. Samples were taken in early, middle and late stationary phase for Cath 001 and Cath 004. The results of the HPLC analysis are shown in figure 3.34. Catharanthine was the only alkaloid present in detectable amounts in this experiment. For Cath 004 there is a clear increase of the catharanthine content compared to the control. The effect is especially clear in the early phase, where it increases by a factor of 4.5. In the middle phase, the addition of JA has more than doubled the catharanthine content compared to the control. Even in the late phase an increase over the control can be seen, but not quite as clear, since in the late phase the catharanthine content visibly decreases under JA treatment compared to the middle phase. At 7.7 mg/g, the highest value for Cath 004 under JA treatment was detected in the middle stationary phase. For Cath 001 only very low values of catharanthine were measured, which steadily decreased.

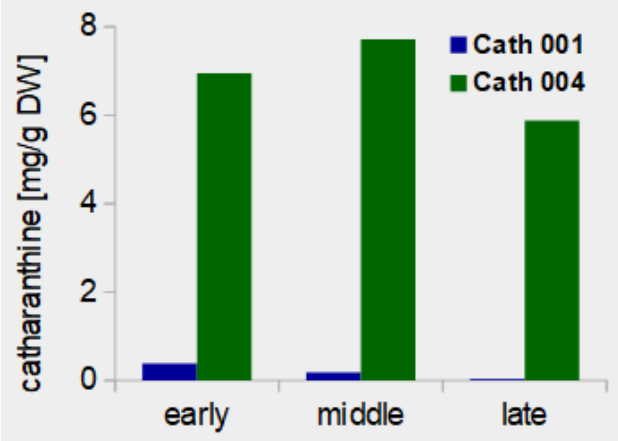


**Fig. 3.34: HPLC profile of Cath 001 and Cath 004 after JA elicitation**
Catharanthine content in Cath 001 and Cath 004 after treatment with 100 µM JA in mg/g dry weight in early, middle and late stationary phase.

In addition to the alkaloid content, the expression of the vindoline pathway genes *t16h1*, *t16h2*, *d4h* and *dat* was also investigated by semi-quantitative PCR, since very little or no expression was shown for these genes in the controls (figure 3.28). However, no appreciable change in expression was recorded.

Furthermore, the length and breadth of the cells were measured, and from this the volume as well as the aspect ratio were calculated in order to determine whether there was a rounding or elongation of the cells. In the case of Cath 001, the volume was much higher in the early stationary phase under JA treatment compared to the control, but then remained more or less constant instead of increasing as in the control. In Cath 004, on the other hand, the volume in both the control and the treatment increased, with the increase being slightly faster under the influence of JA. Cath 001 cells elongated under JA, while they rounded up in the control over time. In the case of Cath 004 the development was reversed. Instead of elongating as in the control, the cells remained round.

## Elicitation with MeJA strongly increases catharanthine in Cath 004

For treatment with MeJA, cells were transferred to auxin-free medium on weekly subcultivation and MeJA was added at a final concentration of 100 µM. The filters of the culture bottles were sealed with tissue paper and aluminum foil due to the volatility of MeJA. Since, in case of JA treatment, the catharanthine content increased sharply even in the early stationary phase and visibly declined in the late stationary phase (figure 3.34), and the viability of the cells was already visibly reduced on day 6 under MeJA treatment and also suffered slightly from closing the filters (figure 3.30), the MeJA

treated cells were sampled on days 1, 3 and 6 after the treatment instead of early, middle and late stationary phase.

The HPLC results of the MeJA treatment and the ethanol control for Cath 001 and Cath 004 are summarized in figure 3.35 A. In the ethanol control there is a slight increase in the catharanthine content for both cell lines. For the MeJA treatment, the content in Cath 001 rises slightly, while from day 3 there is a clear increase for Cath 004, which is approximately 10 mg/g dry weight on day 6, even exceeding the effect of JA.

Since the effect of MeJA was so severe on Cath 004, the MeJA treatment was repeated for this cell line in three biological replicates. The results of this experiment are shown in figure 3.35 B. The increase in the catharanthine content in response to MeJA is very similar to that in the first experiment, but reaches even above 11 mg/g at day 6.

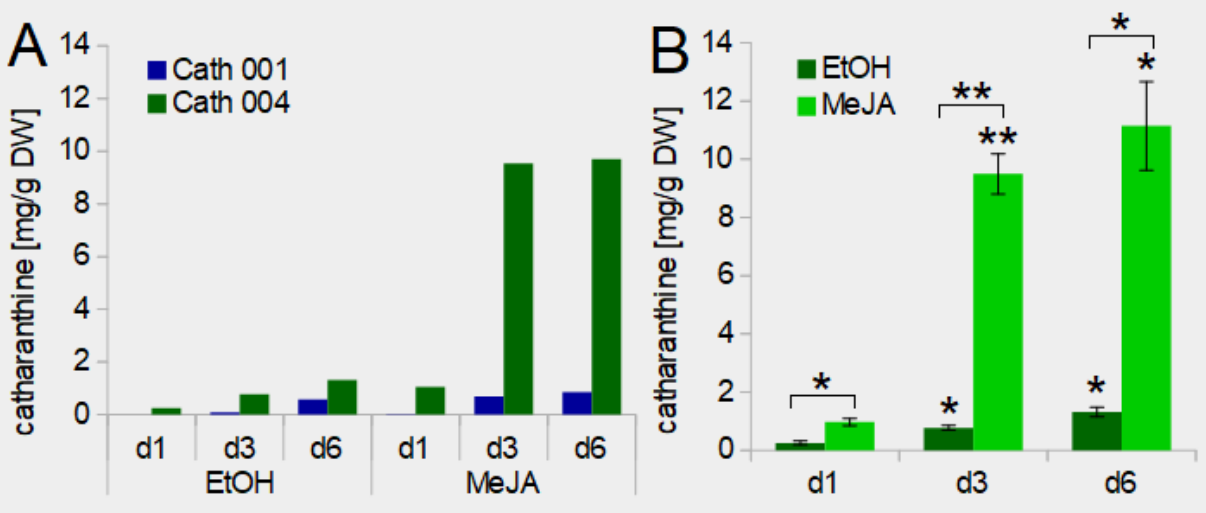


**Fig. 3.35: HPLC profile of Cath 001 and Cath 004 after MeJA elicitation**
A: Catharanthine content in the cell lines Cath 001 and Cath 004 after treatment with EtOH and MeJA in mg/g dry weight. B: Catharanthine content in Cath 004 after treatment with EtOH and MeJA. Each data point represents the average of three biological replicates. Error bars indicate ± SE. Statistically significant differences to the starting point (day 1) are indicated by one or two asterisks above the bar. Statistically significant differences between MeJA and the ethanol control are indicated by one or two asterisks above the bracket (student's *t*-test, *: $p < 0.05$, **: $p < 0.01$).

In the more sensitive non-quantitative LC-MS analysis tabersonine could be found in addition to catharanthine and even traces of vindoline. Figure 3.36 shows a section of the MS spectra. Catharanthine and tabersonine both have a mass of 337. Catharanthine is detected at about 11.4 minutes, tabersonine after about 16.7 minutes. The mass of vindoline is 457 and the retention time about 10.2 minutes. The spectra for the masses

of vinblastine (mass of 811, retention time of 10.8) and vincristine (mass of 825, retention time of 10.1 minutes) do not show defined peaks.

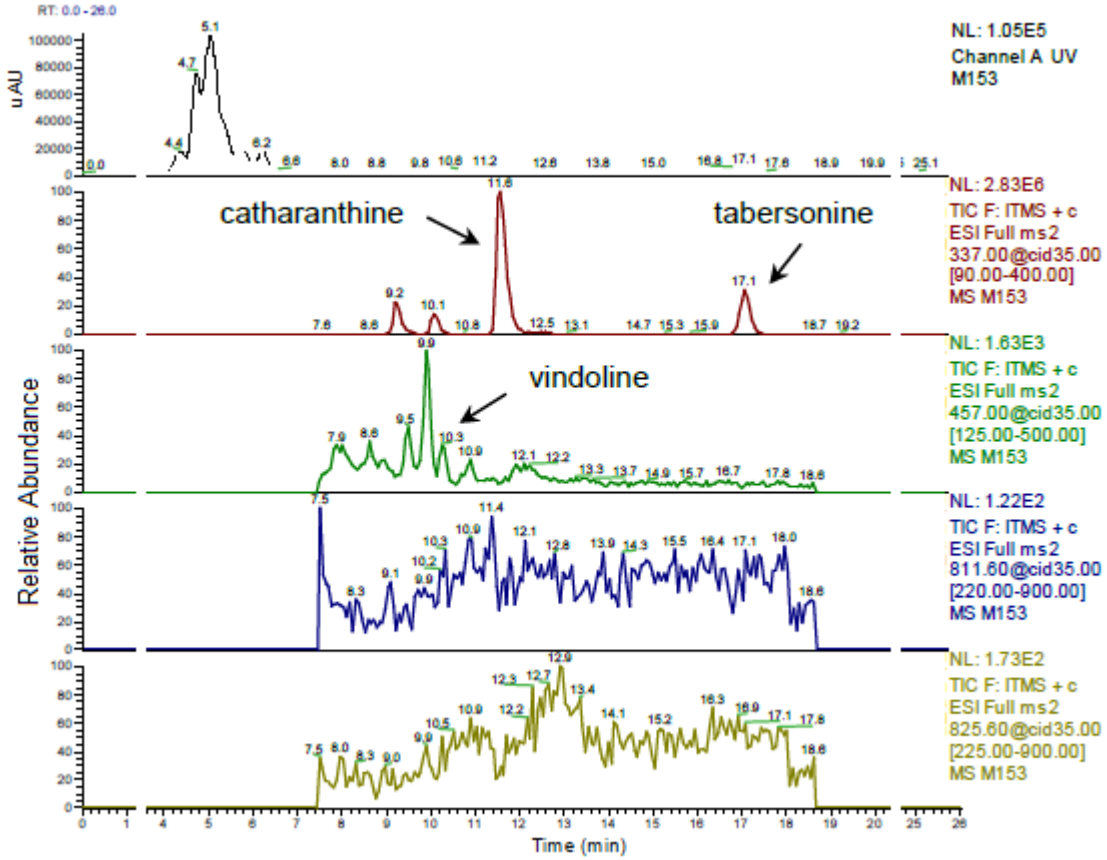


**Fig. 3.36: LC-MS profile of Cath 004 after elicitation with MeJA**
Section of the LC-MS chromatogram. Different masses are noted in different colors. Red: chromatogram of *m/z* 337 (catharanthine and tabersonine), green: chromatogram of *m/z* 457 (vindoline), blue: chromatogram of *m/z* 811 (vinblastine), yellow: chromatogram of *m/z* 825 (vincristine). Height of the peak indicates the relative abundance of a molecule, normalized according to the highest peak in each spectrum. Corresponding retention times are given above.

The examination of the expression of the vindoline pathway genes after MeJA treatment revealed that *t16h1* and *t16h2* are no longer expressed in Cath 001, while slight expression of *dat* was seen three and six days after the treatment. On day 6 there is a slight expression even in the ethanol control (figure 3.37).

For Cath 004 the expression of *t16h1* showed an increase at day 3 after MeJA, in *t16h2* there was a clear increase in expression by MeJA at every day tested. For *dat*, the control showed a very weak band for Cath 004, which is clearly pronounced on days 3 and 6 after the addition of MeJA, on day 6 also in the ethanol control (figure 3.37).

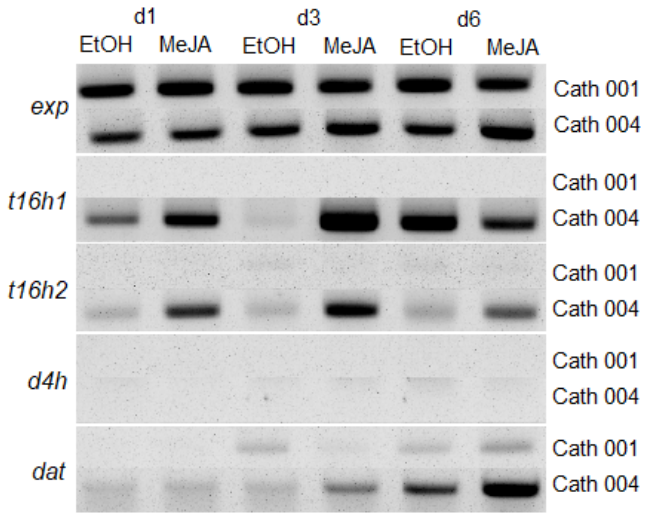


**Fig. 3.37: Gene expression profile of vindoline pathway genes after MeJA elicitation**
Semi-quantitative gene expression profile of *exp*, *t16h1*, *t16h2*, *d4h* and *dat* for Cath 001 and Cath 004 after MeJA elicitation on day 1, day 3 and day 6 after the treatment.

Concerning the aspect ratio and volume after MeJA treatment, Cath 001 cells elongate as in the control, but the volume is much lower. The Cath 004 cells are rounding up a little more compared to the control, the volume is much larger after the MeJA treatment.

## Sugar feeding slightly increases catharanthine in Cath 004

Since sucrose is the carbon source of *Catharanthus* cells, and terpenoid indole alkaloids are complex, carbon-rich compounds, the influence of varying sugar concentrations in stationary phase on alkaloid synthesis, gene expression, and cellular parameters was tested.

Auxin-free medium of different sugar concentrations was prepared and the cells were transferred to the appropriate medium on weekly cell transfer. The extraction of the alkaloids was conducted after 6 days.

Figure 3.38 shows the catharanthine content of the samples. Cath 001 has a slight increase with rising sugar concentration, but does not exceed 0.63 mg/g dry weight at 60 g/l sucrose (figure 3.38 A). In case of Cath 004, the increase with rising sugar concentration is much stronger. The highest value is found for 60 g/l and is 2.55 mg/g dry weight. If the sugar content of the medium increases further, however, there is a drop in the catharanthine content (figure 3.38 B).

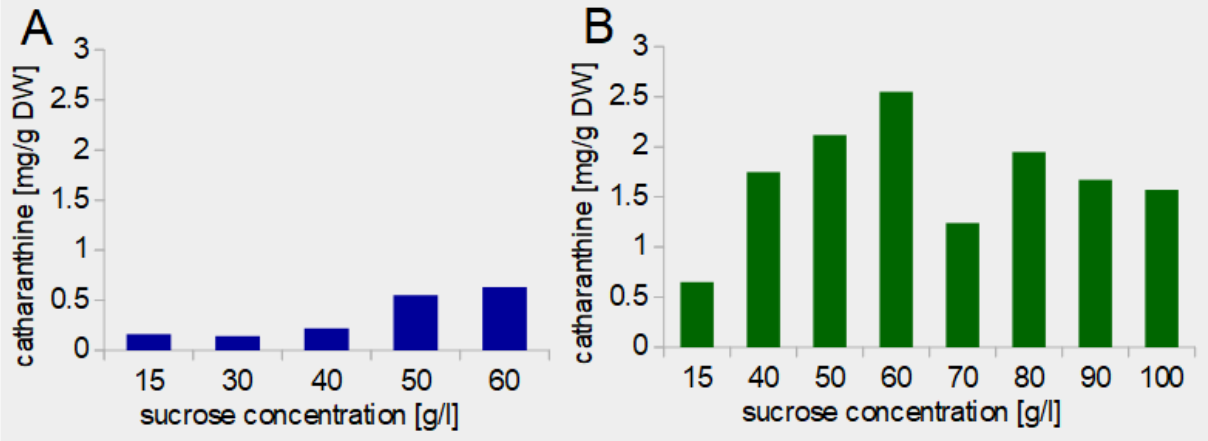


**Fig. 3.38: HPLC profile of Cath 001 and Cath 004 at different sucrose concentrations**
A: Catharanthine content of Cath 001 in mg/g dry weight after 6 days in stationary phase with sucrose concentrations between 15 and 60 g/l. B: Catharanthine content of Cath 004 in mg/g dry weight after 6 days in stationary phase with sucrose concentrations between 15 and 100 g/l.

In terms of gene expression of the vindoline synthesis genes, the increasing sugar concentration had no appreciable effect.

In LC-MS analysis, in addition to catharanthine, small amounts of tabersonine were found in all samples of Cath 001 and Cath 004, but non of the other vinca alkaloids for which standards were used in this study.

In case of Cath 001, the cells are rounding up at 30 and 40 g/l and elongate again at 50 and 60 g/l progressively over time. With Cath 004 there is an elongation over time at 15 and 40 g/l, whereas at the higher sucrose concentrations the cell shape remains very constant.

Concerning the volume, there is an opposite pattern. Here, the values for Cath 001 are mostly stable, with a strong increase of day 6 at 40 g/l, while the volume of Cath 004 cells decreases steadily with increasing sugar concentration, with a rapid progression from 70 g/l (figure 3.39). The development of the volume as response to the change in sucrose concentration correlates with the alkaloid content and the viability of the cells (figure 3.38, 3.30 C and 3.30 D).

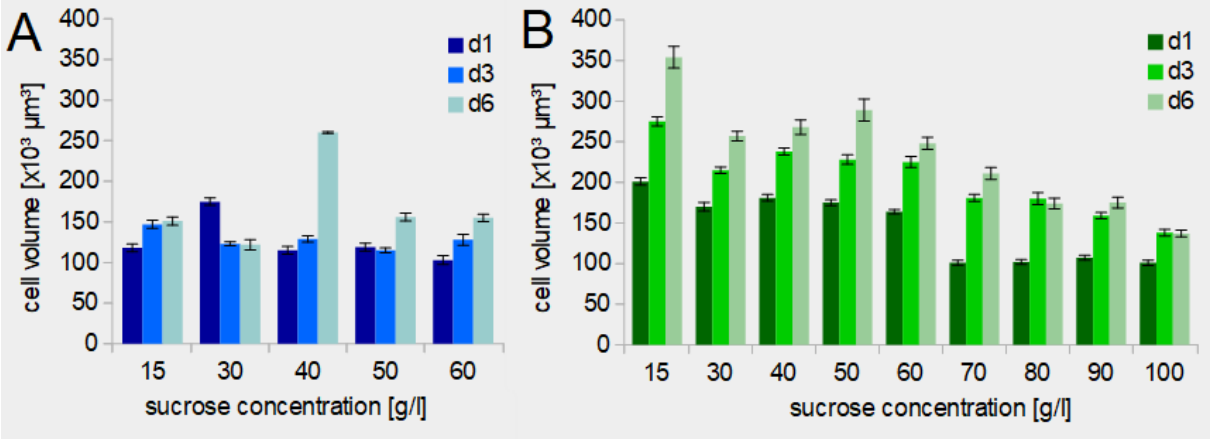


**Fig. 3.39: Cell volume of Cath 001 and Cath 004 at different sucrose concentrations**
A: Cell volume of Cath 001 in x10³ µm³ at day 1, 3 and 6 after addition to sucrose concentrations between 15 g/l and 60 g/l. B: Cell volume of Cath 004 in x10³ µm³ at day 1, 3 and 6 after addition to sucrose concentrations between 15 g/l and 100 g/l Each data point represents the average of at least 400 cells. Error bars indicate ± SE.

To determine whether a higher availability of sugar also leads to a higher consumption by the cells, sugar content in the medium was measured by brix refractometer at day 6. From these values the sugar consumption of both cultures was calculated (figure 3.40).

As with brix measurement over time in growth medium (figure 3.23), Cath 001 shows a much higher sugar consumption compared to Cath 004. In Cath 001, the sugar consumption increases up to a concentration of 40 g/l and then declines. In the case of Cath 004, there is an increase in sugar consumption up to a concentration of 60 g/l, which then decreases, but increases again at very high sugar concentrations.

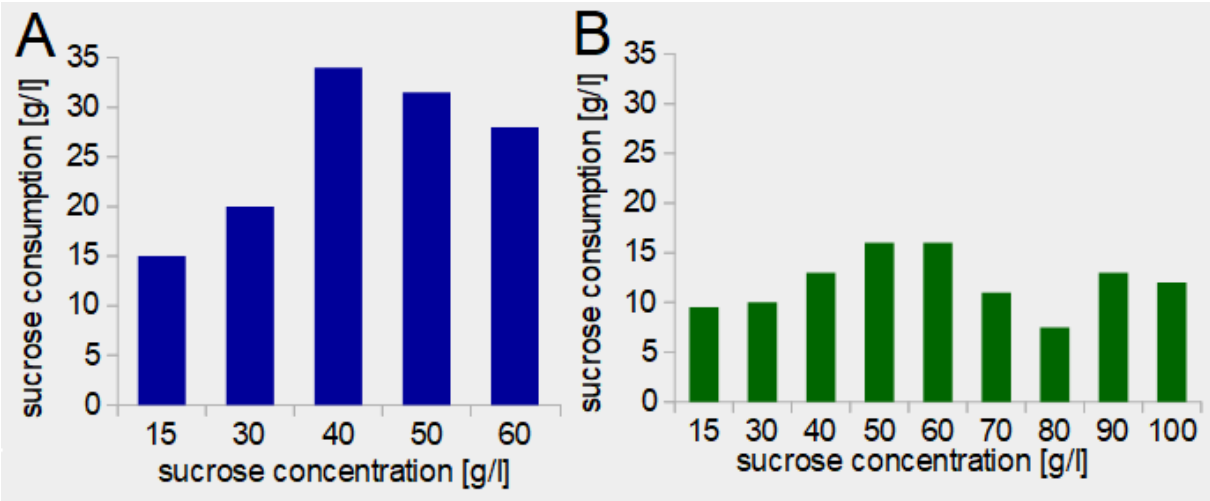


**Fig. 3.40: Sucrose consumption in Cath 001 and Cath 004 depending on the concentration**
Sugar consumption of Cath 001 (A) and Cath 004 (B) after 6 days at different sucrose concentrations, calculated based on the brix values.

## NAA and kinetin inhibit catharanthine production in Cath 004

Auxins and cytokinins are plant hormones that affect the growth and development. In order to find out if these hormones influence the formation of alkaloids, corresponding treatments of the two cell lines Cath 001 and Cath 004 with 1-naphthaleneacetic acid (NAA) and kinetin (K) were carried out and an interaction with the phytohormone methyl jasmonate (MeJA) was investigated, which has already proven to be a strong positive regulator of catharanthine production. Samples for alkaloid extraction were taken 6 days after the treatment. Results of the HPLC analysis of these samples are shown in figure 3.41.

The addition of NAA and K leads to a repression of catharanthine production in Cath 004 compared to the control. In conjunction with MeJA there is an increase in production, but remains below the amount that was achieved by an exclusive MeJA treatment. NAA and K thus diminish the effect of MeJA. In Cath 001, the content of catharanthine is very low in all treatments. There was only a slight increase in treatment with MeJA and NAA, but it falls far short of Cath 004.

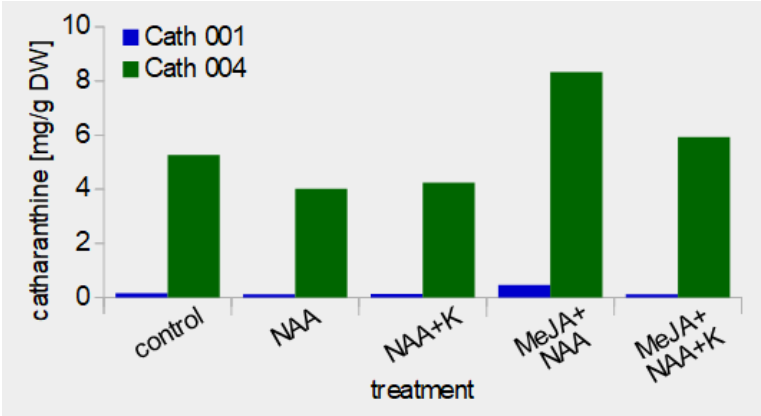


**Fig. 3.41: HPLC profile of Cath 001 and Cath 004 after elicitation with NAA and K**
Catharanthine content in mg/g dry weight of Cath 001 and Cath 004 in response to elicitation with NAA and K and combinations with MeJA 6 days after the treatment.

The more sensitive LC-MS analysis showed in addition to catharanthine also tabersonine in some samples, but no traces of vindoline, vinblastine or vincristine.

The analysis of the gene expression of the vindoline biosynthesis pathway did not reveal any appreciable influence of NAA and K.

In terms of morphology, Cath 001 shows elongation over time in almost all treatments, which corresponds to the development in the control. Only in a combination of MeJA, NAA and K the cells were rather rounding up.

Cath 004 also showed elongation in almost all treatments, except for the NAA+K treatment, where the cell shape remained unchanged, as in the case of the control.

In terms of volume, Cath 001 only showed an increase in the NAA treatment, which is comparable to the control. In all other treatments, volume remained constant over time.

In Cath 004 there was an increase in all treatments and in the control. In combinations with MeJA, the increase in volume was quite large compared to the control.

## Precursor feeding stimulates alkaloid production in Cath 004

As previous experiments have shown, production of catharanthine in Cath 004 is possible. Vindoline or downstream biosynthesis products, however, are not detected or in the smallest amounts. In order to understand whether the administration of additional tabersonine shifts the biosynthesis in the direction of vindoline or the direct administration of vindoline or combination of vindoline and catharanthine leads to a biosynthesis of downstream products, the corresponding precursors were added to the cell medium and extraction of alkaloids was carried out after 6 days (figure 3.42 A). Since MeJA has proven to be the strongest elicitor, combinations of MeJA and precursors were also added to the cell medium to see if this could provide an additional effect (figure 3.42 B). The added precursors were the alkaloids dissolved in MeOH which were used as standards for HPLC. The concentration of tabersonine (Tab) and catharanthine (Cat) stock solution was 3 mM, the concentration of vindoline (Vin) stock solution was 2 mM. Since Cath 001 did not respond to treatments with elicitors in the previous experiments, the precursor feeding was only performed on Cath 004.

As shown in figure 3.42, the exclusive addition of precursors had no discernible effect on catharanthine biosynthesis. Only in combination with MeJA an increase in catharanthine could be detected for small amounts of tabersonine. The administration of higher amounts of tabersonine or vindoline, however, had no or even a negative effect on the catharanthine content.

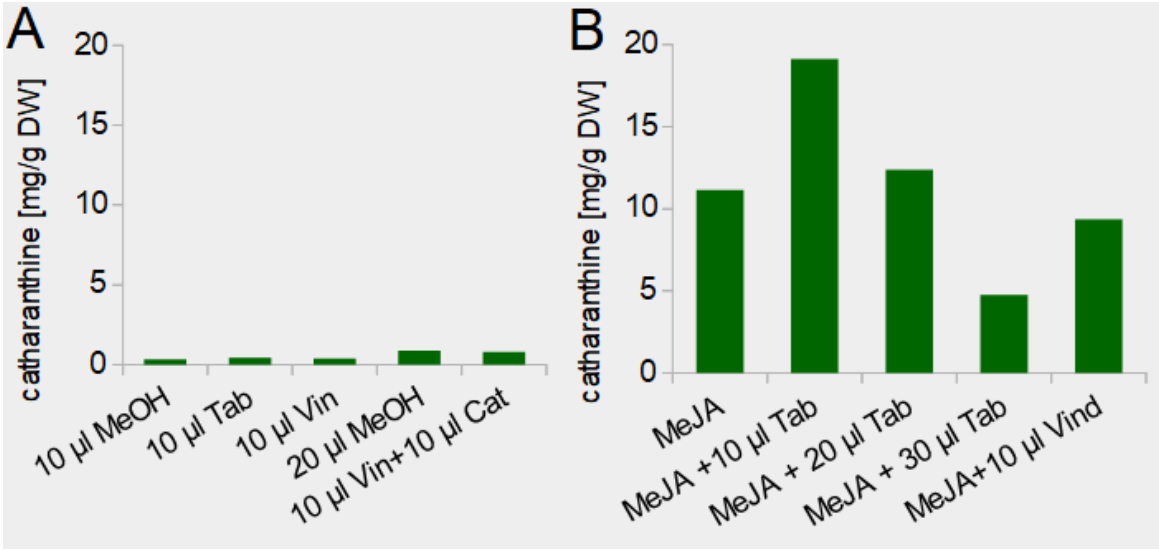


**Fig. 3.42: HPLC profile of Cath 004 after precursor feeding and combination with MeJA**
A: Catharanthine content of Cath 004 in mg/g dry weight after precursor feeding with tabersonine (1.2 µM), vindoline (0.8 µM) and combination of vindoline (0.8 µM) and catharanthine (1.2 µM) as well as the according solvent controls (0.04 % and 0.08 % MeOH).
B: Catharanthine content of Cath 004 in mg/g dry weight after combined precursor feeding (tabersonine: 1.2 µM, 2.4 µM, 3.6 µM, vindoline: 0.8 µM) and MeJA (100 µM) elicitation.

In the LC-MS analysis, in addition to the usual peaks for tabersonine and catharanthine, there was also a small peak in the mass and retention time of vincristine in the combined MeJA and vindoline treatment. A section of the LC-MS chromatogram of this experiment is shown in figure 3.43.

Although this peak is very small, it clearly stands out from the noise and consideration of the mass spectrum for this peak showed that the most abundant masses are 765.51 and 807.59, which corresponds to the fragmentation pattern of vincristine. Figure 3.44 shows a section of the mass spectrum of the peak labeled as vincristine in the *m/z* 825 in figure 3.43.

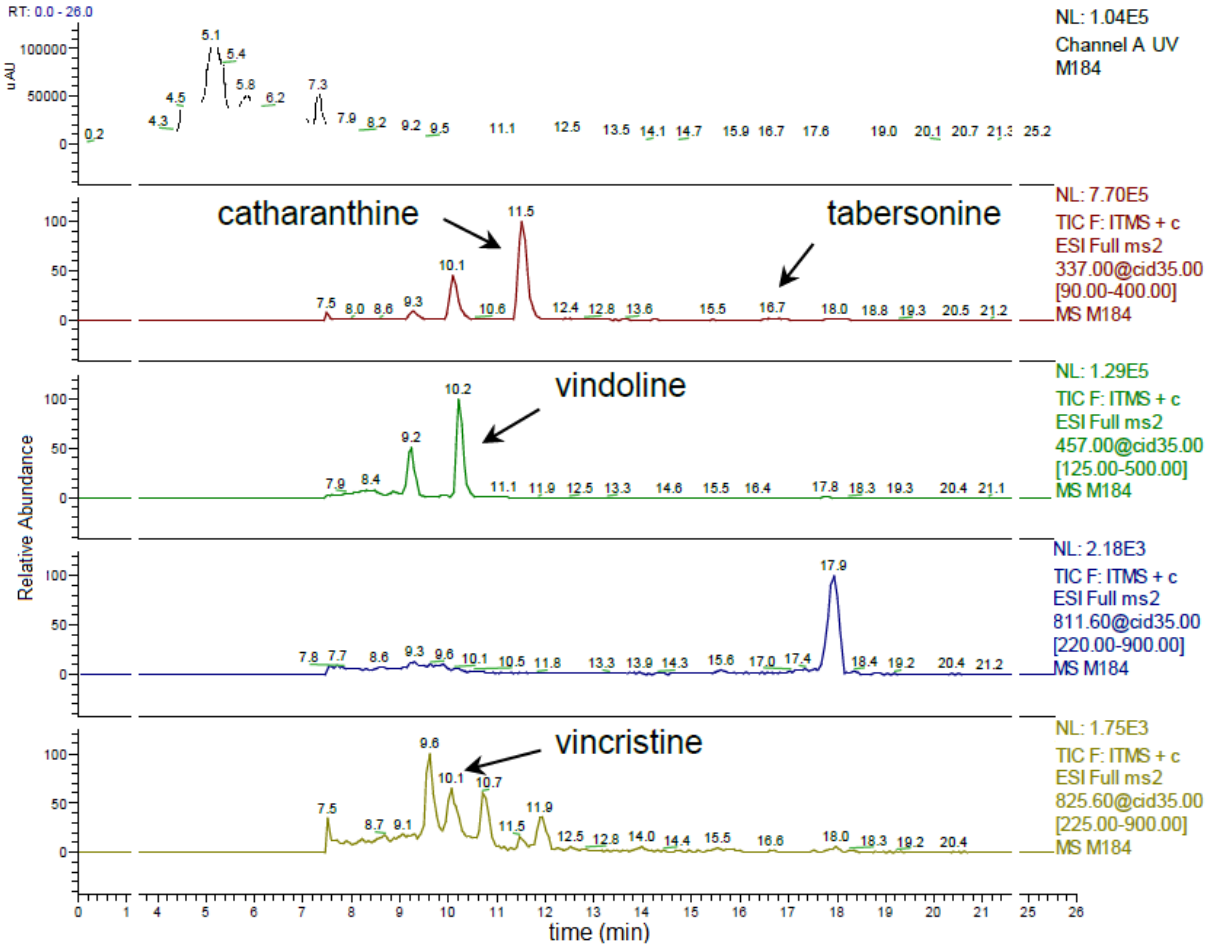


**Fig. 3.43: LC-MS profile of Cath 004 after treatment with MeJA and 10 µl of vindoline**
Section of the LC-MS chromatogram. Different masses are noted in different colors. Red: chromatogram of *m/z* 337 (catharanthine and tabersonine), green: chromatogram of *m/z* 457 (vindoline), blue: chromatogram of *m/z* 811 (vinblastine), yellow: chromatogram of *m/z* 825 (vincristine). Height of the peak indicates the relative abundance of a molecule, normalized according to the highest peak in each spectrum. Corresponding retention times are given above.

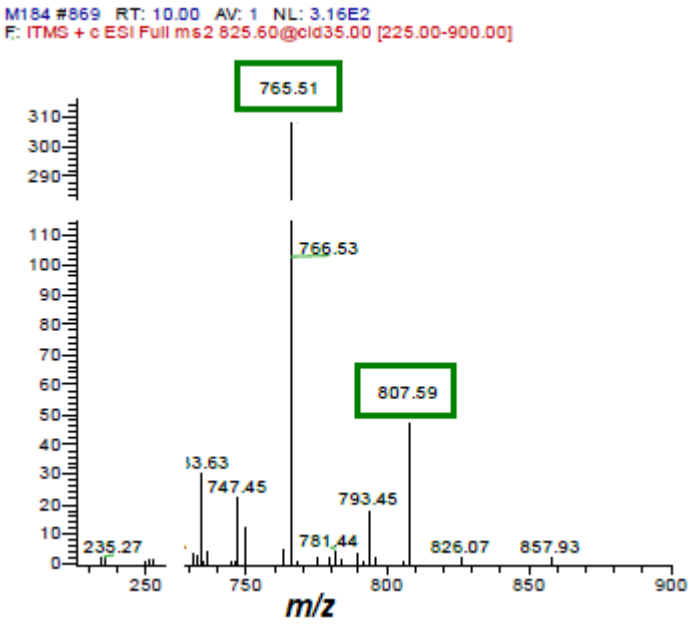


**Fig. 3.44: Mass spectrum of *m/z* 825 (vincristine)**
Section of the MS fragmentation pattern of *m/z* 825. Marked with green boxes are the two most abundant fractions (765.51 & 807.59) which correspond to the mass/charge ratio of vincristine.

The treatment with a combination of MeJA and vindoline on Cath 004 was repeated in three further biological replicates, in which additional treatments with 20 and 30 ml vindoline were performed. The peak in the vincristine spectrum could not be clearly reproduced or even increased in any of these experiments. Although the masses 765.51 and 807.59 were occasionally found in the corresponding spectrum for the appropriate retention time, they were superimposed by other masses, which were more abundant.

Regarding the expression of vindoline biosynthesis genes, treatments with tabersonine have not led to major changes. There was a slight upregulation of *t16h2*, *d4h* and *dat* with downregulation of *t16h1* (figure 3.45).

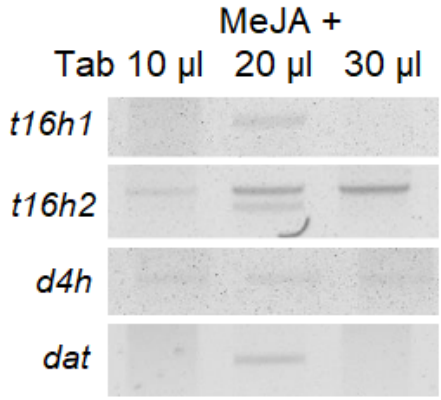


**Fig. 3.45: Gene expression profile of vindoline pathway genes after MeJA elicitation and tabersonine treatment**
Downregulation of *t16h1* with slight upregulation of *t16h2*, *dat* and *d4h*.

Concerning the cell shape the cells were more rounding up compared to the control, except for the combination of vindoline and catharanthine. In terms of volume, vindoline and catharanthine had no change compared to the control. There was a strong increase in the solvent control and a drop after day 3 for tabersonine.

## Cath 001 eliminates Cath 004 in long-term co-cultivation

Investigation of Cath 001 and Cath 004 regarding different growth parameters and expression of vinca alkaloid biosynthesis genes revealed large differences between the two cell lines. Obvious differences were also observed in the study of alkaloid production, with Cath 004 showing a higher level of catharanthine and a much stronger response to treatments than Cath 001. In order to find out whether the two cell lines complement or possibly inhibit one another in the production of alkaloids, a combination experiment was carried out. In this combination experiment, 0.75 g of each cell line were transferred to 25 ml of medium during the weekly cell transfer, so that the usual

experimental setup of 1.5 g cells and 25 ml medium was used. In a short-term experiment, these cells were sampled on days 3 and 6 of the culture cycle and the alkaloid content examined, while in a long-term experiment, the combined cell culture was first subcultured weekly for 4 weeks and then sampled on days 3 and 6. The fact that the Cath 004 cells form larger aggregates and are therefore heavier and perhaps settling faster when transferred to the filter, was accommodated by taking cells from the surface and the bottom of the filter when transferring them to the new culture flask. However, after four weeks of common cell transfer, the cell material in the filter looked like a pure Cath 001 culture (compare figure 3.20 left). Also in the investigation of the alkaloid content the level of catharanthine was very low and corresponding to that of Cath 001 in the long-term experiment (figure 3.46). In the short-term experiment, however, the catharanthine content in the combination study corresponds to that of Cath 004 (compare figure. 3.31), although only half of the cells used in the combination study was Cath 004.

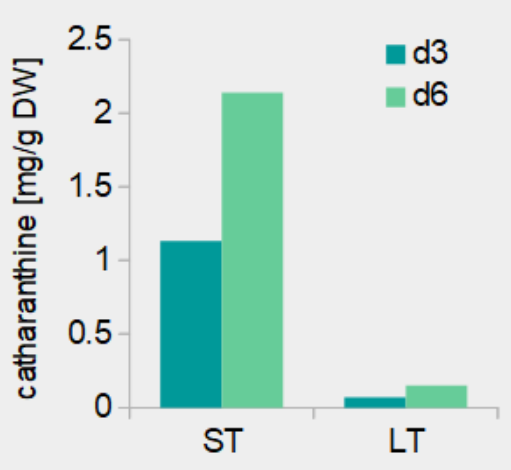


**Fig. 3.46: HPLC profile of Cath 001 and Cath 004 combined cell culture in growth medium**
Catharanthine content in mg/g DW of a cell culture containing Cath 001 and Cath 004 cells at day 3 and day 6 of the cell cycle in a short term (ST) and long-term (LT) experiment in growth medium.

There was no difference between combined and separate *Catharanthus* cell lines in the LC-MS study. Tabersonine and catharanthine were the only detected alkaloids in all experimental approaches.

### 3.2.4 Summary *Catharanthus*

The study of the two *Catharanthus* cell lines Cath 001 and Cath 004 should clarify whether there are differences between cell cultures of same origin in terms of cellular characteristics, growth and metabolic potential. In addition, it should be shown if treatments of the cultures can stimulate the production of valuable alkaloids. The observations listed below represent the most important results:

- Despite the same origin, there are significant differences between Cath 001 and Cath 004, in phenotype, growth and energy potential.
- Cath 001 displaced Cath 004 in long-term co-cultivation.
- Expression analysis by qPCR showed clear differences in expression of *str*, *t16h1*, *d4h* and *prx1* between Cath 001 and Cath 004. Except for *t16h1* expression was higher in Cath 001.
- MeJA treatment could upregulate the *dat* expression in Cath 004 at day 6.
- Cath 001 could not be induced to produce appreciable amounts of alkaloids by any treatment.
- Production of catharanthine in Cath 004 was significantly enhanced by MeJA and a combination of MeJA and tabersonine.
- With a combination of MeJA and vindoline, vincristine could be detected in one experiment.

## 3.3 Chip experiments

This final section of the result chapter is about the experiments performed on the microfluidic bioreactor. First, the detection of alkaloids in a variety of setups is shown, then an attempt to detect communication between cells of individual chips is described.

### 3.3.1 Detection of vinca alkaloids in *Catharanthus* chip experiments is possible

As shown in the combination experiment, it is not possible to grow the two cell lines Cath 001 and Cath 004 together in flasks, as Cath 001 displaces Cath 004 over time. An effective way to cultivate the two cell lines together, without bringing them into direct contact and risking their mutual elimination, is the microfluidic chip. Cath 001 and Cath 004 were cultured alone or together in different setups as described in 2.11 and the

alkaloid profile of medium and cells determined by LC-MS after 7 days. The respective experimental setups and detected alkaloids are listed in Table 3.1.

With a few exceptions, catharanthine (C) was always detected in the medium, in some cases even in the cells despite the small sample size. In the vindoline precursor feeding experiments vindoline (VD) could also be detected in the medium and in the cells. In experiments 1 and 2, vindoline was detected in the medium, although it was not added. It was therefore possible to detect the same alkaloids that were detected on a larger scale in the flask experiments, however, additional alkaloids were not promoted by the chip setup.

**Table 3.1: Experimental setup and detected alkaloids in the chip approach**

| number of experiment | number of chips | volume of chips | cell line used | treatment | alkaloids detected by LC-MS | |
|---|---|---|---|---|---|---|
| | | | | | medium | cells |
| 1 | 2 | 200 µl | Cath 001 + Cath 004 | MeJA 100 µM | C, VD | / |
| 2 | 2 | 200 µl | Cath 004 | MeJA 100 µM | C, VD | / |
| 3 | 2 | 200 µl | Cath 001 + Cath 004 | MeJA 100 µM | C | / |
| 4 | 2 | 200 µl | Cath 004 + Cath 001 | MeJA 100 µM | C | / |
| 5 | 1 | 100 µl | Cath 004 | MeJA 100 µM | C | / |
| 6 | 1 | 200 µl | Cath 004 | MeJA 100 µM | C | / |
| 7 | 1 | 800 µl | Cath 004 | MeJA 100 µM | C | / |
| 8 | 1 | 100 µl | Cath 004 | MeJA 100 µM, vindoline 0.8 µM | C, VD | VD |
| 9 | 1 | 200 µl | Cath 004 | MeJA 100 µM, vindoline 0.8 µM | C, VD | VD |
| 10 | 1 | 800 µl | Cath 004 | MeJA 100 µM, vindoline 0.8 µM | C, VD | VD |
| 11 | 1 | 100 µl | Cath 004 | MeJA 100 µM, vindoline 1.6 µM | C, VD | C, VD |
| 12 | 1 | 200 µl | Cath 004 | MeJA 100 µM, vindoline 1.6 µM | C, VD | C, VD |
| 13 | 1 | 800 µl | Cath 004 | MeJA 100 µM, vindoline 1.6 µM | C, VD | C, VD |
| 14 | 3 | 800 µl | Cath 004 | MeJA 100 µM, vindoline 1.6 µM | / | C, VD |
| 15 | 2 | 800 µl | Cath 001 + Cath 004 | MeJA 100 µM | C | / |
| 16 | 2 | 800 µl | Cath 004 + Cath 001 | MeJA 100 µM | / | / |
| 17 | 1 | 800 µl | Cath 001 | MeJA 100 µM | C | / |
| 18 | 1 | 800 µl | Cath 004 | MeJA 100 µM | / | / |

### 3.3.2 Proof of concept for cell interaction on chip using BY-2

To investigate whether cells in different chips, which are coupled via a medium flow, interact with each other, the experiment described in 2.11 and shown in figure 2.5 was performed.

Two setups were used, one combining two chips with strongly diluted cells, and one combining a chip with strongly diluted cells and a chip with normally concentrated cells. At high dilutions, cells stop proliferating. This effect can be reversed by adding the medium of normally concentrated cells to strongly diluted cells. Proliferating cells apparently give a signal that can be perceived by other cells. If an interaction between the cells in different chips is possible, the strongly diluted cells that are coupled to each other (chip 1A and chip 1B) should show no proliferation, while the diluted cells (chip 2B) that are coupled to undiluted cells (chip 2A) should start dividing again. Since both *Taxus* and *Catharanthus* cells form large aggregates, this experiment was carried out with BY-2. To assess cell division, the cells were counted on day 0, just after the dilution before loading them on the chip and removed from the chip after three days and counted again. The experiment was conducted in three biological replicates. For each replicate, 5 cell counts per data point were performed. The result of the experiment is shown in figure 3.47. The growth factor of the cells in chip 1A and chip 1B, which were strongly diluted and coupled to each other, is 1 or even lower, which means that no cell division occurred. In contrast, the cells in chip 2B, which were also strongly diluted but coupled to normally concentrated cells in chip 2A, have doubled within 3 days. Obviously there is an interaction between the cells in different chips, which are connected via the medium flow.

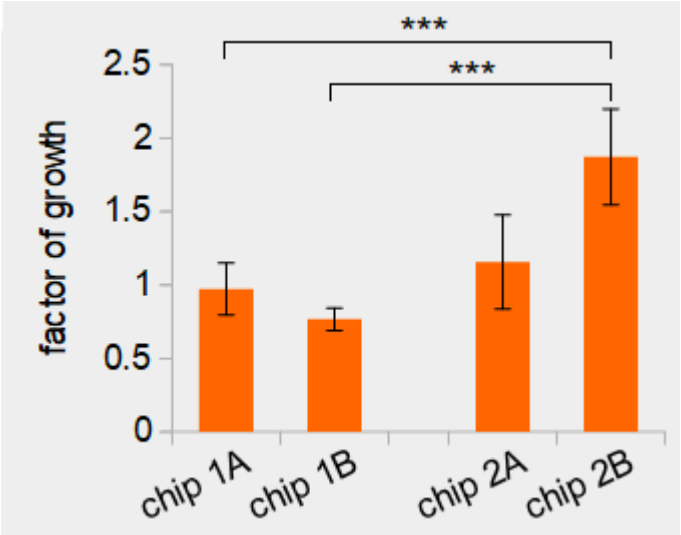


**Fig. 3.47: Growth factor of the BY-2 cells during the dilution experiment in the chip**
Chips 1A, 1B and 2B contained diluted cells, chip 2A undiluted cells. The chips 1A and 1B were coupled together in the experiment, as well as chip 2A and 2B. Error bars indicate ± SE. Statistically significant differences between the diluted cells of the different setups are indicated by asterisks above the brackets (student's *t*-test, ***: $p < 0{,}001$). Data basis for the *t*-test were the 15 individual values of the cell counting from three biological replicates.

### 3.3.3 Summary chip experiments

Experimental setups with the microfluidic bioreactor should show whether a miniaturization of the experimental approaches with cell cultures is possible. In addition, it was to be investigated whether an interaction of cells in different microfluidic chips via the medium flow is possible. It has been shown that:

- Even in the much smaller chip scale the same alkaloids could be detected in *Catharanthus*, which were also formed in the flask experiments.
- Cellular signals can be exchanged and interpreted between cells in coupled chips.

## 3.4 Summary of results

The subject of the present work are fermentation processes in plant cell cultures, which provide a promising approach for production of complex pharmaceutically active plant derived compounds. *Taxus* cell cultures are used successfully for the production of the anticancer drug paclitaxel on an industrial scale, although the biosynthetic pathway and mechanisms of production are not yet fully revealed. The aim of the present dissertation was to find cellular markers for the production of paclitaxel. Of particular interest was a special cell type, which was especially present in production cultures of *Taxus* and was referred to as shiny cells due to its phenotype. The mechanism of formation of these shiny cells was investigated, as well as the relationship between this cell type and paclitaxel biosynthesis and expression of biosynthetic genes. Immunofluorescence staining showed that paclitaxel is found mainly in the area of the cell wall and membrane. Nile red, a lipophilic dye was tested as a marker for paclitaxel and showed a correlation between staining intensity and paclitaxel production of the cells. The formation of shiny cells was significantly increased by MeJA and $AlCl_3$, whereas auxin had an inhibitory effect. The influence of $AlCl_3$ on the formation of shiny cells could be blocked by the administration of DPI. Examination of selected biosynthetic genes showed that auxin did not regulate expression whereas $AlCl_3$ stimulated expression of *tasy* and *dbat* and downregulated expression of *dbtnbt* six days after the treatment. MeJA treatments also stimulated the formation of baccatin VI, which is an analouge of paclitaxel.

Examination of two *Catharanthus* cell lines, Cath 001 and Cath 004, did not only show great differences in phenotype and growth behavior, but also in terms of gene

expression and metabolic potential. While a qPCR analysis revealed a remarkably higher expression in 3 out of 4 tested key genes in the biosynthetic pathway for Cath 001, hardly any alkaloid production could be recorded in this cell line. Cath 004, on the other hand, responded to various elicitor and precursor treatments with markedly increased production of catharanthine, which is an important intermediate in the production of anticancer drugs. The highest value was measured with 20 mg/g dry weight as a result of MeJA treatment with combined tabersonine precursor feeding. In a combination of MeJA and vindoline precursor feeding, traces of vincristine could be measured. In an attempt to co-cultivate the two cell lines, Cath 001 displaced Cath 004 in a long-term approach.

The spatial separation of the vinblastine and vincristine biosynthetic pathway within the plant is a major setback in the production of these valuable compounds in plant cell cultures. In order to test if a technical simulation of a plant tissue using a microfluidic bioreactor is possible in principle, it was investigated whether experimental approaches can be provided on a chip scale and whether the cells in different chips communicate. Even on much smaller chip scale, the same alkaloids could be detected, which were also present in flask experiments. In addition, it was shown that cells can perceive the cell density in another chip via the medium flow and react accordingly.

# 4 Discussion

Plants produce a wide range of secondary metabolites that are beneficial to humans. Prominent examples are the alkaloids paclitaxel from several *Taxus* species and vinblastine and vincristine from *Catharanthus roseus*, which are used as anticancer drugs. However, plants produce these alkaloids only in small quantities, which leads to costly and labor-intensive extraction and has a negative impact on environment and biodiversity (Lin et al., 2018). Technical synthesis would be inefficient and expensive. Plant cell cultures have great potential to solve this problem and produce medically effective alkaloids in a satisfactory amount. In the case of *Taxus*, this has been successfully carried out for several years, although the biosynthetic pathway and mechanism of production is not yet fully understood (Malik et al., 2011). In the case of *Catharanthus*, the desired success despite many years of research failed to date. The strict spatiotemporal developmental regulation of TIA biosynthesis has restricted the utility of these cell cultures for large-scale production (Sharma et al., 2018).

Investigation of *Taxus* and *Catharanthus* cell cultures in the scope of this study should provide insights into the alkaloid production mechanisms and metabolic potential in plant cell cultures. The development and testing of a microfluidic bioreactor also represents an important step in overcoming the limitations in plant cell cultures.

The aim of this work was to clarify if there are cellular markers for paclitaxel production which enable to predict whether a cell line will yield high amounts. Immunofluorescent staining showed that paclitaxel is localized between the cell wall and the membrane. Staining with the lipophilic dye Nile red showed similar patterns and correlation between signal intensity and paclitaxel production.

It should also be clarified whether there is a relationship between a certain shiny cell phenotype, paclitaxel production and expression of biosynthesis genes and what mechanism underlies the formation of shiny cells. MeJA, $AlCl_3$ and auxin proved to have a major influence on the number of shiny cells, with the effect of $AlCl_3$ being inhibited by the administration of DPI. While MeJA increased the production of the paclitaxel analogue baccatin VI, the other elicitors had no effect on production of secondary metabolites. Auxin is not regulating any of the genes under investigation, while $AlCl_3$ showed slight induction of the expression of *tasy* and *dbat*.

The study of the two *Catharanthus* cell lines Cath 001 and Cath 004 should clarify whether there are differences between cell cultures of same origin in terms of cellular

characteristics, growth, metabolic potential, gene expression and inducibility of alkaloid biosynthesis by elicitation. There were significant differences between the two cell cultures in all aforementioned points, suggesting that Cath 004 has greater potential for producing large amounts of alkaloids. Nevertheless, Cath 001 displaced Cath 004 in long-term co-cultivation.

Investigations using the microfluidic bioreactor should show whether a miniaturization of the experimental approaches is possible and whether an interaction of cells in different microfluidic chips via the medium flow takes place. It has been shown that even in the much smaller chip scale the same alkaloids could be detected in *Catharanthus*, which were also formed in the flask experiments. BY-2 dilution experiments showed that the cells in different chips can interact with each other and cellular signals can be exchanged and interpreted.

## 4.1 Phenotypic properties and growth pattern of the cell cultures

Cell cultures are highly heterogeneous with significant variability in terms of growth, metabolism and productivity of key metabolites. Still, few studies emphasize culture heterogeneity but focus on cell culture optimization, reactor design and nutrient utilization (Gaurav et al., 2010). In the present work, a comprehensive study of the growth behavior and cellular parameters of the cell cultures used was conducted.

### 4.1.1 Cell growth in *Taxus* indicates two proliferation cycles

*Taxus* cells form large aggregates in suspension culture, which can range from a few to several hundred cells. The determination of growth index 7 has shown that the fresh weight of *Taxus* cells approximately doubles within the 7-day growth cycle. Despite certain variations, the cell growth of the *Taxus* cultures is quite stable. The packed cell volume (PCV) shows a clear increase between day 2 and 5 and a further increase after day 10. An increase in PCV may be due to cell division or cell swelling. Considering the development of the cell number, a strong, approximately exponential increase from day 11 is visible, demonstrating a second cycle of cell division. The fact that the increase in cell number is so strong during the second cycle can be explained by the higher total number of cells after the first proliferation. The decrease in cell size around the same

time confirms the second cell division phase. Therefore, the cells apparently have a kind of internal clock, so they remember their proliferation cycle, even if there is no transfer into fresh medium. The fact that dry weight increases proportionally faster than the fresh weight suggests that the first increase in PCV is predominantly caused by cell division, while the second proliferation phase is accompanied by an increase in volume. This is also shown by the increase in water content of the cells to 97 % at the end of the measurement period. The values of cell measurement, on the other hand, rather indicate a decrease in the cell volume, as cell length and width decrease from day 11. This supposed contradiction can be explained by the assumption that the growth behavior of the cells in the interior of large aggregates, which are difficult to measure, differs from that of peripheral cells. Cell aggregation creates distinct microenvironments owing to differences in oxygen and nutrient availabilities (Gaurav et al., 2010). Therefore, it is possible that cells inside aggregates, which have less access to oxygen and nutrients, tend to grow by volume increase, whereas marginal cells rather grow by division. The more rapid decrease of the sugar content in the medium between day 10 and 12 also coincides with the second proliferation event.

### 4.1.2 Phenotype and growth in Cath 001 and Cath 004 are linked to their metabolic potential

Phenotype and growth behavior of the two *Catharanthus* cultures show clear differences. Growth index 7 displays an increase of fresh weight by a factor of 2.5 during the 7-day culture cycle over the entire sampling period for Cath 001. The increase for Cath 004 is much higher but has a lot of fluctuations. The PCV shows a moderate, almost linear increase for Cath 001, while Cath 004 shows an exponential increase, followed by a plateau phase from day 8. Cath 001 reaches about 60 % of PCV at day 15, while Cath 004 is so dense at this time that cells no longer settle. The measurement of cells shows that cells of Cath 004 are significantly larger than those of Cath 001. There is a sharp increase in cell size for Cath 004 starting from day 8, indicating a strong increase of the cell volume. The cell counting shows that the number of Cath 001 cells increases much stronger compared to Cath 004. While the fresh weight is much higher for Cath 004 showing the same trend as the PCV, the dry weight is clearly higher in Cath 001. All these observations suggest that Cath 001 rather grows by proliferation, while the enormous growth of Cath 004 is primarily due to an increase in cell volume. This is already a first explanation for the higher production of alkaloids in Cath 004. It

has long been known that the production of alkaloids in the stationary phase is higher (Lindsey & Yeoman, 1983). Cell proliferation and alkaloid production are negatively correlated. Consequently, the less divisible Cath 004 line also has the greater potential to form alkaloids. The higher proliferation rate of Cath 001 might also explain the observation that Cath 001 displaces Cath 004 in long-term co-cultivation (figure 3.46). The strong increase in cell number for Cath 001 between day 12 and 13 may indicate a second proliferation phase, which, however, is not as pronounced as in the case of *Taxus*. Cell counting and measurement indicate that the strongest cell division for both *Catharanthus* cell lines occurs between days 4 and 9, as cell number increases clearly, while the cell size decreases. This is a relatively long proliferation period.

As shown in figures 3.20 and 3.21 the cell aggregates of Cath 004 are larger than those of Cath 001. The size of aggregates is determined by size of individual cells and number of cells within the aggregate. Both the individual cell size and cell number are larger in the aggregates of Cath 004. This difference in the size of cell aggregates between the two cultures is another explanation for the differences in alkaloid production. There is a direct correlation between aggregate size and productivity of cell cultures. Oxygen transport models indicate that large aggregates face oxygen depletion at their center, which is proposed to stimulate secondary metabolic activity, as plant secondary metabolites are often a response to stress (Kolewe et al., 2008). It has been shown that production of thiophene increased with increasing aggregate diameter in *Tagetes patula* cell cultures (Hulst et al., 1989). Same has been shown for the production of tryptamine. The production of ajmalicine anyway shows the limitation of this correlation as it is produced less in very large aggregates (Keßler et al., 1999).

The advantage of Cath 004 over Cath 001 in production of alkaloids can therefore be explained by the larger size of aggregates and the lower proliferation rate. Furthermore, the quantification of mitochondria showed that the percentage of mitochondria is more stable in Cath 004 over time (figure 3.27) which might indicate a better energy level of Cath 004 cells.

The advantage of Cath 001 over Cath 004 in the long-term co-cultivation can be explained by the observation that Cath 001 rather grows through proliferation, while Cath 004 grows mainly by increase of the cell volume. In addition, the measurement of sugar content in the medium shows that Cath 001 used up the sugar in the medium completely after six days, while the decrease of sugar in the Cath 004 medium is

delayed and much slower. This may be an indication that Cath 001 has an advantage over Cath 004 in the utilization of nutrients.

## 4.2 Mitochondrial study of *Taxus*, Cath 001 and Cath 004

Mitochondria are double membrane bound organelles, the inner membrane bounding the matrix and the outer membrane bounding the inter-membrane space (Mitra, 2013). Mitochondria play a central role in the eukaryotic cell. Their function is not limited to their key role in providing energy in the form of ATP through oxidative phosphorylation (Chaban et al., 2014). They are also responsible for synthesis of vitamins like biotin and folic acid (Rébeillé et al., 2007) and as major site of ROS production they are involved in cellular signalling (Rhoads et al., 2006). In addition, they are participants in metabolic and physiological pathways (Law et al., 2014) and play a central role in programmed cell death (Reape & McCabe, 2010). Considering their importance in all these processes, mitochondria were subject to extensive investigations in the present work.

### 4.2.1 Mitochondrial shape is linked to stress response and alkaloid production

The analysis of mitochondria in *Taxus* and *Catharanthus* cultures has shown, that under growth conditions in *Taxus* cultures mesh-like structures are dominant at the beginning of the cell cycle, which are more and more replaced by shorter and dot shaped mitochondria. In production cultures of *Taxus*, the dot like mitochondria make up a very small proportion, especially in the shiny cells. In comparison between normal and shiny cells, shiny cells show a higher proportion of reticular structures. *Catharanthus* cultures show on average a higher percentage of dot shaped mitochondria in Cath 001, while in Cath 004 the proportion of linear and reticular structures is higher. In both cultures, there is an oscillatory progression in the proportion of dot shaped mitochondria, which increases until day 7, then decreases until day 10, followed by another increase.

Mitochondria in animal and yeast cells are typically tubular-reticulate structures of several micro-meters in length. In green plants they are predominantly observed as small spherical structures (Jaipargas et al., 2015). However, mitochondria are highly dynamic and continuously shaped by antagonistic fission and fusion events, to change their number, morphology and distribution (Pan & Hu, 2015). Some proteins involved in the fission and fusion machinery in plants are already identified (Logan, 2010; Pan & Hu, 2015) but the underlying mechanisms are still far from understood. The shape of

mitochondria has been shown to be also cell cycle dependent (Mitra, 2013) and recently endoplasmic reticulum has been identified as a player in fission and fusion of mitochondria (Jaipargas et al., 2015). The physiological role of mitochondrial fusion and fission in cell function is poorly understood but the importance of mitochondrial dynamics in cell homeostasis is illustrated by the serious effects of their disruption on animal and human health and survival (Alexander et al., 2000; Chen et al., 2003; Züchner et al., 2004). While mitochondrial fission is a crucial process in apoptosis (Martinou & Youle, 2006), abnormally large mitochondria have been observed under suboptimal conditions of growth and development (Jaipargas et al., 2015). UV irradiation, actinomycin D and cycloheximide lead to stress-induced mitochondrial hyperfusion in mouse embryonic fibroblasts and induced ATP production (Tondera et al., 2009). In tobacco cells, giant mitochondria are formed in response to hypoxia (van Gestel & Verbelen, 2002). Wakabayashi (2002) describes formation of megamitochondria as a mechanism to decrease intracellular ROS levels by decreasing the consumption of oxygen. The findings agree that the formation of large mitochondrial structures is a response of the cell to stress.

In the present work, longer mitochondrial structures are particularly numerous in *Taxus* production cultures, where they are a little more dominant in shiny cells, which show hardly any dot like and a high proportion of reticular mitochondria. Since the production of most secondary metabolites is associated with pathogen defense or wound response (Zhong, 2002) and shiny cells are also particularly present under stress conditions, the formation of complex mitochondrial structures is correlated with the formation of alkaloids and stress response. Another indication of the relationship between size of mitochondrial structures and the formation of alkaloids is the observation that the mitochondrial structures in Cath 004 tend to be larger than those in Cath 001 and that alkaloid production is significantly higher in Cath 004 even under control conditions. The correlation between complex mitochondrial structures and production of alkaloids can be explained by the fact that both phenomena are stress responses. The strong increase in punctuated mitochondria in *Taxus* growth cultures and the corrugation of the dot pattern in both *Catharanthus* cultures may be explained by the interrelation between mitochondrial shape and cell cycle. The dot pattern is more dominant when there is a strong increase in cell number in all three cell lines. Further evidence for this conjecture is that cells in production medium do not divide and hardly any dot like mitochondria are found in *Taxus* production cultures.

### 4.2.2 Mitochondrial quantity is correlated to alkaloid production

Mitochondria occupy 10-20 % of the internal volume of the cell (Denisenko, & Kuzmina, 2013). In cells with high energy requirements, such as cardiac myocytes, they can even account for up to 40 % of the volume (Yan et al., 2008). Since the mitochondrial quantification in the present study did not consider the cell volume, but the area of the cell in microscopic images, the percentage is correspondingly higher. In *Taxus* growth culture, the percentage coverage of mitochondria is 30 % at the beginning of the cell cycle and decreases to 22 % by day 15. In the production culture, the amount of mitochondria in the non-shiny cells increases over time and reaches 36 % 19 days after transfer to production medium. Accordingly, there is a correlation between alkaloid production and mitochondrial quantity. In the shiny cells, there are no significant changes in the amount of mitochondria, indicating that the shiny cells are not very productive. The mitochondrial abundance of the two *Catharanthus* lines shows, despite some fluctuations, that mitochondrial coverage in Cath 004 remains fairly stable over time, whereas it decreases markedly in Cath 001. Since Cath 004 shows a higher production of alkaloids than Cath 001, there is again a correlation between mitochondria quantity and alkaloide production.

## 4.3 Cellular marker for paclitaxel production

It has been shown that not all cells within a cell culture are equally productive in terms of alkaloid biosynthesis. By flow cytometry Naill & Roberts (2005b) identified a small subpopulation of single cells (3-5 %) which accumulated paclitaxel in unelicited cell cultures of *T. cuspidata*. Hall & Yeoman (1987) report the same about anthocyanin production in *C. roseus* cultures. They also report that the accumulation of anthocyanin primarily depends on percentage of producer cells rather than the production level of each cell. Being able to determine in advance whether a cell line contains a high proportion of producer cells would be an advantage in cell fermentation processes.

As previously described, the amount of mitochondria could provide an indication of the productivity of a culture. However, this analysis needs comparative values and has to be performed on culture level, not on single cell level. For this reason the search for cellular markers for paclitaxel production was part of this dissertation.

### 4.3.1 Nile red as marker for paclitaxel production

The paclitaxel double-immunofluorescence staining of *Taxus* cells in production phase showed that paclitaxel is majorly found at the cell wall and membrane. This localization is conclusive, as in contrast to vinca alkaloids, which are stored mainly in the vacuole (Neumann et al., 1983), paclitaxel is secreted to the medium (Lee et al., 2010).

Since paclitaxel is localized in the area of cell wall and cell membrane, the lipophilic dye Nile red was used for staining of cells from growth, production and bioreactor samples. High-resolution images have shown that the localization of Nile red and paclitaxel is consistent. In addition, it has been shown that the intensity of Nile red staining correlates with the productivity of the cells. The Nile red signal of cells in production phase was more intense compared to cells from growth phase. Staining of cells from the bioreactor showed a strong accumulation of Nile red in some cells, which was visible even in bright field. Interestingly, it was also shown that some cells in the bioreactor were not stained at all. This result indicates that Nile red is suitable for determining the proportion of producer cells in culture.

### 4.3.2 Shiny cells as cellular marker for paclitaxel production

Shiny cells are much more present in production cultures with an increased paclitaxel content than in growth phase cultures (see figs. 3.12 and 3.14 A). As already mentioned, Naill & Roberts (2005b) identified a subpopulation comprising 3-5 % of the cells, which accumulates paclitaxel under unelicitated conditions. Interestingly, the number of shiny cells under control conditions is also in this range (figure 3.14 A). In order to clarify whether shiny cells represent producer cells, their increase after elicitation was compared to the content of secondary metabolites and an expression analysis of selected paclitaxel biosynthesis genes was performed.

The elicitors used in the shiny cell study were the synthetic auxin picloram, MeJA, $AlCl_3$ and $AgNO_3$. The latter, however, led to a high cell mortality. Since other studies reported an additive effect of combined elicitors as with copper and ethylene in the gene transcript profile of TIA (Pan et al., 2015), co-treatment with $AlCl_3$ and MeJA was also performed. While picloram had an inhibitory effect on shiny cell formation, there was a notable increase after application of MeJA and $AlCl_3$. Co-treatment of both also increased the formation of shiny cells. However, an additive effect can only be recorded on day 1.

MeJA is a powerful elicitor which has been repeatedly reported to increase the content of paclitaxel, its precursors and expression of the corresponding biosynthetic genes (Yukimune et al., 1996; Laskaris et al., 1999; Onrubia et al., 2010; Sun et al., 2013). Although no paclitaxel was detected in the present study, the production of the paclitaxel analogue baccatin VI was significantly increased under MeJA treatment. The effect was strongest when MeJA was administered alone. Samples treated with picloram showed a slightly lower baccatin III level compared to the control. This observation is consistent with other studies. Picloram only enhanced the growth of callus but not taxane production in *Taxus* in the work of Furmanowa et al. (1997). Ketchum & Gibson (1996) reported that auxin rather reduces paclitaxel production. Expression of the selected biosynthetic genes showed no discernible change after treatment with picloram. Elicitation with $AlCl_3$ showed no change in content of secondary metabolites but a slight induction of the biosynthesis genes *tasy* and *dbat* six days after the application. $AlCl_3$ is not as common an elicitor as MeJA so there is no indication of its use in *Taxus* cell cultures. However, $AlCl_3$ has been reported to slightly enhance biosynthesis of withanolides in cell suspension cultures of *Withania somnifera* (Sivanandhan et al., 2014) and it increases the production of brachycerine, a monoterpene indole alkaloid (MIA) from *Psychotria brachyceras* (do Nascimento et al., 2013). An effect on paclitaxel production therefore would have been conceivable, although it was not confirmed. An induction of stress related genes by $AlCl_3$ has also been shown by Richards et al. (1998) who reported an induction of oxidative stress genes in *Arabidopsis thaliana*.

The results indicate that the increased formation of shiny cells is not directly related to increased production of secondary metabolites. Although an increase in shiny cells and baccatin VI was observed after MeJA treatment, $AlCl_3$ application only resulted in an increase in shiny cell content. While the synthetic auxin picloram visibly inhibited the formation of shiny cells, the reduction of baccatin III content was not equally pronounced. Shiny cell formation and production of secondary metabolites therefore seem to have a common cause but no direct connection. Shiny cells therefore do not represent producer cells and are only conditionally suitable as marker for paclitaxel production.

## 4.4 Model for shiny cell formation

Besides the question whether shiny cells are suitable as marker for paclitaxel production, it should also be clarified, which mechanism underlies the formation of shiny cells. In a certain percentage, shiny cells are already present unter control conditions. There is evidence that shiny cells are not just an observation of the present work. In a publication of Kolewe et al. (2008), a microscopic image of the *Taxus cuspidata* cell line P991 is shown. The image should exemplarily show the size and structure of a cell aggregate, but also provides an indication that shiny cells are probably present in this cell line (figure 4.1). Shiny cells are easiest to detect as single cells or peripheral to larger aggregates. But they can also be recognized within larger aggregates, even if they are not in focus, as highly reflective spots that look slightly overexposed (fig.5.4), which is exactly what can be seen on the picture mentioned.

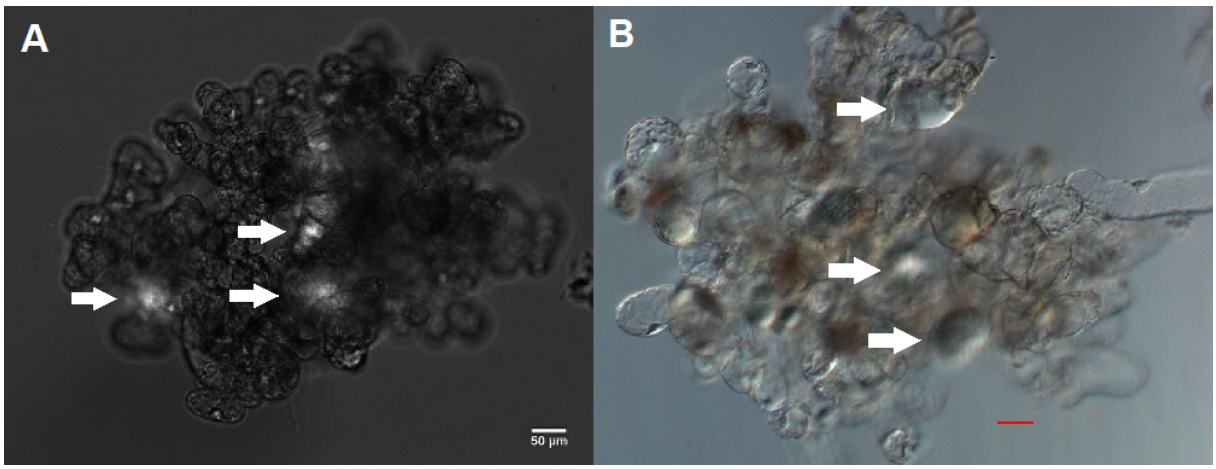


**Fig. 4.1: Indication for existence of shiny cells in other *Taxus* cell lines**
A: Aggregate of *Taxus cuspidata* P991 cells in suspension culture. Arrows indicate the position of three supposed shiny cells. Adapted from (Kolewe et al., 2008).
B: Aggregate of *Taxus chinensis* cells from the present study containing numerous shiny cells. Arrows indicate the position of three shiny cells within the aggregate.
(Scale bars indicate 50 µm.)

In the present study the most pronounced increase in number of shiny cells was seen after treatment with $AlCl_3$. Aluminum ions are very phytotoxic as they induce oxidative burst by activating the NADPH oxidase RboH, which produces superoxide (Kawano et al., 2001; Kawano et al., 2003). It has also been shown, that treatments with the NADPH oxidase inhibitor DPI have inhibitory effect on trivalent cation-induced generation of superoxide (Kawano et al., 2001).

A working model was proposed by Eggenberger et al. (2017) where elevated levels of reactive oxygen species caused by the NADPH oxidase RboH interfere with actin dynamicity. They also found DPI to act antagonistically to the cell penetrating peptide, that caused the superoxide induced actinbundling. As the $AlCl_3$ mediated formation of shiny cells could also be reversed by application of DPI, it is reasonable to assume that the formation of shiny cells also depends on the production of superoxide and the subsequent bundling of actin. This assumption is supported by considering the effect of auxin and the relationship between auxin and actin.

The organization of actin is under control of auxin (Nick, 2010). This has been confirmed in various experiments. The administration of auxin was able to prevent the harpin-induced bundling of actin and the resulting cell death in grapevine cells (Chang et al., 2015). The overexpression of the actin-binding protein talin in rice caused bundling of actin filaments and therefore impaired gravitropism, which could be restored by exogenous auxins (Nick et al., 2009). This relationship between actin and auxin and the fact that shiny cell formation is inhibited under application of auxin encourages the assumption that actinbundling plays a crucial role in shiny cell formation.

The involvement of MeJA in this model can be explained by the cross-talk between auxin- and JA-signalling, which was described by Nick (2006). There is a competition between both pathways for a common key factor, namely, AXR1. Activation of the jasmonate pathway has the consequence that auxin signalling becomes depleted from this key player leading to reduced auxin responsiveness. This cross-talk becomes evident, when considering the *axr1* mutant in *Arabidopsis*, which was isolated as an auxin mutant, but still showed a defective jasmonate response (Tiryaki, Staswick, 2002). The inhibitory effect of jasmonate on auxin signaling also becomes apparent in the rice mutant *hebiba*, which is not able to produce JA and exhibits elevated auxin responsiveness (Riemann et al., 2003). It is therefore very conceivable, that the positive effect of MeJA on the number of shiny cells is achieved by inhibiting the effect of auxin, which is reducing the number of shiny cells. In this way JA has an indirect effect on actin. All these observations and interactions suggest a model for the formation of shiny cells in dependence of actin organization, which is shown in figure 4.2.

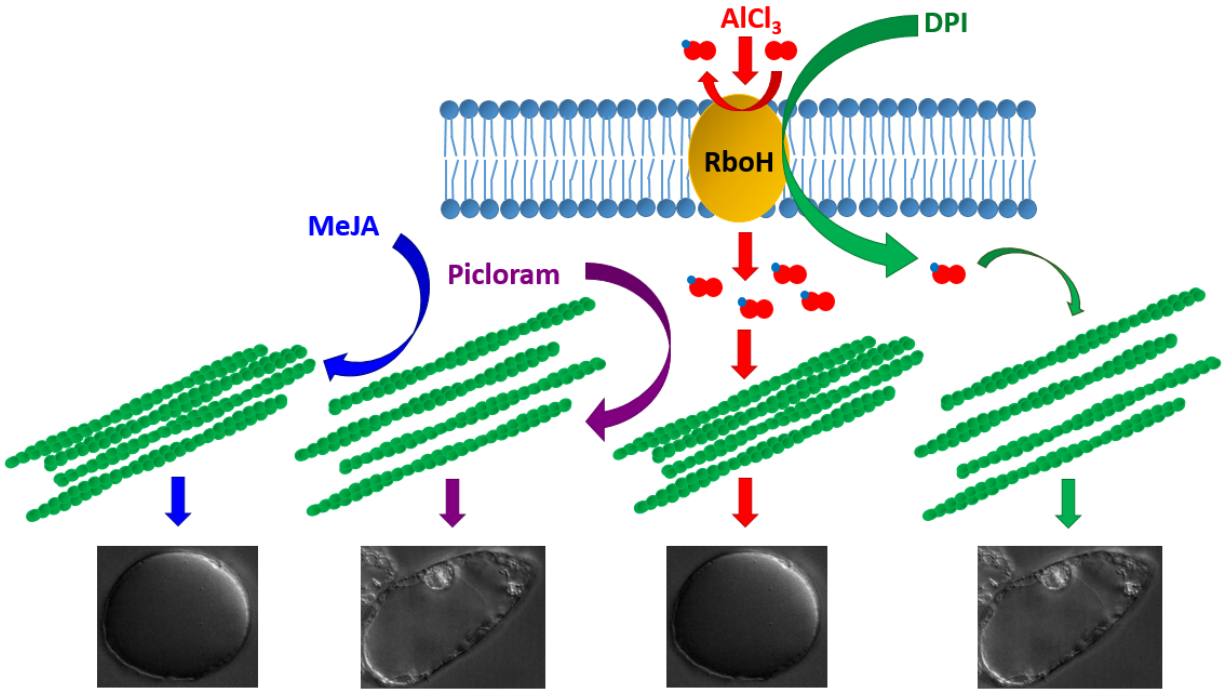


**Fig. 4.2: Model for shiny cell formation**
$AlCl_3$ induces oxidative burst by activating NADPH oxidase RboH (respiratory burst oxidase homolog) mediated $O_2^-$ production, resulting in actinbundling and shiny cell formation (red arrows). DPI, an inhibitor of RboH, reduces $O_2^-$ production leading to debundling of actin and reduction of shiny cells number (green arrows). Auxin directly acts on actin, causing debundling and reduction of shiny cell number (purple arrows). MeJA is antagonistic to auxin, leading to actinbundling and shiny cell formation (blue arrows).

## 4.5 *Catharanthus* elicitation and alkaloid production

In biosynthesis of vinblastine and vincristine the precursor tabersonine is transformed into vindoline by seven enzymatic reaction steps. Vindoline and catharanthine are combined to anhydrovinblastine which is further converted to vinblastine and vincristine (Qu et al., 2015; Liu et al., 2016).

### 4.5.1 Vinca alkaloid biosynthesis pathway is blocked in the vindoline pathway

Tabersonine and catharanthine were detected in Cath 001 and Cath 004, while vindoline could only be detected in traces after elicitation. There was also no detection of the downstream alkaloids vinblastine and vincristine except for one Cath 004 sample which showed traces of vincristine after combined elicitation and precursor feeding. The vindoline pathway is therefore obviously blocked, which is a very common observation in *Catharanthus* suspension cultures as reported by van der Heijden et al. (1989)

decades ago. However, ability to produce vindoline is not generally lost in plant cell cultures, as regenerated shoots recover the ability to produce vindoline (Constabel et al., 1982). These observations suggest, that biosynthesis of catharanthine and vindoline are differentially regulated and that vindoline biosynthesis is under more rigid tissue-, development-, and environment-specific control than that of catharanthine (St-Pierre, 1999). Metabolic engineering on vindoline pathway is challenging, as there are many branches in the biosynthesis pathway leading to the products vinblastine and vinciristine which means that there are a lot of competing pathways. As reported by Kellner et al. (2015), Qu et al. (2015) and Edge et al. (2018) shunt products of the vindoline pathway are formed by the same enzymes involved in the production of vindoline. Knockout or silencing of these genes will therefore not just lead to blocking of the shunt pathways but also to disruption of the vindoline pathway. Sun et al. (2018) managed to shift tabersonine from competing pathways to the vindoline pathway by overexpressing *t16h* and *16omt*, the genes for the first two enzymes in the vindoline pathway, in hairy root cultures. But in consequence they also detected new metabolites, indicating that this shift also activated other biosynthesis pathways, branching off from the vindoline pathway. The complex network of biosynthetic pathways of secondary metabolism generally makes manipulation difficult. While Canel et al. (1998) reported a strong positive effect of overexpression of *str* on the production of downstream TIAs in *Catharanthus* cell cultures, overexpression of *tdc* was detrimental to growth. Yao et al. (1995) report a reduction in lignin biosynthesis by overexpression of *tdc*. To shift the biosynthesis in one direction by overexpression of individual genes is therefore problematic and the vindoline pathway and its modification definitely remains a bottleneck in the production of downstream alkaloids in plant cell cultures.

### 4.5.2 Alkaloid production and gene expression show no correlation in Cath 001 and Cath 004

Among the alkaloids analyzed, catharanthine was the only one produced in quantities quantifiable by HPLC. Cath 004 showed a significantly higher production of catharanthine than Cath 001. However, gene expression was higher for Cath 001 in three out of four biosynthetic genes tested, especially for *prx1*. This suggests that there is posttranslational regulation or that Cath 001 is in principle capable of forming downstream alkaloids, but the biosynthetic pathway is interrupted at an earlier point. Treatments with different elicitors have also shown that alkaloid production is barely

inducible in Cath 001, while Cath 004 responded by production of varying amounts of catharanthine.

### 4.5.3 Jasmonate and MeJA increase alkaloid production

Jasmonates are probably the most common elicitor for induction of TIA production in *Catharanthus* cell cultures. There is a network of jasmonate-responsive transcription factors, modulating the TIA biosynthesis in *C. roseus* (Geyter et al., 2012; Patra et al., 2018), which is probably the reason for the strong positive effects on alkaloid production seen after treatments with jasmonates. JA is also reported to inhibit cell division (Swiatek et al., 2002) and trigger cell wall synthesis (Koda, 1997). This is another indicator for its positive effect on alkaloid production as proliferation and alkaloid production are negatively correlated as already mentioned (Lindsey & Yeoman, 1983). Also in the present work the application of JA showed a positive effect on alkaloid production. This effect was significantly higher in Cath 004, where JA more than doubled the catharanthine content in the middle stationary phase. With prolonged duration of the incubation time, the catharanthine level decreased again, which may indicate that JA inhibits alkaloid production in long-term. The effect of MeJA was even stronger than that of JA, although there was again a clear difference between Cath 004 and Cath 001. The latter hardly responded to the treatment. MeJA is described as a potent elicitor of alkaloids biosynthesis in *C. roseus* by a variety of authors. MeJA activates the production of vinca alkaloids in plants (Aerts et al., 1994), cells (Rischer et al., 2006; Guo et al., 2013), rootless shoots (Vázquez-Flota et al., 2009) and hairy roots (Ruiz-May et al., 2009). Also the expression of a wide range of TIA biosynthesis genes is induced by MeJA (van der Fits, 2000) such as *sgd* (Geerlings et al., 2000) and *str* (Menke et al., 1999). In the present study semi-quantitative PCR also indicated an upregulation of expression of vindoline biosynthesis genes in Cath 004 (figure 3.37) and LC-MS profile showed a small peak for vindoline after the treatment (figure 3.36).

### 4.5.4 Positive effect of sugar on alkaloid production is limited

30 g/l is a very common sugar concentration used for *Catharanthus* growth cell culture medium, as in the present study, where this concentration showed the highest cell viability (figure 3.30 C and 3.30 D). As also shown in the present work, the production of catharanthine in Cath 004 increases clearly with an increase in the sugar

concentration in the medium (figure 3.38 B). Although the effect of sugar is not as strong as that of JA or MeJA, Cath 004 has a fivefold increase in catharanthine production at 60 g/l compared to 15 g/l. A similar effect is also seen for Cath 001 (figure 3.38 A) but as in other treatments, the effect in Cath 001 is not nearly as pronounced as in Cath 004. The strongest catharanthine production was seen at a sugar concentration of 60 g/l. Other authors report similar observations. For example Zhao et al. (2001b) recorded the highest alkaloid production in compact callus cultures of *C. roseus* with sugar concentrations between 50 and 60 g/l. In their study on hairy root cultures Jung et al. (1992) observed a slightly higher catharanthine production at 45 g/l compared to 30 g/l. The effect of sugar is not just seen in *Catharanthus*. Dong & Zhong (2002) report that sucrose feeding increased taxane production in *Taxus* in bioreactor. Nevertheless, the effect of increased sugar levels is limited. At 70 g/l, the catharanthine content in Cath 004 decreases markedly compared to 60 g/l and remains relatively stable but visibly lower at higher concentrations. Not only the production of alkaloids, but also the viability of the cells decreases markedly at sugar levels of more than 70 g/l (figure 3.30 D). The cell volume also shows a dramatic decrease at high sugar concentrations (figure 3.39 B). This observation is most likely explained by the strong osmotic effect with high sugar content. Investigation of sugar consumption at various concentrations confirmed that the sugar consumption of Cath 001 is much higher compared to Cath 004 (figure 3.40). It also showed that from a concentration of 70 g/l, sugar utilization decreases strongly in Cath 004. For Cath 001, this decline is even evident at lower concentrations. Therefore, although the supply of sugar is higher, the cells are unable to use more sugar. This observation was also made by Fowler (1982), who reports that efficiency of sucrose utilization of *C. roseus* cell cultures declines with increasing sugar concentration. Also Knobloch & Berlin (1980) report a low culture growth in *C. roseus* cell cultures with 80 g/l sucrose, although high levels of ajmalicine are produced.

### 4.5.5 Auxin and cytokinin inhibit alkaloid production

Kim et al. (1994) showed that cell shape and alkaloid production are linked. They reported that catharanthine production was increased in elongated cells. Campanoni & Nick (2005) reported that NAA is promoting cell elongation, while 2,4-D is supporting cell division in tobacco cell cultures. Therefore, NAA was used in order to support cell elongation and thus production of alkaloids. NAA treatment resulted in an elongation in

Cath 004 compared to the auxin-free control, while cell shape and its development were unchanged in Cath 001.

Smith et al. (1987) reported that NAA and kinetin as growth regulators generally increase yields of catharanthine in suspension cell cultures. Zhao et al. (2001a) used NAA and kinetin in their production medium, when they treated *Catharanthus* cell cultures with different elicitors, increasing the amount of indole alkaloids. In 1998 the group of Joël Crèche showed that cytokinin has a positive effect on the accumulation of alkaloids in *Catharanthus* cell suspension cultures (Yahia et al., 1998). In 2005, they reported an upregulation of *g10h* expression by cytokinin (Papon et al., 2005). Nevertheless, no positive effect of NAA and kinetin on catharanthine production could be observed in the present study. Treatments with NAA and combined NAA and kinetin actually decreased the amount of catharanthine compared to the control. Combined treatments of NAA, kinetin and MeJA showed an increased level of catharanthine, which nevertheless was lower than the level in samples exclusively treated with MeJA, indicating that NAA and kinetin application rather has an inhibiting effect on TIA biosynthesis. Same can be seen for the synthetic auxin 2,4-D. As shown in figure 3.33, the absence of 2,4-D in the medium already caused a large increase in catharanthine production in Cath 004 without application of any elicitors. These results are in line with the findings of Goddijn et al. (1992), who report an auxin induced decrease in expression of *tdc* and Pasquali et al. (1992) who showed an additional downregulation of *str* expression by auxin, which both encode for key enzymes in the TIA biosynthesis pathway. In the study of Kim et al. (1994) shape of the tested cell lines was rather uneffected by treatments with auxin or cytokinin. It therefore appears that the internally determined morphology of the cells is crucial for the production of alkaloids rather than the induced morphology. This would correlate with the results of the present study, where Cath 004 showed slightly higher degree of cell elongation in the control (figure 5.1) and higher production of alkaloids.

### 4.5.6 Precursor feeding strongly induces alkaloid production

At an early stage of this work, it has been shown that the vindoline biosynthetic pathway in Cath 004 is blocked. While catharanthine production was stimulated by various treatments, little or no vindoline was detected and no downstream products. The idea of precursor feeding was to stimulate the production of downstream products by adding intermediates that are not formed by Cath 004. Evidence that this approach is effective

was provided by El-Sayed et al. (2004), who were able to stimulate the production of tabersonine and catharanthine by adding the common precursor stemmadenine. The addition of vindoline with simultaneous elicitation by MeJA actually revealed traces of vincristine in Cath 004 (figures 3.43 & 3.44). Interestingly, the exogenous addition of tabersonine did not lead to the formation of vindoline, but increased the production of catharanthine (figure 3.42). Since catharanthine and tabersonine are located in different branches of the vinca alkaloid biosynthesis pathway and therefore catharanthine is no downstream product of tabersonine, this result was unexpected (figure 1.2). This correlation can only be explained by a feedback activation of common precursors by exogenous tabersonine. A similar observation was also made by Whitmer et al. (2002). The application of loganin to their *str* overexpression line resulted in a flux to tryptamine, which is also located in a different branch of the biosynthetic pathway than loganin and is no downstream product (figure 1.2). Evidence for feedback activation in alkaloid biosynthesis was also found by Expósito et al. (2009), who showed increased production of paclitaxel and other taxanes in *Taxus* by exogenous addition of paclitaxel. Interestingly, higher amounts of tabersonine not necessarily lead to higher amounts of catharanthine. The effect is decreasing at higher concentrations (figure 3.42). Again, a similar observation was made by Whitmer et al. (2002), where accumulation of tryptamine seems to reduce the flux through feedback inhibition. These results indicate complex regulatory mechanisms of the vinca biosynthetic and branching pathways.

## 4.6 Chip

In plants, production of secondary metabolites with pharmaceutical activity typically involves different cell types. This impedes biotechnological production, since differentiation of cells is suppressed in suspension cultures. By use of a microfluidic chamber system, where plant cells can be integrated into a process flow, the situation in a real tissue can be simulated. A prerequisite for the implementation of this project is that fermentation processes also take place on a chip scale and interaction between cells in different chips is possible. These two points have been addressed in the present work.

### 4.6.1 Miniaturization of fermentation processes

It has already been shown for the tobacco cell culture BY-2 that cells can be successfully cultivated in the chip system and physiological parameters (viability, mitotic index, division synchrony) can be preserved over several days the way they are in culture flasks (Maisch et al., 2016b). It was still to be clarified whether the same fermentation processes that take place in culture flasks also proceed at the much smaller chip scale. For this purpose *Catharanthus* cells were introduced into the microfluidic system in the setup described under 2.11 and elicited with MeJA. Alkaloids were extracted from cells and medium and the alkaloid profile determined by LC-MS. It has been shown that the alkaloid profile in the chip corresponds to that of the culture flask. This proves that miniaturization of the fermentation process to chip scale is possible, allowing a variety of new applications. Microfluidic devices have already been used in plant research, for example for high throughput studies on gene expression in seedlings (Busch et al., 2012), investigation of cell growth and differentiation using protoplasts (Wu et al., 2011) or quantification of cellular penetrative forces on pollen tubes (Sanati Nezhad et al., 2013) but so far not for studies on fermentation processes in plant cell cultures.

### 4.6.2 Cell communication in the chip system

To allow the simulation of a plant tissue, the microfluidic chip approach has to enable cells to communicate via the medium flow. To prove this requirement, the experiment shown in figure 2.8 was performed. It has been shown on several occasions that high dilutions lead to a block of cell division in liquid cell cultures, although the same amount of nutrients is available (figure 5.3). Therefore, cells are able to perceive the density of surrounding cells and respond accordingly. This ability is called quorum sensing and is especially well characterized for amoebae (Gomer et al., 2011). It has also been shown that this block of cell division can be abolished when the highly diluted cells are cultured in medium of normally concentrated, dividing cells (unpublished data). This conditioned medium is a cell-free filtrate that contains all the molecular signals released by cells. The use of conditioned medium to restore cell functions is also described by other authors. For propagation of superior cell populations Naill and Roberts isolated single cells from aggregated *Taxus cuspidata* cultures to grow them in suspension culture. High seeding density showed no cell growth. Conditioned medium with growth stimulating factors secreted by cells induced growth at high seeding density (Naill & Roberts, 2005a). In carrot cell cultures a density of less than 10,000 cells per ml

activates a cell death process. By addition of cell-conditioned growth medium this process could be impeded and cells survived at low density (McCabe et al., 1997). Based on these findings, the attempt to detect cell communication in the chip system was conducted. In a control approach, two chips were coupled together containing a highly diluted BY-2 cell suspension. In the second approach, a chip with a highly diluted cell suspension was coupled to a chip of normal cell concentration. While cell division did not occur in the control setup, cell division of the diluted cells was re-initiated in the second setup. The diluted cells were therefore able to perceive the signals of the cells in the second chip and responded accordingly. The microfluidic chip approach thus enables cell communication.

## 4.7 Conclusion

Plant cell cultures are not only a promising platform for the production of secondary metabolites but can also serve as a system of reduced complexity for approaches on cellular mechanisms. Plant cell lines/strains and calli are often considered as “dedifferantiated” (Opatrný et al., 2014) and cells growing in biofermenters are referred to as “biomass” (Nick, 2016). These terms are misleading and superficial and therefore, the great potential of cell culture systems might neither be recognized nor fully exploited. It was noted by Gaurav et al. (2010) that cell cultures are highly heterogeneous with significant variability amongst cells in terms of growth, metabolism and productivity and as mentioned by Nick (2016), it has become clear that a cell is more than just a “bag of enzymes”. As reviewed by Opatrný, cell lines often preserve certain features from their source tissue (Opatrný et al., 2014) and a callus is not a chaotic group of confused cells but a dynamic complex of molecularly determined cells, exhibiting certain functional and morphogenic competencies (Opatrný, 2014).

This conception has also been confirmed in the present work. Not only was a stress-inducible cellular phenotype found in *Taxus* cell culture, it was also shown in detail that two *Catharanthus* cell cultures, despite their same origin, show remarkable differences in phenotype, growth, gene expression profile and metabolic potential. Therefore, cells in suspension cultures are definitely more than dedifferentiated biomass.

In this dissertation, a model was developed, demonstrating that formation of the stress-inducible shiny cells is related to the bundling of actin, and that shiny cells and alklaiod production share a common cause without being directly coupled.

The search for cellular markers for paclitaxel production showed that paclitaxel is localized at the cell wall and membrane and Nile red has proven to be a useful indicator of paclitaxel production.
The TIA biosynthesis pathway has been shown to be blocked in the vindoline pathway in Cath 001 and Cath 004. Cath 004 has proven to be a high performer in alkaloid production and its inducibility compared to Cath 001. However, differences in growth behavior and nutrient utilization provide an advantage for Cath 001 in competition with Cath 004. The effects of elicitor and precursor treatments suggest complex regulatory mechanisms in alkaloid biosynthesis, involving feedback mechanisms. The highest accumulation of alkaloids was achieved by simultaneous MeJA elicitation and tabersonine precursor feeding.

Furthermore, the microfluidic bioreactor in chip design has been found to be suitable for technical simulation of plant tissues, allowing metabolic processes and cell communication.

## 4.8 Outlook

For the extension and confirmation of the model for shiny cell formation by actinbundling, further treatments should be performed and their effect on the number of shiny cells quantified. Co-treatment of auxin and $AlCl_3$ is useful to see if the actin debundling effect of auxin can abolish the effect of $AlCl_3$ as seen for DPI. Treatments with other cytoskeletal drugs like latrunculin B, which sequesters G-actin monomers and eliminates actin filaments or phalloidin, which stabilizes actin (Durst et al., 2013, Zaban et al., 2013), can also give a better understanding of the mechanism and prove the role of actin as key regulator in shiny cell formation. Another aim is the visualization of actin to directly compare its structure between shiny and non shiny cells. Visualization of actin by transient transformation has already been demonstrated in the present work (figure 3.5).

The suitability of Nile red as marker for paclitaxel production can be confirmed by quantifying the number of stained cells and comparison to the alkaloid production of different cell cultures.

Examination of gene expression and alkaloid production in Cath 001 and Cath 004 already indicated a posttranslational regulation. In order to determine regulatory

mechanisms in the formation of vinca alkaloids in Cath 001 and Cath 004 more precisely, a gene expression analysis using qPCR should be conducted after various elicitor treatments, which can then be correlated with alkaloid production. Since evidence has been found that size of aggregates is relevant for the accumulation of alkaloids, the size of the aggregates should be determined and compared to the metabolic productivity of the cell lines after elicitation and precursor feeding.

The microfluidic bioreactor in chip design has already been proven to be suitable for technical simulation of plant tissue and miniaturization of fermentation processes. Microscopic examination of cells in the chip has already been made possible in the course of the present work (figure 5.5) by means of the cooperation between IMT and BOT I. Currently, the chip is equipped with a system for pH measurement, which can detect slight pH changes in the medium during the experiment. To further extend the application of the chip and to enable an even more detailed investigation of cellular processes in the chip, the microfluidic bioreactor can be equipped with additional features.

# 5 Appendix

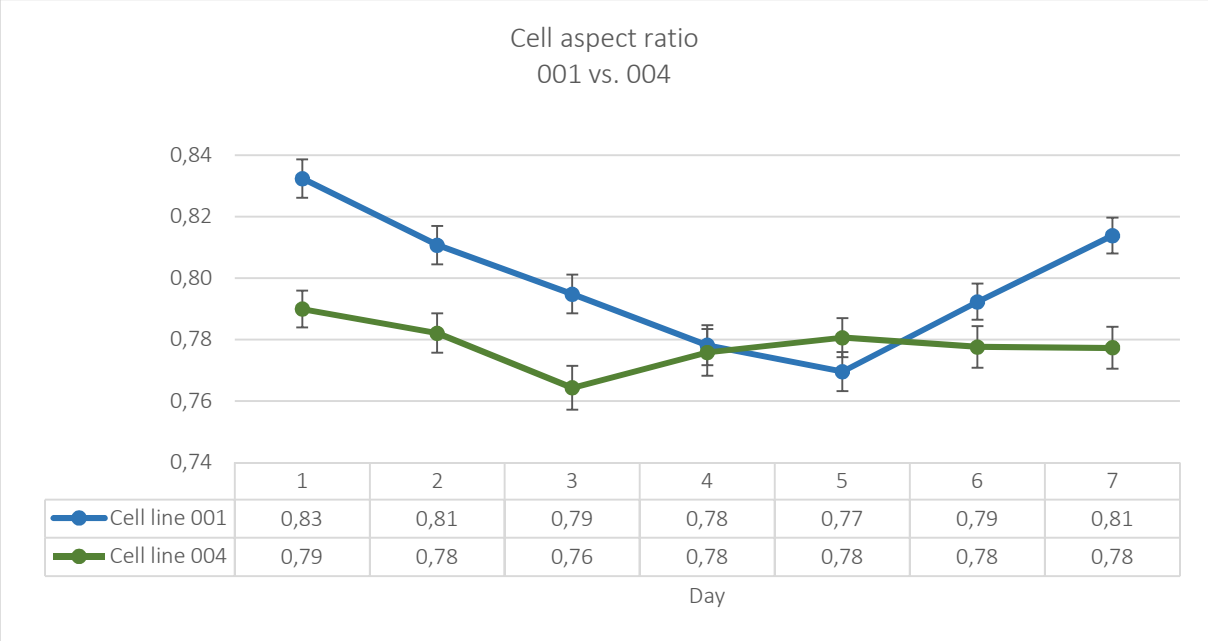


**Fig. 5.1: Cell aspect ratio of Cath 001 and Cath 004 control over time**
Average ratio between breadth and length of Cath 001 and Cath 004 cells over 7 days. Values closer to 1 indicate round cell shape, values closer to 0 indicate cell elongation. Each data point represents an average of at least 500 cells. Error bars indicate ±SE

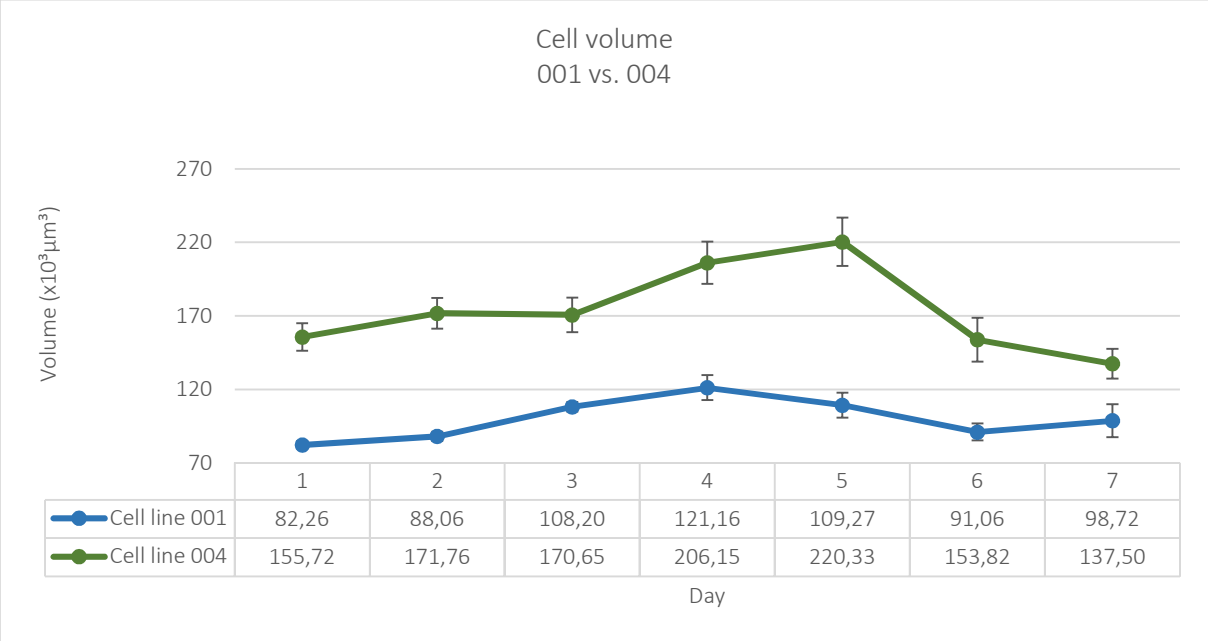


**Fig. 5.2: Cell volume of Cath 001 and Cath 004 control over time**
Average cell volume of Cath 001 and Cath 004 over 7 days. Each data point represents an average of at least 500 cells. Error bars indicate ±SE

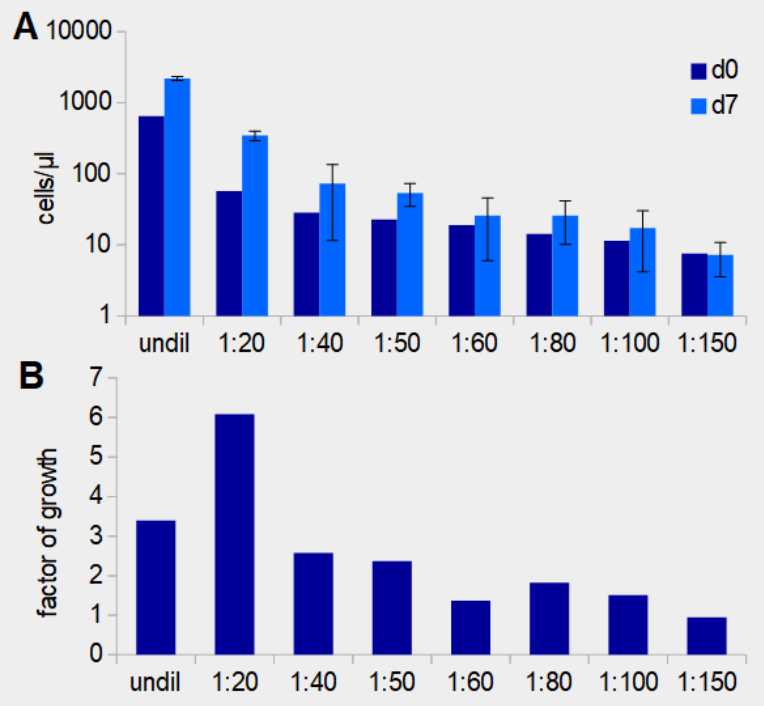


**Fig. 5.3: Inhibition of cell division in Cath 001 after dilution**
A: Number of Cath 001 cells per µl at the time of inoculation (d0) and after seven days (d7) in logarithmic scale for different dilutions. Values for d0 are calculated from the control, values of d7 represent the average of at least 6 technical replicates. Error bars indicate ± SE
B: Factor of growth in Cath 001 cell cultures for different dilutions, calculated from d7 values divided by d0 values. Low dilution promotes cell division, higher dilution inhibits cell division. In very high dilution cells stop dividing.

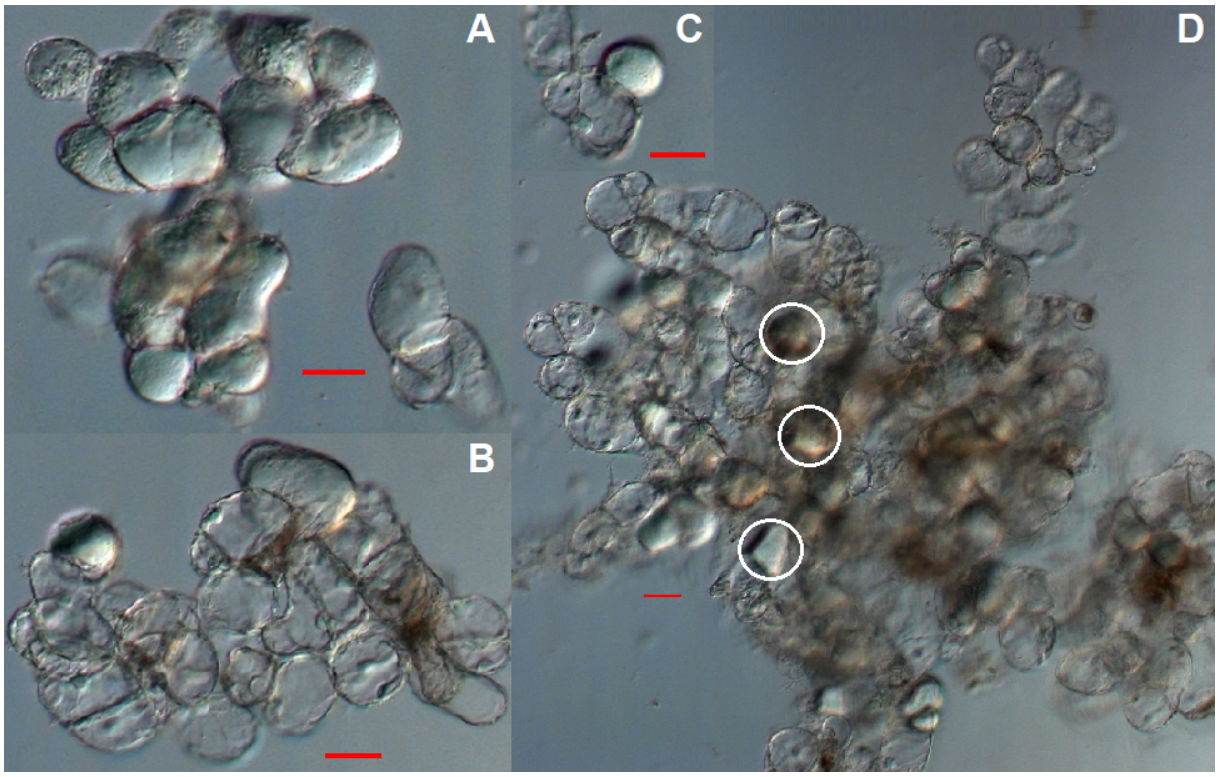


**Fig. 5.4: Exemplary sections of microscopic images for the evaluation of the shiny cell study**
Shown is a selection of arrangements in which the shiny cells are present within the aggregates.
A: Medium sized aggregate consisting almost excluxively of shiny cells
B: Medium sized aggregate with occasional occurrence of shiny cells
C: Shiny cell as part of very small aggregate
D: Large aggregate with varying numbers of shiny cells. Three shiny cells inside the aggregate are exemplarily marked by white circles.
(Scale bars represent 50 µm.)

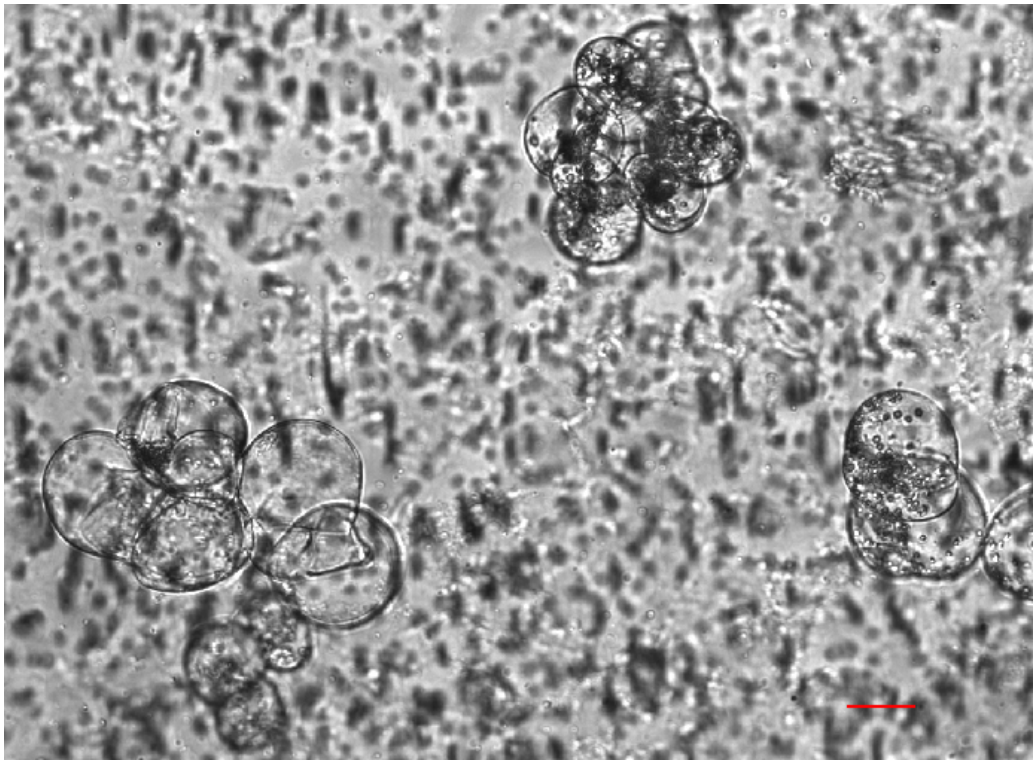

**Fig. 5.5: Microscopic image of Cath 001 cell aggregates taken in the chip**
Shown is a section of a microskopic image of Cath 001 cell aggregates in the microfluidic bioreactor. In the background, the semipermeable membrane with its pores can be seen, which separates the chip chamber from the medium chamber.
(Scale bar represents 50 µm.)

# 6 References

Aerts, R. J.; Gisi, D.; Carolis, E.; Luca, V.; Baumann, T. W. Methyl jasmonate vapor increases the developmentally controlled synthesis of alkaloids in Catharanthus and Cinchona seedlings. *Plant J* **1994,** *5* (5), 635–643. DOI: 10.1111/j.1365-313X.1994.00635.x.

Agnello, M.; Morici, G.; Rinaldi, A. M. A method for measuring mitochondrial mass and activity. *Cytotechnology* **2008,** *56* (3), 145–149. DOI: 10.1007/s10616-008-9143-2.

Alexander, C.; Votruba, M.; Pesch, U. E.A.; Thiselton, D. L.; Mayer, S.; Moore, A.; Rodriguez, M.; Kellner, U.; Leo-Kottler, B.; Auburger, G.; Bhattacharya, S. S.; Wissinger, B. *OPA1*, encoding a dynamin-related GTPase, is mutated in autosomal dominant optic atrophy linked to chromosome 3q28. *Nature Genetics* **2000,** *26* (2), 211. DOI: 10.1038/79944.

Almagro, L.; Fernández-Pérez, F.; Pedreño, M. A. Indole alkaloids from Catharanthus roseus: bioproduction and their effect on human health. *Molecules (Basel, Switzerland)* **2015,** *20* (2), 2973–3000. DOI: 10.3390/molecules20022973.

Asada, K.; Salim, V.; Masada-Atsumi, S.; Edmunds, E.; Nagatoshi, M.; Terasaka, K.; Mizukami, H.; Luca, V. de. A 7-deoxyloganetic acid glucosyltransferase contributes a key step in secologanin biosynthesis in Madagascar periwinkle. *The Plant cell* **2013,** *25* (10), 4123–4134. DOI: 10.1105/tpc.113.115154.

Barbulova, A.; Apone, F.; Colucci, G. Plant Cell Cultures as Source of Cosmetic Active Ingredients. *Cosmetics* **2014,** *1* (2), 94–104. DOI: 10.3390/cosmetics1020094.

Bentley, R. The shikimate pathway--a metabolic tree with many branches. *Critical reviews in biochemistry and molecular biology* **1990,** *25* (5), 307–384. DOI: 10.3109/10409239009090615.

Besseau, S.; Kellner, F.; Lanoue, A.; Thamm, A. M. K.; Salim, V.; Schneider, B.; Geu-Flores, F.; Höfer, R.; Guirimand, G.; Guihur, A.; Oudin, A.; Glevarec, G.; Foureau, E.; Papon, N.; Clastre, M.; Giglioli-Guivarc'h, N.; St-Pierre, B.; Werck-Reichhart, D.; Burlat, V.; Luca, V. de; O'Connor, S. E.; Courdavault, V. A pair of tabersonine 16-hydroxylases initiates the synthesis of vindoline in an organ-dependent manner in Catharanthus roseus. *Plant physiology* **2013,** *163* (4), 1792–1803. DOI: 10.1104/pp.113.222828.

Besumbes, O.; Sauret-Güeto, S.; Phillips, M. A.; Imperial, S.; Rodríguez-Concepción, M.; Boronat, A. Metabolic engineering of isoprenoid biosynthesis in Arabidopsis for the production of taxadiene, the first committed precursor of Taxol. *Biotechnology and bioengineering* **2004,** *88* (2), 168–175. DOI: 10.1002/bit.20237.

Blom, T. J.; Sierra, M.; van Vliet, T. B.; Franke-van Dijk, M. E.; Koning, P. de; van Iren, F.; Verpoorte, R.; Libbenga, K. R. Uptake and accumulation of ajmalicine into isolated vacuoles of cultured cells of Catharanthus roseus (L.) G. Don. and its conversion into serpentine. *Planta* **1991,** *183* (2), 170–177. DOI: 10.1007/BF00197785.

Brandizzi, F. Membrane Protein Transport between the Endoplasmic Reticulum and the Golgi in Tobacco Leaves Is Energy Dependent but Cytoskeleton Independent: Evidence from Selective Photobleaching. *THE PLANT CELL ONLINE* **2002,** *14* (6), 1293–1309. DOI: 10.1105/tpc.001586.

Brown, S.; Clastre, M.; Courdavault, V.; O'Connor, S. E. De novo production of the plant-derived alkaloid strictosidine in yeast. *Proceedings of the National Academy of Sciences of the United States of America* **2015,** *112* (11), 3205–3210. DOI: 10.1073/pnas.1423555112.

Burlat, V.; Oudin, A.; Courtois, M.; Rideau, M.; St-Pierre, B. Co-expression of three MEP pathway genes and geraniol 10-hydroxylase in internal phloem parenchyma of Catharanthus roseus implicates multicellular translocation of intermediates during the biosynthesis of monoterpene indole alkaloids and isoprenoid-derived primary metabolites. *Plant J* **2004,** *38* (1), 131–141. DOI: 10.1111/j.1365-313X.2004.02030.x.

Busch, W.; Moore, B. T.; Martsberger, B.; Mace, D. L.; Twigg, R. W.; Jung, J.; Pruteanu-Malinici, I.; Kennedy, S. J.; Fricke, G. K.; Clark, R. L.; Ohler, U.; Benfey, P. N. A microfluidic device and computational platform for high-throughput live imaging of gene expression. *Nature Methods* **2012,** *9* (11), 1101. DOI: 10.1038/nmeth.2185.

Campanoni, P.; Nick, P. Auxin-dependent cell division and cell elongation. 1-Naphthaleneacetic acid and 2,4-dichlorophenoxyacetic acid activate different pathways. *Plant physiology* **2005,** *137* (3), 939–948. DOI: 10.1104/pp.104.053843.

Canel, C.; Lopes-Cardoso, M. I.; Whitmer, S.; van der Fits, L.; Pasquali, G.; van der Heijden, R.; Hoge, J. H. C.; Verpoorte, R. Effects of over-expression of strictosidine synthase and tryptophan decarboxylase on alkaloid production by cell cultures of Catharanthus roseus. *Planta* **1998,** *205* (3), 414–419. DOI: 10.1007/s004250050338.

Carqueijeiro, I.; Noronha, H.; Duarte, P.; Gerós, H.; Sottomayor, M. Vacuolar transport of the medicinal alkaloids from Catharanthus roseus is mediated by a proton-driven antiport. *Plant physiology* **2013,** *162* (3), 1486–1496. DOI: 10.1104/pp.113.220558.

Chaban, Y.; Boekema, E. J.; Dudkina, N. V. Structures of mitochondrial oxidative phosphorylation supercomplexes and mechanisms for their stabilisation. *Biochimica et biophysica acta* **2014,** *1837* (4), 418–426. DOI: 10.1016/j.bbabio.2013.10.004.

Chang, X.; Riemann, M.; Liu, Q.; Nick, P. Actin as deathly switch? How auxin can suppress cell-death related defence. *PloS one* **2015,** *10* (5), e0125498. DOI: 10.1371/journal.pone.0125498.

Chemler, J. A.; Koffas, M. A. G. Metabolic engineering for plant natural product biosynthesis in microbes. *Current opinion in biotechnology* **2008,** *19* (6), 597–605. DOI: 10.1016/j.copbio.2008.10.011.

Chen, H.; Detmer, S. A.; Ewald, A. J.; Griffin, E. E.; Fraser, S. E.; Chan, D. C. Mitofusins Mfn1 and Mfn2 coordinately regulate mitochondrial fusion and are essential for embryonic development. *The Journal of cell biology* **2003,** *160* (2), 189–200. DOI: 10.1083/jcb.200211046.

Constabel, F.; Gaudet-Laprairie, P.; Kurz, W. G.; Kutney, J. P. Alkaloid production in Catharanthus roseus cell cultures : XII. Biosynthetic capacity of callus from original explants and regenerated shoots. *Plant cell reports* **1982,** *1* (4), 139–142. DOI: 10.1007/BF00269182.

Costa, M. M. R.; Hilliou, F.; Duarte, P.; Pereira, L. G.; Almeida, I.; Leech, M.; Memelink, J.; Barceló, A. R.; Sottomayor, M. Molecular cloning and characterization of a vacuolar class III peroxidase involved in the metabolism of anticancer alkaloids in Catharanthus roseus. *Plant physiology* **2008,** *146* (2), 403–417. DOI: 10.1104/pp.107.107060.

Covello, P. S. Making artemisinin. *Phytochemistry* **2008,** *69* (17), 2881–2885. DOI: 10.1016/j.phytochem.2008.10.001.

Cusido, R. M.; Onrubia, M.; Sabater-Jara, A. B.; Moyano, E.; Bonfill, M.; Goossens, A.; Angeles Pedreño, M.; Palazon, J. A rational approach to improving the biotechnological production of taxanes in plant cell cultures of Taxus spp. *Biotechnology advances* **2014,** *32* (6), 1157–1167. DOI: 10.1016/j.biotechadv.2014.03.002.

d'Amato, T. A.; Ganson, R. J.; Gaines, C. G.; Jensen, R. A. Subcellular localization of chorismate-mutase isoenzymes in protoplasts from mesophyll and suspension-cultured cells of Nicotiana silvestris. *Planta* **1984,** *162* (2), 104–108. DOI: 10.1007/BF00410205.

Denisenko, V. Y.; Kuzmina, T. I. On the problem of identification of intracellular signaling pathways. *Biochemistry. Biokhimiia* **2013,** *78* (4), 431–432. DOI: 10.1134/S0006297913040135.

D'haene, B.; Vandesompele, J.; Hellemans, J. Accurate and objective copy number profiling using real-time quantitative PCR. *Methods (San Diego, Calif.)* **2010,** *50* (4), 262–270. DOI: 10.1016/j.ymeth.2009.12.007.

do Nascimento, N. C.; Menguer, P. K.; Henriques, A. T.; Fett-Neto, A. G. Accumulation of brachycerine, an antioxidant glucosidic indole alkaloid, is induced by abscisic acid, heavy metal, and osmotic stress in leaves of Psychotria brachyceras. *Plant physiology and biochemistry : PPB* **2013,** *73*, 33–40. DOI: 10.1016/j.plaphy.2013.08.007.

Dong, H.-D.; Zhong, J.-J. Enhanced taxane productivity in bioreactor cultivation of Taxus chinensis cells by combining elicitation, sucrose feeding and ethylene incorporation. *Enzyme and Microbial Technology* **2002,** *31* (1-2), 116–121. DOI: 10.1016/S0141-0229(02)00079-0.

Durst, S.; Nick, P.; Maisch, J. Nicotiana tabacum actin-depolymerizing factor 2 is involved in actin-driven, auxin-dependent patterning. *Journal of plant physiology* **2013,** *170* (12), 1057–1066. DOI: 10.1016/j.jplph.2013.03.002.

Edge, A.; Qu, Y.; Easson, M. L. A. E.; Thamm, A. M. K.; Kim, K. H.; Luca, V. de. A tabersonine 3-reductase Catharanthus roseus mutant accumulates vindoline pathway intermediates. *Planta* **2018,** *247* (1), 155–169. DOI: 10.1007/s00425-017-2775-8.

Eggenberger, K.; Sanyal, P.; Hundt, S.; Wadhwani, P.; Ulrich, A. S.; Nick, P. Challenge Integrity: The Cell-Penetrating Peptide BP100 Interferes with the Auxin-Actin Oscillator. *Plant & cell physiology* **2017,** *58* (1), 71–85. DOI: 10.1093/pcp/pcw161.

El-Sayed, M.; Choi, Y. H.; Frédérich, M.; Roytrakul, S.; Verpoorte, R. Alkaloid accumulation in Catharanthus roseus cell suspension cultures fed with stemmadenine. *Biotechnology letters* **2004,** *26* (10), 793–798. DOI: 10.1023/B:BILE.0000025879.53632.f2.

El-Sayed, M.; Verpoorte, R. Catharanthus terpenoid indole alkaloids: biosynthesis and regulation. *Phytochem Rev* **2007,** *6* (2-3), 277–305. DOI: 10.1007/s11101-006-9047-8.

Expósito, O.; Bonfill, M.; Onrubia, M.; Jané, A.; Moyano, E.; Cusidó, R. M.; Palazón, J.; Piñol, M. T. Effect of taxol feeding on taxol and related taxane production in Taxus baccata suspension cultures. *New biotechnology* **2009,** *25* (4), 252–259. DOI: 10.1016/j.nbt.2008.11.001.

Farmer, E. E.; Ryan, C. A. Interplant communication: airborne methyl jasmonate induces synthesis of proteinase inhibitors in plant leaves. *Proceedings of the National Academy of Sciences* **1990,** *87* (19), 7713–7716. DOI: 10.1073/pnas.87.19.7713.

Fiedler, E.; Schultz, G. Localization, Purification, and Characterization of Shikimate Oxidoreductase-Dehydroquinate Hydrolyase from Stroma of Spinach Chloroplasts. *Plant physiology* **1985,** *79* (1), 212–218. DOI: 10.1104/pp.79.1.212.

Fowler, M. W. Substrate utilisation by plant-cell cultures. *J. Chem. Technol. Biotechnol.* **1982,** *32* (1), 338–346. DOI: 10.1002/jctb.5030320139.

Furmanowa, M.; Glowniak, K.; Syklowska-Baranek, K.; Zgórka, G.; Józefczyk, A. Effect of picloram and methyl jasmonate on growth and taxane accumulation in callus culture of Taxus

× media var. Hatfieldii. *Plant Cell, Tissue and Organ Culture* **1997,** *49* (1), 75–79. DOI: 10.1023/A:1005858329430.

Gaurav, V.; Kolewe, M. E.; Roberts, S. C. Flow cytometric methods to investigate culture heterogeneities for plant metabolic engineering. *Methods in molecular biology (Clifton, N.J.)* **2010,** *643*, 243–262. DOI: 10.1007/978-1-60761-723-5_17.

Geerlings, A.; Ibañez, M. M.-L.; Memelink, J.; van der Heijden, R.; Verpoorte, R. Molecular Cloning and Analysis of Strictosidine β-d-Glucosidase, an Enzyme in Terpenoid Indole Alkaloid Biosynthesis in Catharanthus roseus. *J. Biol. Chem.* **2000,** *275* (5), 3051–3056. DOI: 10.1074/jbc.275.5.3051.

Geyter, N. de; Gholami, A.; Goormachtig, S.; Goossens, A. Transcriptional machineries in jasmonate-elicited plant secondary metabolism. *Trends in plant science* **2012,** *17* (6), 349–359. DOI: 10.1016/j.tplants.2012.03.001.

Goddijn, O. J. M.; Kam, R. J. de; Zanetti, A.; Schilperoort, R. A.; Hoge, J. H. C. Auxin rapidly down-regulates transcription of the tryptophan decarboxylase gene from Catharanthus roseus. *Plant molecular biology* **1992,** *18* (6), 1113–1120. DOI: 10.1007/BF00047714.

Gomer, R. H.; Jang, W.; Brazill, D. Cell density sensing and size determination. *Development, growth & differentiation* **2011,** *53* (4), 482–494. DOI: 10.1111/j.1440-169X.2010.01248.x.

Gómez-Galera, S.; Pelacho, A. M.; Gené, A.; Capell, T.; Christou, P. The genetic manipulation of medicinal and aromatic plants. *Plant cell reports* **2007,** *26* (10), 1689–1715. DOI: 10.1007/s00299-007-0384-x.

Gonçalves, S.; Romano, A. Production of Plant Secondary Metabolites by Using Biotechnological Tools. In *Secondary Metabolites - Sources and Applications*; Vijayakumar, R., Raja, S. S.S., Eds.; InTech, 2018. DOI: 10.5772/intechopen.76414.

Goossens, A.; Häkkinen, S. T.; Laakso, I.; Seppänen-Laakso, T.; Biondi, S.; Sutter, V. de; Lammertyn, F.; Nuutila, A. M.; Söderlund, H.; Zabeau, M.; Inzé, D.; Oksman-Caldentey, K.-M. A functional genomics approach toward the understanding of secondary metabolism in plant cells. *Proceedings of the National Academy of Sciences* **2003,** *100* (14), 8595–8600. DOI: 10.1073/pnas.1032967100.

Guirimand, G.; Burlat, V.; Oudin, A.; Lanoue, A.; St-Pierre, B.; Courdavault, V. Optimization of the transient transformation of Catharanthus roseus cells by particle bombardment and its application to the subcellular localization of hydroxymethylbutenyl 4-diphosphate synthase and geraniol 10-hydroxylase. *Plant cell reports* **2009,** *28* (8), 1215–1234. DOI: 10.1007/s00299-009-0722-2.

Guirimand, G.; Courdavault, V.; Lanoue, A.; Mahroug, S.; Guihur, A.; Blanc, N.; Giglioli-Guivarc'h, N.; St-Pierre, B.; Burlat, V. Strictosidine activation in Apocynaceae: towards a "nuclear time bomb"? *BMC plant biology* **2010,** *10*, 182. DOI: 10.1186/1471-2229-10-182.

Guirimand, G.; Guihur, A.; Ginis, O.; Poutrain, P.; Héricourt, F.; Oudin, A.; Lanoue, A.; St-Pierre, B.; Burlat, V.; Courdavault, V. The subcellular organization of strictosidine biosynthesis in Catharanthus roseus epidermis highlights several trans-tonoplast translocations of intermediate metabolites. *The FEBS journal* **2011a,** *278* (5), 749–763. DOI: 10.1111/j.1742-4658.2010.07994.x.

Guirimand, G.; Guihur, A.; Poutrain, P.; Héricourt, F.; Mahroug, S.; St-Pierre, B.; Burlat, V.; Courdavault, V. Spatial organization of the vindoline biosynthetic pathway in Catharanthus roseus. *Journal of plant physiology* **2011b,** *168* (6), 549–557. DOI: 10.1016/j.jplph.2010.08.018.

Guo, Z.-G.; Liu, Y.; Gong, M.-Z.; Chen, W.; Li, W.-Y. Regulation of vinblastine biosynthesis in cell suspension cultures of catharanthus roseus. *Plant Cell Tiss Organ Cult* **2013,** *112* (1), 43–54. DOI: 10.1007/s11240-012-0213-y.

Hall, R. D. Plant Cell Culture Initiation: Practical Tips. *MB* **2000,** *16* (2), 161–174. DOI: 10.1385/MB:16:2:161.

Hall, R. D.; Yeoman, M. M. Intercellular and Intercultural Heterogeneity in Secondary Metabolite Accumulation in Cultures of Catharanthus roseus following Cell Line Selection. *J Exp Bot* **1987,** *38* (8), 1391–1398. DOI: 10.1093/jxb/38.8.1391.

Harborne, J. B. Classes and funktions of secondary products from plants. In *Chemicals from plants*: *Perspectives on plant secondary products*; Walton, N. J., Brown, D. E., Eds.; Distributed by World Scientific: London, 1999; pp 1–25. DOI: 10.1142/9789812817273_0001.

Hashimoto, T.; Yamada, Y. Alkaloid Biogenesis: Molecular Aspects. *Annual review of plant physiology and plant molecular biology* **1994,** *45* (1), 257–285. DOI: 10.1146/annurev.pp.45.060194.001353.

He, C.-T.; Li, Z.-L.; Zhou, Q.; Shen, C.; Huang, Y.-Y.; Mubeen, S.; Yang, J.-Z.; Yuan, J.-G.; Yang, Z.-Y. Transcriptome profiling reveals specific patterns of paclitaxel synthesis in a new Taxus yunnanensis cultivar. *Plant physiology and biochemistry : PPB* **2018,** *122*, 10–18. DOI: 10.1016/j.plaphy.2017.10.028.

Hefner, J.; Ketchum, R. E.; Croteau, R. Cloning and functional expression of a cDNA encoding geranylgeranyl diphosphate synthase from Taxus canadensis and assessment of the role of this prenyltransferase in cells induced for taxol production. *Archives of biochemistry and biophysics* **1998,** *360* (1), 62–74. DOI: 10.1006/abbi.1998.0926.

Heijden, R.; Jacobs, D.; Snoeijer, W.; Hallard, D.; Verpoorte, R. The Catharanthus Alkaloids:Pharmacognosy and Biotechnology. *CMC* **2004,** *11* (5), 607–628. DOI: 10.2174/0929867043455846.

Hellemans, J.; Mortier, G.; Paepe, A. de; Speleman, F.; Vandesompele, J. qBase relative quantification framework and software for management and automated analysis of real-time quantitative PCR data. *Genome biology* **2007,** *8* (2), R19. DOI: 10.1186/gb-2007-8-2-r19.

Herrmann, K. M.; Weaver, L. M. THE SHIKIMATE PATHWAY. *Annual review of plant physiology and plant molecular biology* **1999,** *50*, 473–503. DOI: 10.1146/annurev.arplant.50.1.473.

Hildebrand, A. A.; Kohn, B. N.; Pfeiffer, E.; Wefers, D.; Metzler, M.; Bunzel, M. Conjugation of the mycotoxins alternariol and alternariol monomethyl ether in tobacco suspension cells. *Journal of agricultural and food chemistry* **2015,** *63* (19), 4728–4736. DOI: 10.1021/acs.jafc.5b00806.

Hill, A.; Barber, M. Unexplained rises in UK cancer drug prices between 2011 and 2016. *European Journal of Cancer* **2017,** *72*, S113-S114. DOI: 10.1016/S0959-8049(17)30455-0.

Howat, S.; Park, B.; Oh, I. S.; Jin, Y.-W.; Lee, E.-K.; Loake, G. J. Paclitaxel: biosynthesis, production and future prospects. *New biotechnology* **2014,** *31* (3), 242–245. DOI: 10.1016/j.nbt.2014.02.010.

Hulst, A. C.; Meyer, M.M.T.; Breteler, H.; Tramper, J. Effect of aggregate size in cell cultures of Tagetes patula on thiophene production and cell growth. *Appl Microbiol Biotechnol* **1989,** *30* (1). DOI: 10.1007/BF00255991.

Irmler, S.; Schröder, G.; St-Pierre, B.; Crouch, N. P.; Hotze, M.; Schmidt, J.; Strack, D.; Matern, U.; Schröder, J. Indole alkaloid biosynthesis in Catharanthus roseus: new enzyme activities and identification of cytochrome P450 CYP72A1 as secologanin synthase. *Plant J* **2000,** *24* (6), 797–804. DOI: 10.1111/j.1365-313X.2000.00922.x.

Jain, M.; Nijhawan, A.; Tyagi, A. K.; Khurana, J. P. Validation of housekeeping genes as internal control for studying gene expression in rice by quantitative real-time PCR. *Biochemical and biophysical research communications* **2006,** *345* (2), 646–651. DOI: 10.1016/j.bbrc.2006.04.140.

Jaipargas, E.-A.; Barton, K. A.; Mathur, N.; Mathur, J. Mitochondrial pleomorphy in plant cells is driven by contiguous ER dynamics. *Frontiers in plant science* **2015,** *6*, 783. DOI: 10.3389/fpls.2015.00783.

Jennewein, S.; Long, R. M.; Williams, R. M.; Croteau, R. Cytochrome p450 taxadiene 5alpha-hydroxylase, a mechanistically unusual monooxygenase catalyzing the first oxygenation step of taxol biosynthesis. *Chemistry & biology* **2004a,** *11* (3), 379–387. DOI: 10.1016/j.chembiol.2004.02.022.

Jennewein, S.; Rithner, C. D.; Williams, R. M.; Croteau, R. B. Taxol biosynthesis: taxane 13 alpha-hydroxylase is a cytochrome P450-dependent monooxygenase. *Proceedings of the National Academy of Sciences* **2001,** *98* (24), 13595–13600. DOI: 10.1073/pnas.251539398.

Jennewein, S.; Wildung, M. R.; Chau, M.; Walker, K.; Croteau, R. Random sequencing of an induced Taxus cell cDNA library for identification of clones involved in Taxol biosynthesis. *Proceedings of the National Academy of Sciences* **2004b,** *101* (24), 9149–9154. DOI: 10.1073/pnas.0403009101.

Jordan, M. A.; Wilson, L. Microtubules as a target for anticancer drugs. *Nature reviews. Cancer* **2004,** *4* (4), 253–265. DOI: 10.1038/nrc1317.

Jovanović, A. M.; Durst, S.; Nick, P. Plant cell division is specifically affected by nitrotyrosine. *Journal of experimental botany* **2010,** *61* (3), 901–909. DOI: 10.1093/jxb/erp369.

Joyce, C. Taxol: Search for a Cancer Drug. *BioScience* **1993,** *43* (3), 133–136. DOI: 10.2307/1312015.

Jung, K. H.; Kwak, S. S.; Kim, S. W.; Lee, H.; Choi, C. Y.; Liu, J. R. Improvement of the catharanthine productivity in hairy root cultures ofCatharanthus roseus by using monosaccharides as a carbon source. *Biotechnology letters* **1992,** *14* (8), 695–700. DOI: 10.1007/BF01021645.

Kawano, T.; Kadono, T.; Furuichi, T.; Muto, S.; Lapeyrie, F. Aluminum-induced distortion in calcium signaling involving oxidative bursts and channel regulation in tobacco BY-2 cells. *Biochemical and biophysical research communications* **2003,** *308* (1), 35–42. DOI: 10.1016/S0006-291X(03)01286-5.

Kawano, T.; Kawano, N.; Muto, S.; Lapeyrie, F. Cation-induced superoxide generation in tobacco cell suspension culture is dependent on ion valence. *Plant Cell Environ* **2001,** *24* (11), 1235–1241. DOI: 10.1046/j.1365-3040.2001.00766.x.

Kellner, F.; Geu-Flores, F.; Sherden, N. H.; Brown, S.; Foureau, E.; Courdavault, V.; O'Connor, S. E. Discovery of a P450-catalyzed step in vindoline biosynthesis: a link between the aspidosperma and eburnamine alkaloids. *Chemical communications (Cambridge, England)* **2015,** *51* (36), 7626–7628. DOI: 10.1039/c5cc01309g.

Keßler, M.; Hoopen, H. J.G. ten; Furusaki, S. The effect of the aggregate size on the production of ajmalicine and tryptamine in Catharanthus roseus suspension culture. *Enzyme and Microbial Technology* **1999,** *24* (5-6), 308–315. DOI: 10.1016/S0141-0229(98)00121-5.

Ketchum, R. E. B.; Gibson, D. M. Paclitaxel production in suspension cell cultures of Taxus. *Plant Cell Tiss Organ Cult* **1996,** *46* (1), 9–16. DOI: 10.1007/BF00039691.

Kim, S. W.; Jung, K. H.; Kwak, S. S.; Liu, J. R. Relationship between cell morphology and indole alkaloid production in suspension cultures of Catharanthus roseus. *Plant cell reports* **1994,** *14* (1), 23–26. DOI: 10.1007/BF00233292.

Kingston, D. G. I.; Chordia, M. D.; Jagtap, P. G.; Liang, J.; Shen, Y.-C.; Long, B. H.; Fairchild, C. R.; Johnston, K. A. Synthesis and Biological Evaluation of 1-Deoxypaclitaxel Analogues. *J. Org. Chem.* **1999,** *64* (6), 1814–1822. DOI: 10.1021/jo981406l.

Knobloch, K.-H.; Berlin, J. Influence of Medium Composition on the Formation of Secondary Compounds in Cell Suspension Cultures of Catharanthus roseus (L.) G. Don. *Zeitschrift für Naturforschung C* **1980,** *35* (7-8), 551–556. DOI: 10.1515/znc-1980-7-805.

Koda, Y. Possible involvement of jasmonates in various morphogenic events. *Physiol Plant* **1997,** *100* (3), 639–646. DOI: 10.1111/j.1399-3054.1997.tb03070.x.

Kolewe, M. E.; Gaurav, V.; Roberts, S. C. Pharmaceutically active natural product synthesis and supply via plant cell culture technology. *Molecular pharmaceutics* **2008,** *5* (2), 243–256. DOI: 10.1021/mp7001494.

Kovacs, K.; Zhang, L.; Linforth, R. S. T.; Whittaker, B.; Hayes, C. J.; Fray, R. G. Redirection of carotenoid metabolism for the efficient production of taxadiene taxa-4(5),11(12)-diene in transgenic tomato fruit. *Transgenic research* **2007,** *16* (1), 121–126. DOI: 10.1007/s11248-006-9039-x.

Küpeli, E.; Erdemoğlu, N.; Yeşilada, E.; Şener, B. Anti-inflammatory and antinociceptive activity of taxoids and lignans from the heartwood of Taxus baccata L. *Journal of Ethnopharmacology* **2003,** *89* (2-3), 265–270. DOI: 10.1016/j.jep.2003.09.005.

Laskaris, G.; Bounkhay, M.; Theodoridis, G.; van der Heijden, R.; Verpoorte, R.; Jaziri, M. Induction of geranylgeranyl diphosphate synthase activity and taxane accumulation in Taxus baccata cell cultures after elicitation by methyl jasmonate. *Plant Science* **1999,** *147* (1), 1–8. DOI: 10.1016/S0168-9452(99)00078-3.

Law, S. R.; Narsai, R.; Whelan, J. Mitochondrial biogenesis in plants during seed germination. *Mitochondrion* **2014,** *19 Pt B*, 214–221. DOI: 10.1016/j.mito.2014.04.002.

Le Zhao; Sander, G. W.; Shanks, J. V. Perspectives of the metabolic engineering of terpenoid indole alkaloids in Catharanthus roseus hairy roots. *Advances in biochemical engineering/biotechnology* **2013,** *134*, 23–54. DOI: 10.1007/10_2013_182.

Lee, E.-K.; Jin, Y.-W.; Park, J. H.; Yoo, Y. M.; Hong, S. M.; Amir, R.; Yan, Z.; Kwon, E.; Elfick, A.; Tomlinson, S.; Halbritter, F.; Waibel, T.; Yun, B.-W.; Loake, G. J. Cultured cambial meristematic cells as a source of plant natural products. *Nature Biotechnology* **2010,** *28* (11), 1213. DOI: 10.1038/nbt.1693.

Lenka, S. K.; Nims, N. E.; Vongpaseuth, K.; Boshar, R. A.; Roberts, S. C.; Walker, E. L. Jasmonate-responsive expression of paclitaxel biosynthesis genes in Taxus cuspidata cultured cells is negatively regulated by the bHLH transcription factors TcJAMYC1, TcJAMYC2, and TcJAMYC4. *Frontiers in plant science* **2015,** *6*, 115. DOI: 10.3389/fpls.2015.00115.

Levac, D.; Murata, J.; Kim, W. S.; Luca, V. de. Application of carborundum abrasion for investigating the leaf epidermis: molecular cloning of Catharanthus roseus 16-hydroxytabersonine-16-O-methyltransferase. *Plant J* **2008,** *53* (2), 225–236. DOI: 10.1111/j.1365-313X.2007.03337.x.

Li, J.; Last, R. L. The Arabidopsis thaliana trp5 Mutant Has a Feedback-Resistant Anthranilate Synthase and Elevated Soluble Tryptophan. *Plant physiology* **1996,** *110* (1), 51–59. DOI: 10.1104/pp.110.1.51.

Lin, S.-L.; Wei, T.; Lin, J.-F.; Guo, L.-Q.; Wu, G.-P.; Wei, J.-B.; Huang, J.-J.; Ouyang, P.-L. Bio-production of Baccatin III, an Important Precursor of Paclitaxel by a Cost-Effective Approach. *Molecular biotechnology* **2018,** *60* (7), 492–505. DOI: 10.1007/s12033-018-0090-7.

Lindsey, K.; Yeoman, M. M. The Relationship between Growth Rate, Differentiation and Alkaloid Accumulation in Cell Cultures. *J Exp Bot* **1983,** *34* (8), 1055–1065. DOI: 10.1093/jxb/34.8.1055.

Liscombe, D. K.; Usera, A. R.; O'Connor, S. E. Homolog of tocopherol C methyltransferases catalyzes N methylation in anticancer alkaloid biosynthesis. *Proceedings of the National Academy of Sciences of the United States of America* **2010,** *107* (44), 18793–18798. DOI: 10.1073/pnas.1009003107.

Liu, J.; Cai, J.; Wang, R.; Yang, S. Transcriptional Regulation and Transport of Terpenoid Indole Alkaloid in Catharanthus roseus: Exploration of New Research Directions. *International journal of molecular sciences* **2016,** *18* (1). DOI: 10.3390/ijms18010053.

Liu, Q. Mechanosensing in Plants - Mechanosensitive Calcium Channels versus the Cell Wall-Plasma Membrane-Cytoskeleton Continuum [Online] **2014**.

Logan, D. C. Mitochondrial fusion, division and positioning in plants. *Biochemical Society transactions* **2010,** *38* (3), 789–795. DOI: 10.1042/BST0380789.

Luca, V. de; Cutler, A. J. Subcellular Localization of Enzymes Involved in Indole Alkaloid Biosynthesis in Catharanthus roseus. *Plant physiology* **1987,** *85* (4), 1099–1102. DOI: 10.1104/pp.85.4.1099.

Luca, V. de; Marineau, C.; Brisson, N. Molecular cloning and analysis of cDNA encoding a plant tryptophan decarboxylase: comparison with animal dopa decarboxylases. *Proceedings of the National Academy of Sciences* **1989,** *86* (8), 2582–2586. DOI: 10.1073/pnas.86.8.2582.

Mahroug, S.; Burlat, V.; St-Pierre, B. Cellular and sub-cellular organisation of the monoterpenoid indole alkaloid pathway in Catharanthus roseus. *Phytochem Rev* **2007,** *6* (2-3), 363–381. DOI: 10.1007/s11101-006-9017-1.

Maisch, J.; Ahrens, R.; Sobich, S.; Guber, A.; Kreppenhofer, K.; Nick, P. Microfluidic Bioreactor with modular Design for Synthesizing Cell Metabolites, Method for Using same, and use thereof. *United States Patent Application Publication* [Online] **2016a**.

Maisch, J.; Fiserová, J.; Fischer, L.; Nick, P. Tobacco Arp3 is localized to actin-nucleating sites in vivo. *Journal of experimental botany* **2009,** *60* (2), 603–614. DOI: 10.1093/jxb/ern307.

Maisch, J.; Kreppenhofer, K.; Büchler, S.; Merle, C.; Sobich, S.; Görling, B.; Luy, B.; Ahrens, R.; Guber, A. E.; Nick, P. Time-resolved NMR metabolomics of plant cells based on a microfluidic chip. *Journal of plant physiology* **2016b,** *200*, 28–34. DOI: 10.1016/j.jplph.2016.06.004.

Maisch, J.; Nick, P. Actin is involved in auxin-dependent patterning. *Plant physiology* **2007,** *143* (4), 1695–1704. DOI: 10.1104/pp.106.094052.

Malik, S.; Cusidó, R. M.; Mirjalili, M. H.; Moyano, E.; Palazón, J.; Bonfill, M. Production of the anticancer drug taxol in Taxus baccata suspension cultures: A review. *Process Biochemistry* **2011,** *46* (1), 23–34. DOI: 10.1016/j.procbio.2010.09.004.

Martinou, J.-C.; Youle, R. J. Which came first, the cytochrome c release or the mitochondrial fission? *Cell death and differentiation* **2006,** *13* (8), 1291–1295. DOI: 10.1038/sj.cdd.4401985.

Marty, F. Plant Vacuoles. *THE PLANT CELL ONLINE* **1999,** *11* (4), 587–600. DOI: 10.1105/tpc.11.4.587.

Mathur, J.; Mathur, N.; Hülskamp, M. Simultaneous visualization of peroxisomes and cytoskeletal elements reveals actin and not microtubule-based peroxisome motility in plants. *Plant physiology* **2002,** *128* (3), 1031–1045. DOI: 10.1104/pp.011018.

McCabe, P. F.; Levine, A.; Meijer, P.-J.; Tapon, N. A.; Pennell, R. I. A programmed cell death pathway activated in carrot cells cultured at low cell density. *Plant J* **1997,** *12* (2), 267–280. DOI: 10.1046/j.1365-313X.1997.12020267.x.

McKnight, T. D.; Roessner, C. A.; Devagupta, R.; Scott, A. I.; Nessler, C. L. Nucleotide sequence of a cDNA encoding the vacuolar protein strictosidine synthase from Catharanthus roseus. *Nucleic Acids Research* **1990,** *18* (16), 4939.

Meijer, A. H.; Cardoso, M. I. L.; Voskuilen, J. T.; Waal, A.; Verpoorte, R.; Hoge, J. H. C. Isolation and characterization of a cDNA clone from Catharanthus roseus encoding NADPH:cytochrome P-450 reductase, an enzyme essential for reactions catalysed by cytochrome P-450 mono-oxygenases in plants. *Plant J* **1993,** *4* (1), 47–60. DOI: 10.1046/j.1365-313X.1993.04010047.x.

Menke, F. L.; Champion, A.; Kijne, J. W.; Memelink, J. A novel jasmonate- and elicitor-responsive element in the periwinkle secondary metabolite biosynthetic gene Str interacts with a jasmonate- and elicitor-inducible AP2-domain transcription factor, ORCA2. *The EMBO journal* **1999,** *18* (16), 4455–4463. DOI: 10.1093/emboj/18.16.4455.

Miettinen, K.; Dong, L.; Navrot, N.; Schneider, T.; Burlat, V.; Pollier, J.; Woittiez, L.; van der Krol, S.; Lugan, R.; Ilc, T.; Verpoorte, R.; Oksman-Caldentey, K.-M.; Martinoia, E.; Bouwmeester, H.; Goossens, A.; Memelink, J.; Werck-Reichhart, D. The seco-iridoid pathway from Catharanthus roseus. *Nature Communications* **2014,** *5*, 3606. DOI: 10.1038/ncomms4606.

Mitra, K. Mitochondrial fission-fusion as an emerging key regulator of cell proliferation and differentiation. *BioEssays : news and reviews in molecular, cellular and developmental biology* **2013,** *35* (11), 955–964. DOI: 10.1002/bies.201300011.

Moudi, M.; Go, R.; Yien, C. Y. S.; Nazre, M. Vinca Alkaloids. *International Journal of Preventive Medicine* **2013,** *4* (11), 1231–1235.

Mousdale, D. M.; Coggins, J. R. Subcellular localization of the common shikimate-pathway enzymes in Pisum sativum L. *Planta* **1985,** *163* (2), 241–249. DOI: 10.1007/BF00393514.

Mousdale, D. M.; Coggins, J. R. Detection and subcellular localization of a higher plant chorismate synthase. *FEBS Letters* **1986,** *205* (2), 328–332. DOI: 10.1016/0014-5793(86)80922-X.

Murata, J.; Luca, V. de. Localization of tabersonine 16-hydroxylase and 16-OH tabersonine-16-O-methyltransferase to leaf epidermal cells defines them as a major site of precursor biosynthesis in the vindoline pathway in Catharanthus roseus. *Plant J* **2005,** *44* (4), 581–594. DOI: 10.1111/j.1365-313X.2005.02557.x.

Murata, J.; Roepke, J.; Gordon, H.; Luca, V. de. The leaf epidermome of Catharanthus roseus reveals its biochemical specialization. *The Plant cell* **2008,** *20* (3), 524–542. DOI: 10.1105/tpc.107.056630.

Nagappa, M.; Bhat, R. R.; Sudeep, K.; Mishra, S. K.; Badhe, A. S.; Hemavathi, B. Vincristine-induced acute life-threatening hyponatremia resulting in seizure and coma. *Indian Journal of Critical Care Medicine : Peer-reviewed, Official Publication of Indian Society of Critical Care Medicine* **2009,** *13* (3), 167–168. DOI: 10.4103/0972-5229.58545.

Nagata, T.; Nemoto, Y.; Hasezawa, S. Tobacco BY-2 Cell Line as the “HeLa” Cell in the Cell Biology of Higher Plants. In *International review of cytology*: *A survey of cell biology*; Jeon, K. W., Friedlander, M., Eds.; International Review of Cytology 132; Elsevier: London, 1992; pp 1–30. DOI: 10.1016/S0074-7696(08)62452-3.

Naik, P. M.; Al-Khayri, J. M. Abiotic and Biotic Elicitors–Role in Secondary Metabolites Production through In Vitro Culture of Medicinal Plants. In *Abiotic and biotic stress in plants - recent advances and future perspectives*; Shanker, A. K., Shanker, C., Eds.; InTech: Rijeka, Croatia, op. 2016. DOI: 10.5772/61442.

Naill, M. C.; Roberts, S. C. Culture of isolated single cells from Taxus suspensions for the propagation of superior cell populations. *Biotechnology letters* **2005a,** *27* (21), 1725–1730. DOI: 10.1007/s10529-005-2738-1.

Naill, M. C.; Roberts, S. C. Flow cytometric identification of Paclitaxel-accumulating subpopulations. *Biotechnology progress* **2005b,** *21* (3), 978–983. DOI: 10.1021/bp049544l.

Narayani, M.; Srivastava, S. Elicitation: a stimulation of stress in in vitro plant cell/tissue cultures for enhancement of secondary metabolite production. *Phytochem Rev* **2017,** *16* (6), 1227–1252. DOI: 10.1007/s11101-017-9534-0.

Nasiri, J.; Naghavi, M. R.; Alizadeh, H.; Moghadam, M. R. F. Seasonal-based temporal changes fluctuate expression patterns of TXS, DBAT, BAPT and DBTNBT genes alongside production of associated taxanes in Taxus baccata. *Plant cell reports* **2016,** *35* (5), 1103–1119. DOI: 10.1007/s00299-016-1941-y.

Neumann, D.; Krauss, G.; Hieke, M.; Gröger, D. Indole Alkaloid Formation and Storage in Cell Suspension Cultures of Catharanthus roseus. *Planta medica* **1983,** *48* (1), 20–23. DOI: 10.1055/s-2007-969871.

Newman, D. J.; Cragg, G. M.; Snader, K. M. Natural products as sources of new drugs over the period 1981-2002. *J. Nat. Prod.* **2003,** *66* (7), 1022–1037. DOI: 10.1021/np030096l.

Nick, P. Noise yields order--auxin, actin, and polar patterning. *Plant biology* **2006,** *8* (3), 360–370. DOI: 10.1055/s-2006-923969.

Nick, P. Probing the actin-auxin oscillator. *Plant Signaling & Behavior* **2010,** *5* (2), 94–98. DOI: 10.4161/psb.5.2.10337.

Nick, P. Life versus 'biomass'-why application needs cell biology. *Protoplasma* **2016,** *253* (5), 1175–1176. DOI: 10.1007/s00709-016-1014-7.

Nick, P.; Han, M.-J.; An, G. Auxin Stimulates Its Own Transport by Shaping Actin Filaments. *Plant physiology* **2009,** *151* (1), 155–167. DOI: 10.1104/pp.109.140111.

Nick, P.; Heuing, A.; Ehmann, B. Plant chaperonins: a role in microtubule-dependent wall formation? *Protoplasma* **2000,** *211* (3-4), 234–244. DOI: 10.1007/BF01304491.

Nicolaou, K. C.; Yang, Z.; Liu, J. J.; Ueno, H.; Nantermet, P. G.; Guy, R. K.; Claiborne, C. F.; Renaud, J.; Couladouros, E. A.; Paulvannan, K.; Sorensen, E. J. Total synthesis of taxol. *Nature* **1994,** *367* (6464), 630. DOI: 10.1038/367630a0.

Nims, E.; Dubois, C. P.; Roberts, S. C.; Walker, E. L. Expression profiling of genes involved in paclitaxel biosynthesis for targeted metabolic engineering. *Metabolic engineering* **2006,** *8* (5), 385–394. DOI: 10.1016/j.ymben.2006.04.001.

Noé, W.; Mollenschott, C.; Berlin, J. Tryptophan decarboxylase from Catharanthus roseus cell suspension cultures: purification, molecular and kinetic data of the homogenous protein. *Plant molecular biology* **1984,** *3* (5), 281–288. DOI: 10.1007/BF00017782.

Ochoa-Villarreal, M.; Howat, S.; Hong, S.; Jang, M. O.; Jin, Y.-W.; Lee, E.-K.; Loake, G. J. Plant cell culture strategies for the production of natural products. *BMB Reports* **2016,** *49* (3), 149–158. DOI: 10.5483/BMBRep.2016.49.3.264.

Odell, L. R.; Skopec, J.; McCluskey, A. Isolation and identification of unique marker compounds from the Tasmanian poppy Papaver somniferum N. Implications for the identification of illicit heroin of Tasmanian origin. *Forensic science international* **2008,** *175* (2-3), 202–208. DOI: 10.1016/j.forsciint.2007.07.002.

O'Keefe, B. R.; Mahady, G. B.; Gills, J. J.; Beecher, C. W. W.; Schilling, A. B. Stable Vindoline Production in Transformed Cell Cultures of Catharanthus roseus. *J. Nat. Prod.* **1997,** *60* (3), 261–264. DOI: 10.1021/np960703n.

Onrubia, M.; Moyano, E.; Bonfill, M.; Expósito, O.; Palazón, J.; Cusidó, R. M. An approach to the molecular mechanism of methyl jasmonate and vanadyl sulphate elicitation in Taxus baccata cell cultures: The role of txs and bapt gene expression. *Biochemical Engineering Journal* **2010,** *53* (1), 104–111. DOI: 10.1016/j.bej.2010.10.001.

Opatrný, Z. From Němec and Haberlandt to Plant Molecular Biology. In *Applied Plant Cell Biology*: *Cellular Tools and Approaches for Plant Biotechnology*; Nick, P., Opatrný, Z., Eds.; Plant Cell Monographs 1 22; Springer Berlin: Berlin, 2014; pp 1–36. DOI: 10.1007/978-3-642-41787-0_1.

Opatrný, Z.; Nick, P.; Petrášek, J. Plant Cell Strains in Fundamental Research and Applications. In *Applied Plant Cell Biology*: *Cellular Tools and Approaches for Plant Biotechnology*; Nick, P., Opatrný, Z., Eds.; Plant Cell Monographs 1 22; Springer Berlin: Berlin, 2014; pp 455–481. DOI: 10.1007/978-3-642-41787-0_15.

Oudin, A.; Mahroug, S.; Courdavault, V.; Hervouet, N.; Zelwer, C.; Rodríguez-Concepción, M.; St-Pierre, B.; Burlat, V. Spatial distribution and hormonal regulation of gene products from methyl erythritol phosphate and monoterpene-secoiridoid pathways in Catharanthus roseus. *Plant molecular biology* **2007,** *65* (1-2), 13–30. DOI: 10.1007/s11103-007-9190-7.

Pan, Q.; Mustafa, N. R.; Tang, K.; Choi, Y. H.; Verpoorte, R. Monoterpenoid indole alkaloids biosynthesis and its regulation in Catharanthus roseus: a literature review from genes to metabolites. *Phytochem Rev* **2016a,** *15* (2), 221–250. DOI: 10.1007/s11101-015-9406-4.

Pan, Q.; Saiman, M. Z.; Mustafa, N. R.; Verpoorte, R.; Tang, K. A simple and rapid HPLC-DAD method for simultaneously monitoring the accumulation of alkaloids and precursors in different parts and different developmental stages of Catharanthus roseus plants. *Journal of chromatography. B, Analytical technologies in the biomedical and life sciences* **2016b,** *1014*, 10–16. DOI: 10.1016/j.jchromb.2016.01.034.

Pan, R.; Hu, J. Plant mitochondrial dynamics and the role of membrane lipids. *Plant Signaling & Behavior* **2015,** *10* (10), e1050573. DOI: 10.1080/15592324.2015.1050573.

Pan, Y.-J.; Liu, J.; Guo, X.-R.; Zu, Y.-G.; Tang, Z.-H. Gene transcript profiles of the TIA biosynthetic pathway in response to ethylene and copper reveal their interactive role in modulating TIA biosynthesis in Catharanthus roseus. *Protoplasma* **2015,** *252* (3), 813–824. DOI: 10.1007/s00709-014-0718-9.

Papon, N.; Bremer, J.; Vansiri, A.; Andreu, F.; Rideau, M.; Crèche, J. Cytokinin and ethylene control indole alkaloid production at the level of the MEP/terpenoid pathway in Catharanthus roseus suspension cells. *Planta medica* **2005,** *71* (6), 572–574. DOI: 10.1055/s-2005-864163.

Pasquali, G.; Goddijn, O. J. M.; Waal, A. de; Verpoorte, R.; Schilperoort, R. A.; Hoge, J. H. C.; Memelink, J. Coordinated regulation of two indole alkaloid biosynthetic genes from Catharanthus roseus by auxin and elicitors. *Plant molecular biology* **1992,** *18* (6), 1121–1131. DOI: 10.1007/BF00047715.

Patra, B.; Pattanaik, S.; Schluttenhofer, C.; Yuan, L. A network of jasmonate-responsive bHLH factors modulate monoterpenoid indole alkaloid biosynthesis in Catharanthus roseus. *The New phytologist* **2018,** *217* (4), 1566–1581. DOI: 10.1111/nph.14910.

Peebles, C. A. M.; Hughes, E. H.; Shanks, J. V.; San, K.-Y. Transcriptional response of the terpenoid indole alkaloid pathway to the overexpression of ORCA3 along with jasmonic acid elicitation of Catharanthus roseus hairy roots over time. *Metabolic engineering* **2009,** *11* (2), 76–86. DOI: 10.1016/j.ymben.2008.09.002.

Pollier, J.; Vanden Bossche, R.; Rischer, H.; Goossens, A. Selection and validation of reference genes for transcript normalization in gene expression studies in Catharanthus roseus. *Plant physiology and biochemistry : PPB* **2014,** *83*, 20–25. DOI: 10.1016/j.plaphy.2014.07.004.

Presley, A. D.; Fuller, K. M.; Arriaga, E. A. MitoTracker Green labeling of mitochondrial proteins and their subsequent analysis by capillary electrophoresis with laser-induced fluorescence detection. *Journal of Chromatography B* **2003,** *793* (1), 141–150. DOI: 10.1016/S1570-0232(03)00371-4.

Qu, Y.; Easson, M. L. A. E.; Froese, J.; Simionescu, R.; Hudlicky, T.; Luca, V. de. Completion of the seven-step pathway from tabersonine to the anticancer drug precursor vindoline and its assembly in yeast. *Proceedings of the National Academy of Sciences of the United States of America* **2015,** *112* (19), 6224–6229. DOI: 10.1073/pnas.1501821112.

Qu, Y.; Thamm, A. M. K.; Czerwinski, M.; Masada, S.; Kim, K. H.; Jones, G.; Liang, P.; Luca, V. de. Geissoschizine synthase controls flux in the formation of monoterpenoid indole alkaloids in a Catharanthus roseus mutant. *Planta* **2018,** *247* (3), 625–634. DOI: 10.1007/s00425-017-2812-7.

Rai, A.; Smita, S. S.; Singh, A. K.; Shanker, K.; Nagegowda, D. A. Heteromeric and homomeric geranyl diphosphate synthases from Catharanthus roseus and their role in monoterpene indole alkaloid biosynthesis. *Molecular plant* **2013,** *6* (5), 1531–1549. DOI: 10.1093/mp/sst058.

Rajabi, F.; Heene, E.; Maisch, J.; Nick, P. Combination of Plant Metabolic Modules Yields Synthetic Synergies. *PloS one* **2017,** *12* (1), e0169778. DOI: 10.1371/journal.pone.0169778.

Ramachandra Rao, S.; Ravishankar, G.A. Plant cell cultures: Chemical factories of secondary metabolites. *Biotechnology advances* **2002,** *20* (2), 101–153. DOI: 10.1016/S0734-9750(02)00007-1.

Ramani, S.; Jayabaskaran, C. Enhanced catharanthine and vindoline production in suspension cultures of Catharanthus roseus by ultraviolet-B light. *Journal of molecular signaling* **2008,** *3*, 9. DOI: 10.1186/1750-2187-3-9.

Ramirez-Estrada, K.; Osuna, L.; Moyano, E.; Bonfill, M.; Tapia, N.; Cusido, R. M.; Palazon, J. Changes in gene transcription and taxane production in elicited cell cultures of Taxus×media and Taxus globosa. *Phytochemistry* **2015,** *117*, 174–184. DOI: 10.1016/j.phytochem.2015.06.013.

Ramirez-Estrada, K.; Vidal-Limon, H.; Hidalgo, D.; Moyano, E.; Golenioswki, M.; Cusidó, R. M.; Palazon, J. Elicitation, an Effective Strategy for the Biotechnological Production of Bioactive High-Added Value Compounds in Plant Cell Factories. *Molecules (Basel, Switzerland)* **2016,** *21* (2), 182. DOI: 10.3390/molecules21020182.

Reape, T. J.; McCabe, P. F. Apoptotic-like regulation of programmed cell death in plants. *Apoptosis : an international journal on programmed cell death* **2010,** *15* (3), 249–256. DOI: 10.1007/s10495-009-0447-2.

Rébeillé, F.; Alban, C.; Bourguignon, J.; Ravanel, S.; Douce, R. The role of plant mitochondria in the biosynthesis of coenzymes. *Photosynthesis Research* **2007,** *92* (2), 149–162. DOI: 10.1007/s11120-007-9167-z.

Rhoads, D. M.; Umbach, A. L.; Subbaiah, C. C.; Siedow, J. N. Mitochondrial reactive oxygen species. Contribution to oxidative stress and interorganellar signaling. *Plant physiology* **2006,** *141* (2), 357–366. DOI: 10.1104/pp.106.079129.

Richards, K. D.; Schott, E. J.; Sharma, Y. K.; Davis, K. R.; Gardner, R. C. Aluminum Induces Oxidative Stress Genes in Arabidopsis thaliana. *Plant physiology* **1998,** *116* (1), 409–418. DOI: 10.1104/pp.116.1.409.

Rieder, C. L.; Maiato, H. Stuck in division or passing through: what happens when cells cannot satisfy the spindle assembly checkpoint. *Developmental cell* **2004,** *7* (5), 637–651. DOI: 10.1016/j.devcel.2004.09.002.

Riemann, M.; Muller, A.; Korte, A.; Furuya, M.; Weiler, E. W.; Nick, P. Impaired induction of the jasmonate pathway in the rice mutant hebiba. *Plant physiology* **2003,** *133* (4), 1820–1830. DOI: 10.1104/pp.103.027490.

Rischer, H.; Oresic, M.; Seppänen-Laakso, T.; Katajamaa, M.; Lammertyn, F.; Ardiles-Diaz, W.; van Montagu, M. C. E.; Inzé, D.; Oksman-Caldentey, K.-M.; Goossens, A. Gene-to-metabolite networks for terpenoid indole alkaloid biosynthesis in Catharanthus roseus cells. *Proceedings of the National Academy of Sciences* **2006,** *103* (14), 5614–5619. DOI: 10.1073/pnas.0601027103.

Roberts, C. W.; Roberts, F.; Lyons, R. E.; Kirisits, M. J.; Mui, E. J.; Finnerty, J.; Johnson, J. J.; Ferguson, D. J. P.; Coggins, J. R.; Krell, T.; Coombs, G. H.; Milhous, W. K.; Kyle, D. E.; Tzipori, S.; Barnwell, J.; Dame, J. B.; Carlton, J.; McLeod, R. The shikimate pathway and its branches in apicomplexan parasites. *The Journal of infectious diseases* **2002,** *185 Suppl 1*, S25-36. DOI: 10.1086/338004.

Roberts, S. C. Production and engineering of terpenoids in plant cell culture. *Nature Chemical Biology* **2007,** *3* (7), 387. DOI: 10.1038/nchembio.2007.8.

Rodríguez-Concepción, M. Early Steps in Isoprenoid Biosynthesis: Multilevel Regulation of the Supply of Common Precursors in Plant Cells. *Phytochem Rev* **2006,** *5* (1), 1–15. DOI: 10.1007/s11101-005-3130-4.

Ruiz-May, E.; Galaz-Avalos, R. M.; Loyola-Vargas, V. M. Differential secretion and accumulation of terpene indole alkaloids in hairy roots of Catharanthus roseus treated with methyl jasmonate. *Molecular biotechnology* **2009,** *41* (3), 278–285. DOI: 10.1007/s12033-008-9111-2.

Runge, T.; Sackmann, J.; Schomburg, W. K.; Blank, L. M. Ultrasonically manufactured microfluidic device for yeast analysis. *Microsyst Technol* **2017,** *23* (6), 2139–2144. DOI: 10.1007/s00542-016-3007-z.

Rusan, N. M.; Fagerstrom, C. J.; Yvon, A. M.; Wadsworth, P. Cell cycle-dependent changes in microtubule dynamics in living cells expressing green fluorescent protein-alpha tubulin. *Molecular biology of the cell* **2001,** *12* (4), 971–980. DOI: 10.1091/mbc.12.4.971.

Sakano, K.; Yazaki, Y.; Okihara, K.; Mimura, T.; Kiyota, S. Lack of Control in Inorganic Phosphate Uptake by Catharanthus roseus (L.) G. Don Cells (Cytoplasmic Inorganic Phosphate Homeostasis Depends on the Tonoplast Inorganic Phosphate Transport System?). *Plant physiology* **1995,** *108* (1), 295–302. DOI: 10.1104/pp.108.1.295.

Salim, V.; Wiens, B.; Masada-Atsumi, S.; Yu, F.; Luca, V. de. 7-deoxyloganetic acid synthase catalyzes a key 3 step oxidation to form 7-deoxyloganetic acid in Catharanthus roseus iridoid biosynthesis. *Phytochemistry* **2014,** *101*, 23–31. DOI: 10.1016/j.phytochem.2014.02.009.

Salim, V.; Yu, F.; Altarejos, J.; Luca, V. de. Virus-induced gene silencing identifies Catharanthus roseus 7-deoxyloganic acid-7-hydroxylase, a step in iridoid and monoterpene indole alkaloid biosynthesis. *The Plant journal : for cell and molecular biology* **2013,** *76* (5), 754–765. DOI: 10.1111/tpj.12330.

Sanati Nezhad, A.; Naghavi, M.; Packirisamy, M.; Bhat, R.; Geitmann, A. Quantification of cellular penetrative forces using lab-on-a-chip technology and finite element modeling. *Proceedings of the National Academy of Sciences of the United States of America* **2013,** *110* (20), 8093–8098. DOI: 10.1073/pnas.1221677110.

Schoendorf, A.; Rithner, C. D.; Williams, R. M.; Croteau, R. B. Molecular cloning of a cytochrome P450 taxane 10 beta-hydroxylase cDNA from Taxus and functional expression in yeast. *Proceedings of the National Academy of Sciences* **2001,** *98* (4), 1501–1506. DOI: 10.1073/pnas.98.4.1501.

Sharma, A.; Verma, P.; Mathur, A.; Mathur, A. K. Overexpression of tryptophan decarboxylase and strictosidine synthase enhanced terpenoid indole alkaloid pathway activity and antineoplastic vinblastine biosynthesis in Catharanthus roseus. *Protoplasma* **2018,** *255* (5), 1281–1294. DOI: 10.1007/s00709-018-1233-1.

Shitan, N.; Yazaki, K. Accumulation and Membrane Transport of Plant Alkaloids. *CPB* **2007,** *8* (4), 244–252. DOI: 10.2174/138920107781387429.

Simkin, A. J.; Miettinen, K.; Claudel, P.; Burlat, V.; Guirimand, G.; Courdavault, V.; Papon, N.; Meyer, S.; Godet, S.; St-Pierre, B.; Giglioli-Guivarc'h, N.; Fischer, M. J. C.; Memelink, J.; Clastre, M. Characterization of the plastidial geraniol synthase from Madagascar periwinkle which initiates the monoterpenoid branch of the alkaloid pathway in internal phloem associated parenchyma. *Phytochemistry* **2013,** *85*, 36–43. DOI: 10.1016/j.phytochem.2012.09.014.

Sivanandhan, G.; Selvaraj, N.; Ganapathi, A.; Manickavasagam, M. Enhanced biosynthesis of withanolides by elicitation and precursor feeding in cell suspension culture of Withania somnifera (L.) Dunal in shake-flask culture and bioreactor. *PloS one* **2014,** *9* (8), e104005. DOI: 10.1371/journal.pone.0104005.

Slichenmyer, W. J.; Hoff, D. D. von. New Natural Products in Cancer Chemotherapy. *The Journal of Clinical Pharmacology* **1990,** *30* (9), 770–788. DOI: 10.1002/j.1552-4604.1990.tb01873.x.

Smetanska, I. Production of secondary metabolites using plant cell cultures. *Advances in biochemical engineering/biotechnology* **2008,** *111*, 187–228. DOI: 10.1007/10_2008_103.

Smith, J. I.; Quesnel, A. A.; Smart, N. J.; Misawa, M.; Kurz, W.G.W. The development of a single-stage growth and indole alkaloid production medium for Catharanthus roseus (L.) G. Don suspension cultures. *Enzyme and Microbial Technology* **1987,** *9* (8), 466–469. DOI: 10.1016/0141-0229(87)90098-6.

Sottomayor, M.; López-Serrano, M.; DiCosmo, F.; Ros Barceló, A. Purification and characterization of α-3′,4′-anhydrovinblastine synthase (peroxidase-like) from Catharanthus roseus (L.) G. Don. *FEBS Letters* **1998,** *428* (3), 299–303. DOI: 10.1016/S0014-5793(98)00551-1.

Srivastava, J. K.; Shankar, E.; Gupta, S. Chamomile: A herbal medicine of the past with bright future. *Molecular medicine reports* **2010,** *3* (6), 895–901. DOI: 10.3892/mmr.2010.377.

Stevens, L. H.; Blom, T. J.; Verpoorte, R. Subcellular localization of tryptophan decarboxylase, strictosidine synthase and strictosidine glucosidase in suspension cultured cells of Catharanthus roseus and Tabernaemontana divaricata. *Plant cell reports* **1993,** *12* (10), 573–576. DOI: 10.1007/BF00233063.

St-Pierre, B. Multicellular Compartmentation of Catharanthus roseus Alkaloid Biosynthesis Predicts Intercellular Translocation of a Pathway Intermediate. *THE PLANT CELL ONLINE* **1999,** *11* (5), 887–900. DOI: 10.1105/tpc.11.5.887.

St-Pierre, B.; Laflamme, P.; Alarco, A.-M.; D, V.; Luca, e. The terminal O-acetyltransferase involved in vindoline biosynthesis defines a new class of proteins responsible for coenzyme A-dependent acyl transfer. *Plant J* **1998,** *14* (6), 703–713. DOI: 10.1046/j.1365-313x.1998.00174.x.

St-Pierre, B.; Vazquez-Flota, F. A.; Luca, V. de. Multicellular Compartmentation of Catharanthus roseus Alkaloid Biosynthesis Predicts Intercellular Translocation of a Pathway Intermediate. *The Plant cell* **1999,** *11* (5), 887–900. DOI: 10.1105/tpc.11.5.887.

Sun, G.; Yang, Y.; Xie, F.; Wen, J.-F.; Wu, J.; Wilson, I. W.; Tang, Q.; Liu, H.; Qiu, D. Deep sequencing reveals transcriptome re-programming of Taxus × media cells to the elicitation with methyl jasmonate. *PloS one* **2013,** *8* (4), e62865. DOI: 10.1371/journal.pone.0062865.

Sun, J.; Le Zhao; Shao, Z.; Shanks, J.; Peebles, C. A. M. Expression of tabersonine 16-hydroxylase and 16-hydroxytabersonine-O-methyltransferase in Catharanthus roseus hairy roots. *Biotechnology and bioengineering* **2018,** *115* (3), 673–683. DOI: 10.1002/bit.26487.

Swiatek, A.; Lenjou, M.; van Bockstaele, D.; Inze, D.; van Onckelen, H. Differential Effect of Jasmonic Acid and Abscisic Acid on Cell Cycle Progression in Tobacco BY-2 Cells. *Plant physiology* **2002,** *128* (1), 201–211. DOI: 10.1104/pp.010592.

Tekoah, Y.; Shulman, A.; Kizhner, T.; Ruderfer, I.; Fux, L.; Nataf, Y.; Bartfeld, D.; Ariel, T.; Gingis-Velitski, S.; Hanania, U.; Shaaltiel, Y. Large-scale production of pharmaceutical proteins in plant cell culture-the Protalix experience. *Plant biotechnology journal* **2015,** *13* (8), 1199–1208. DOI: 10.1111/pbi.12428.

Thamm, A. M. K.; Qu, Y.; Luca, V. de. Discovery and metabolic engineering of iridoid/secoiridoid and monoterpenoid indole alkaloid biosynthesis. *Phytochem Rev* **2016,** *15* (3), 339–361. DOI: 10.1007/s11101-016-9468-y.

Thornburg, C. K.; Walter, T.; Walker, K. D. Biocatalysis of a Paclitaxel Analogue: Conversion of Baccatin III to N-Debenzoyl-N-(2-furoyl)paclitaxel and Characterization of an Amino Phenylpropanoyl CoA Transferase. *Biochemistry* **2017,** *56* (44), 5920–5930. DOI: 10.1021/acs.biochem.7b00912.

Tiryaki, I.; Staswick, P. E. An Arabidopsis mutant defective in jasmonate response is allelic to the auxin-signaling mutant axr1. *Plant physiology* **2002,** *130* (2), 887–894. DOI: 10.1104/pp.005272.

Tondera, D.; Grandemange, S.; Jourdain, A.; Karbowski, M.; Mattenberger, Y.; Herzig, S.; Da Cruz, S.; Clerc, P.; Raschke, I.; Merkwirth, C.; Ehses, S.; Krause, F.; Chan, D. C.; Alexander, C.; Bauer, C.; Youle, R.; Langer, T.; Martinou, J.-C. SLP-2 is required for stress-induced mitochondrial hyperfusion. *The EMBO journal* **2009,** *28* (11), 1589–1600. DOI: 10.1038/emboj.2009.89.

van der Fits, L. ORCA3, a Jasmonate-Responsive Transcriptional Regulator of Plant Primary and Secondary Metabolism. *Science* **2000,** *289* (5477), 295–297. DOI: 10.1126/science.289.5477.295.

van der Heijden, R.; Verpoorte, R.; Hoopen, H. J. G. ten. Cell and tissue cultures ofCatharanthus roseus (L.) G. Don: a literature survey. *Plant Cell Tiss Organ Cult* **1989,** *18* (3), 231–280. DOI: 10.1007/BF00043397.

van der Valk, P.; van Kalken, C. K.; Ketelaars, H.; Broxterman, H. J.; Scheffer, G.; Kuiper, C. M.; Tsuruo, T.; Lankelma, J.; Meijer, C. J. L. M.; Pinedo, H. M.; Scheper, R. J. Original article: Distribution of multi-drug resistance-associated P-glycoprotein in normal and neoplastic human tissues. *Annals of Oncology* **1990,** *1* (1), 56–64. DOI: 10.1093/oxfordjournals.annonc.a057676.

van Gestel, K.; Verbelen, J.-P. Giant mitochondria are a response to low oxygen pressure in cells of tobacco (Nicotiana tabacum L.). *J Exp Bot* **2002,** *53* (371), 1215–1218. DOI: 10.1093/jexbot/53.371.1215.

Vandesompele, J.; Preter, K. de; Pattyn, F.; Poppe, B.; van Roy, N.; Paepe, A. de; Speleman, F. Accurate normalization of real-time quantitative RT-PCR data by geometric averaging of multiple internal control genes. *Genome Biol* **2002,** *3* (7), research0034.1. DOI: 10.1186/gb-2002-3-7-research0034.

Vazquez-Flota, F.; Carolis, E. de; Alarco, A.-M.; Luca, V. de. Molecular cloning and characterization of desacetoxyvindoline-4-hydroxylase, a 2-oxogluterate dependent-dioxygenase involved in the biosynthesis of vindoline in Catharanthus roseus (L.) G. Don. *Plant molecular biology* **1997,** *34* (6), 935–948. DOI: 10.1023/A:1005894001516.

Vázquez-Flota, F.; Hernández-Domínguez, E.; Lourdes Miranda-Ham, M. de; Monforte-González, M. A differential response to chemical elicitors in Catharanthus roseus in vitro cultures. *Biotechnology letters* **2009,** *31* (4), 591–595. DOI: 10.1007/s10529-008-9881-4.

Vereshchagina, E.; Mc Glade, D.; Glynn, M.; Ducrée, J. A hybrid microfluidic platform for cell-based assays via diffusive and convective trans-membrane perfusion. *Biomicrofluidics* **2013,** *7* (3), 34101. DOI: 10.1063/1.4804250.

Verma, P.; Mathur, A. K.; Srivastava, A.; Mathur, A. Emerging trends in research on spatial and temporal organization of terpenoid indole alkaloid pathway in Catharanthus roseus: a literature update. *Protoplasma* **2012,** *249* (2), 255–268. DOI: 10.1007/s00709-011-0291-4.

Vidensek, N.; Lim, P.; Campbell, A.; Carlson, C. Taxol Content in Bark, Wood, Root, Leaf, Twig, and Seedling from Several Taxus Species. *J. Nat. Prod.* **1990,** *53* (6), 1609–1610. DOI: 10.1021/np50072a039.

Wakabayashi, T. Megamitochondria formation - physiology and pathology. *J Cellular Mol Med* **2002,** *6* (4), 497–538. DOI: 10.1111/j.1582-4934.2002.tb00452.x.

Walker, K.; Croteau, R. Molecular cloning of a 10-deacetylbaccatin III-10-O-acetyl transferase cDNA from Taxus and functional expression in Escherichia coli. *Proceedings of the National Academy of Sciences* **2000a,** *97* (2), 583–587. DOI: 10.1073/pnas.97.2.583.

Walker, K.; Croteau, R. Taxol biosynthesis: molecular cloning of a benzoyl-CoA:taxane 2alpha-O-benzoyltransferase cDNA from taxus and functional expression in Escherichia coli. *Proceedings of the National Academy of Sciences* **2000b,** *97* (25), 13591–13596. DOI: 10.1073/pnas.250491997.

Walker, K.; Fujisaki, S.; Long, R.; Croteau, R. Molecular cloning and heterologous expression of the C-13 phenylpropanoid side chain-CoA acyltransferase that functions in Taxol biosynthesis. *Proceedings of the National Academy of Sciences* **2002,** *99* (20), 12715–12720. DOI: 10.1073/pnas.192463699.

Walker, K.; Ketchum, R. E.; Hezari, M.; Gatfield, D.; Goleniowski, M.; Barthol, A.; Croteau, R. Partial purification and characterization of acetyl coenzyme A: taxa-4(20),11(12)-dien-5alpha-ol O-acetyl transferase that catalyzes the first acylation step of taxol biosynthesis. *Archives of biochemistry and biophysics* **1999,** *364* (2), 273–279. DOI: 10.1006/abbi.1999.1125.

Whitesides, G. M. The origins and the future of microfluidics. *Nature* **2006,** *442* (7101), 368–373. DOI: 10.1038/nature05058.

Whitmer, S.; van der Heijden, R.; Verpoorte, R. Effect of precursor feeding on alkaloid accumulation by a strictosidine synthase over-expressing transgenic cell line S1 of Catharanthus roseus. *Plant Cell, Tissue and Organ Culture* **2002,** *69* (1), 85–93. DOI: 10.1023/A:1015090224398.

Widholm, J. M. The Use of Fluorescein Diacetate and Phenosafranine for Determining Viability of Cultured Plant Cells. *Stain Technology* **1972,** *47* (4), 189–194. DOI: 10.3109/10520297209116483.

Wildung, M. R.; Croteau, R. A cDNA Clone for Taxadiene Synthase, the Diterpene Cyclase That Catalyzes the Committed Step of Taxol Biosynthesis. *J. Biol. Chem.* **1996,** *271* (16), 9201–9204. DOI: 10.1074/jbc.271.16.9201.

Wilson, S. A.; Roberts, S. C. Recent advances towards development and commercialization of plant cell culture processes for the synthesis of biomolecules. *Plant biotechnology journal* **2012,** *10* (3), 249–268. DOI: 10.1111/j.1467-7652.2011.00664.x.

Wink, M. Functions and Biotechnology of Plant Secondary Metabolites **2010,** *v.39. DOI:* 10.1002/9781444318876.

Wu, H.; Liu, W.; Tu, Q.; Song, N.; Li, L.; Wang, J.; Wang, J. Culture and chemical-induced fusion of tobacco mesophyll protoplasts in a microfluidic device. *Microfluid Nanofluid* **2011,** *10* (4), 867–876. DOI: 10.1007/s10404-010-0720-2.

Yahia, A.; Kevers, C.; Gaspar, T.; Chénieux, J.-C.; Rideau, M.; Crèche, J. Cytokinins and ethylene stimulate indole alkaloid accumulation in cell suspension cultures of Catharanthus roseus by two distinct mechanisms. *Plant Science* **1998,** *133* (1), 9–15. DOI: 10.1016/S0168-9452(98)00014-4.

Yan, Y.; Liu, J.; Wei, C.; Li, K.; Xie, W.; Wang, Y.; Cheng, H. Bidirectional regulation of Ca2+ sparks by mitochondria-derived reactive oxygen species in cardiac myocytes. *Cardiovascular research* **2008,** *77* (2), 432–441. DOI: 10.1093/cvr/cvm047.

Yao, K.; Luca, V. de; Brisson, N. Creation of a Metabolic Sink for Tryptophan Alters the Phenylpropanoid Pathway and the Susceptibility of Potato to Phytophthora infestans. *The Plant cell* **1995,** *7* (11), 1787–1799. DOI: 10.1105/tpc.7.11.1787.

Yazaki, K. ABC transporters involved in the transport of plant secondary metabolites. *FEBS Letters* **2006,** *580* (4), 1183–1191. DOI: 10.1016/j.febslet.2005.12.009.

Yu, F.; Luca, V. de. ATP-binding cassette transporter controls leaf surface secretion of anticancer drug components in Catharanthus roseus. *Proceedings of the National Academy of Sciences of the United States of America* **2013,** *110* (39), 15830–15835. DOI: 10.1073/pnas.1307504110.

Yue, W.; Ming, Q.-L.; Lin, B.; Rahman, K.; Zheng, C.-J.; Han, T.; Qin, L.-P. Medicinal plant cell suspension cultures: pharmaceutical applications and high-yielding strategies for the desired secondary metabolites. *Critical reviews in biotechnology* **2016,** *36* (2), 215–232. DOI: 10.3109/07388551.2014.923986.

Yukimune, Y.; Tabata, H.; Higashi, Y.; Hara, Y. Methyl jasmonate-induced overproduction of paclitaxel and baccatin III in Taxus cell suspension cultures. *Nature Biotechnology* **1996,** *14*, 1129 EP -. DOI: 10.1038/nbt0996-1129.

Zaban, B.; Maisch, J.; Nick, P. Dynamic actin controls polarity induction de novo in protoplasts. *Journal of integrative plant biology* **2013,** *55* (2), 142–159. DOI: 10.1111/jipb.12001.

Zhang, H.; Boghigian, B. A.; Armando, J.; Pfeifer, B. A. Methods and options for the heterologous production of complex natural products. *Natural product reports* **2011,** *28* (1), 125–151. DOI: 10.1039/c0np00037j.

Zhao, J.; Zhu, W.-H.; Hu, Q. Enhanced catharanthine production in catharanthus roseus cell cultures by combined elicitor treatment in shake flasks and bioreactors. *Enzyme and Microbial Technology* **2001a,** *28* (7-8), 673–681. DOI: 10.1016/S0141-0229(01)00306-4.

Zhao, J.; Zhu, W.-H.; Hu, Q.; He, X.-W. Enhanced indole alkaloid production in suspension compact callus clusters of Catharanthus roseus: impacts of plant growth regulators and sucrose. *Plant Growth Regulation* **2001b,** *33* (1), 33–41. DOI: 10.1023/A:1010732308175.

Zhong, J.-J. Plant Cell Culture for Production of Paclitaxel and Other Taxanes. *J. BIOSCI. BIOENG.* **2002,** *94* (6), 591–599. DOI: 10.1263/jbb.94.591.

Zhong, J.-J.; Yue, C.-J. Plant Cells: Secondary Metabolite Heterogeneity and Its Manipulation. In *Biotechnology for the future*; Nielsen, J. H., Ed.; Advances in Biochemical Engineering/Biotechnology; Springer: Berlin, 2005; pp 53–88. DOI: 10.1007/b136412.

Zhu, J.; Wang, M.; Wen, W.; Yu, R. Biosynthesis and regulation of terpenoid indole alkaloids in Catharanthus roseus. *Pharmacognosy Reviews* **2015,** *9* (17), 24–28. DOI: 10.4103/0973-7847.156323.

Zhu, X.; Zeng, X.; Sun, C.; Chen, S. Biosynthetic pathway of terpenoid indole alkaloids in Catharanthus roseus. *Frontiers of medicine* **2014,** *8* (3), 285–293. DOI: 10.1007/s11684-014-0350-2.

Züchner, S.; Mersiyanova, I. V.; Muglia, M.; Bissar-Tadmouri, N.; Rochelle, J.; Dadali, E. L.; Zappia, M.; Nelis, E.; Patitucci, A.; Senderek, J.; Parman, Y.; Evgrafov, O.; Jonghe, P. D.; Takahashi, Y.; Tsuji, S.; Pericak-Vance, M. A.; Quattrone, A.; Battologlu, E.; Polyakov, A. V.; Timmerman, V.; Schröder, J. M.; Vance, J. M. Mutations in the mitochondrial GTPase mitofusin 2 cause Charcot-Marie-Tooth neuropathy type 2A. *Nature Genetics* **2004,** *36* (5), 449. DOI: 10.1038/ng1341.